Fakultät für Medizin

Helicobacter pylori and colon cancer: interplay between intestinal immune signaling and microbiota

Anna Ralser

Vollständiger Abdruck der von der Fakultät für Medizin der Technischen Universität München zur Erlangung des akademischen Grades eines

Doctor of Philosophy (Ph.D.)

genehmigten Dissertation.

Vorsitzende: Prof. Dr. Alessandra Moretti

Betreuer: Prof. Dr. med. Markus Gerhard

Prüfer der Dissertation:

1. Prof. Dr. Klaus-Peter Janssen

2. Prof. Dr. Dirk Haller

3. Priv-Doz. Dr. Christian Schulz

Die Dissertation wurde am 15.06.2022 bei der Fakultät für Medizin der Technischen Universität München eingereicht und durch die Fakultät für Medizin am 19.09.2022 angenommen.

„Das Wissen, das Wissenschaft produziert, ist indes niemals absolut, immer vorläufig und prinzipiell revidierbar.“

- Lorraine Daston

Abstract

Helicobacter pylori infection affects more than half of the world's population and although colonizing the stomach, chronic infection is also associated with extragastric diseases. *H. pylori*-positive individuals harbor a nearly 2-fold increased risk for colorectal cancer (CRC) development. However, the underlying mechanisms that confer the observed increased risk are unclear.

C57BL/6 mice and mouse models of CRC ($Apc^{+/1638N}$ and $Apc^{+/min}$) were infected with the pathogenic *H. pylori* strain PMSS1 and a comprehensive analysis of *H. pylori*-induced changes in intestinal and colonic immune response, pro-carcinogenic and pro-inflammatory signaling and gut homeostasis via flow cytometry, chip cytometry, immunohistochemistry and single cell RNA sequencing was conducted. Furthermore, the intestinal and colonic microbiota was assessed by 16S rRNA sequencing. To evaluate the phenotype mechanistically, *H. pylori* infected mice were eradicated, germ-free mice were infected and stool transfer experiments were conducted. The observed findings were validated in a human cohort of *H. pylori*-infected individuals.

H. pylori infection was found to promote tumor development in *Apc* mouse models, and to induce a specific proinflammatory T-cell response, accompanied by a reduction of regulatory T-cells, in the intestine and colon. Transcriptomic profiling of immune cells revealed that *H. pylori* induces impaired regulatory T-cell functions and rewires the tumor microenvironment towards CD8+ T-cell exhaustion. Increased activation of STAT3 signaling and a loss of mucus-producing goblet cells was observed in infected animals. This *H. pylori*-induced phenotype was normalized to the levels of non-infected controls upon eradication therapy. 16S rRNA sequencing revealed that *H. pylori* infection shapes microbiota towards mucus degradation, and germ-free mice as well as stool transfer provided evidence of a significant role of the microbiota in the observed phenotype. In colon tissues of *H. pylori* infected individuals, similar changes in colonic immune response, STAT3 signaling and goblet cells differentiation, which were attenuated in eradicated patients, were observed.

These results define distant effects of *H. pylori* on the intestinal and colonic immune response and on the microbiota to be the dominant mechanisms involved in *H. pylori*-driven colorectal carcinogenesis. This study indicates to include *H. pylori* status into an adapted risk score for CRC and suggests including *H. pylori* positive patients in CRC screening programs.

Zusammenfassung

Mehr als die Hälfte der Weltbevölkerung ist mit *Helicobacter pylori* infiziert. Obwohl das Bakterium ausschließlich den Magen kolonisiert, ist eine chronische Infektion mit Krankheiten außerhalb des Magens assoziiert. Epidemiologische Daten haben gezeigt, dass *H. pylori* positive Menschen ein fast 2-fach erhöhtes Risiko haben, ein kolorektales Karzinom zu entwickeln. Die Mechanismen, die zu diesem erhöhten Risiko führen, sind jedoch noch nicht geklärt.

C57BL/6 Mäuse und die Tumormausmodelle $Apc^{+/1638N}$ and $Apc^{+/min}$ wurden mit dem pathogenen *H. pylori* Stamm PMSS1 infiziert und die Immunantwort, dabei induzierte pro-inflammatorische und pro-karzinogene Signalwege und der Einfluss auf das epitheliale Gleichgewicht im Dünn- und Dickdarm der Mäuse mittels Druchflusszytometrie, Chip Zytometrie, Immunhistochemie und RNA Sequenzierung auf Einzelzelllevel charakterisiert.

Außerdem wurden die Mikrobiota des Dünn- und Dickdarms mittels 16S rRNA Sequenzierung untersucht. Um den dadurch identifizierten Phänotypen mechanistisch zu evaluieren, wurden *H. pylori* infizierte Mäuse eradiziert, keimfreie Mäuse infiziert und Stuhltransfer Experimente durchgeführt. Die Ergebnisse wurden schließlich in einer humanen Kohorte verifiziert.

Es konnte gezeigt werden, dass *H. pylori* die Tumorentwicklung in Apc Mausmodellen beschleunigt und einen spezifische, proinflammatorische T-Zell Antwort, begleitet von einer Reduktion von regulatorischen T-Zellen, im Dünn- und Dickdarm auslöst. Analysen auf Genexpressionslevel von Immunzellen ergaben außerdem, dass *H. pylori* regulatorische T-Zellen umprogrammiert und die Tumorumgebung beeinflusst, indem es Erschöpfung von CD8+ T-Zellen induziert. Eine erhöhte Aktivierung des STAT3 Signalwegs und der Verlust von Mucus-produzierenden Goblet Zellen wurde außerdem in infizierten Mäusen beobachtet. Dieser Phänotyp normalisierte sich auf das Level von nicht infizierten Mäusen nach einer Eradikationstherapie. 16S rRNA Sequenzierung zeigte, dass *H. pylori* die Mikrobiota in Richtung Mucus-Degradierung formt und sowohl Experimente in keimfreien Mäusen als auch Stuhltransfer unterstrichen die signifikante Rolle des Mikrobioms in dem beschriebenen Phänotyp. Ähnliche Veränderungen in der Immunantwort, die Aktivierung von STAT3 und der Verlust von Goblet Zellen konnten in *H. pylori* positiven Individuen gezeigt werden und diese Effekte waren in eradizierten Patienten abgeschwächt.

Diese Ergebnisse definieren Effekte von *H. pylori* auf die Immunantwort und das Mikrobiom des Darms als dominante Mechanismen der *H. pylori*-induzierten kolorektalen Karzinogenese. Die Studie liefert den Nachweis, dass *H. pylori* Status in einen angepassten Risikoscore für kolorektale Karzinome aufgenommen werden sollte und suggeriert *H. pylori* positive Patienten für kolorektale Karzinome zu screenen.

List of Contents

1. Introduction 11

1.1. Helicobacter pylori 11

1.1.1. Pathogenesis of *H. pylori* infection 11

1.1.2. Virulence factors of *H. pylori* 13

1.1.3. *H. pylori*-induced immune response 14

1.1.4. *H. pylori*-induced changes in microbiota 18

1.1.5. H. pylori-induced gastric and extragastric diseases 18

1.2. Colorectal Cancer 21

1.2.1. Colorectal Carcinogenesis 21

1.2.2. Inflammation and Colorectal Cancer 25

1.2.3. Microbiota, intestinal homeostasis and Colorectal Cancer 23

1.2.4. Mouse models of Colorectal Cancer 22

1.2.5. Risk factors 24

2. Aims 27

3. Material and Methods 29

3.1. Material 29

3.2. Methods 33

3.2.1. Animal experiments 33

3.2.2. Histological evaluation 34

3.2.3. Quantitative PCR 36

3.2.4. ChipCytometry and automatic image quantification 38

3.2.5. Flow Cytometry 38

3.2.6. 16S rRNA Sequencing 40

3.2.7. Single cell RNA sequencing 41

3.2.8. Human studies 42

3.2.9. Statistical analysis 42

4. Results 43

4.1. Characterization of the influence of H. pylori infection on intestinal/colonic inflammation and signaling pathways 43

4.1.1. *H. pylori*-infected mice exhibit a pro-inflammatory T-cell response in intestine and colon 43

4.1.2. *H. pylori* infection activates STAT3 signaling, enhances proliferation and reduces mucus producing goblet cells in intestine and colon 49

4.1.3. *H. pylori* infection shapes gut microbiota towards mucus-degradation 54

4.1.4. Eradication therapy reverses *H. pylori* induced phenotype to levels of non-infected controls 55

4.2. Characterization of the influence of *H. pylori* infection on intestinal/colonic carcinogenesis 58

4.2.1. *H. pylori* drives tumor development in $Apc^{+/1638N}$ and $Apc^{+/min}$ mice 58

4.2.2. *H. pylori* infection induces pro-inflammatory T-cell response in $Apc^{+/1638N}$ and $Apc^{+/min}$ mice 59

4.2.3. *H. pylori* infection activates STAT3 signaling, enhances proliferation and reduces mucus producing goblet cells in $Apc^{+/1638N}$ and $Apc^{+/min}$ mice 62

4.2.4. *H. pylori* infection shapes gut microbiota in $Apc^{+/1638N}$ and $Apc^{+/min}$ mice 63

4.2.5. *H. pylori*-induced immune and epithelial signatures depend on the presence of gut microbiota and level to non-infected controls upon eradication therapy 65
4.2.6. Single cell RNA Sequencing reveals molecular mechanisms in *H. pylori*-induced colon carcinogenesis 68
4.3. Characterization of the influence of *H. pylori* infection on inflammation and signaling pathways in human colon 74
4.3.1. *H. pylori* induced immune and epithelial signature can be translated into human colon 74
4.3.2. *H. pylori* infection affects microbiota in humans 76
5. Discussion 79
5.1. *H. pylori* shapes intestinal immune response and signaling 79
5.2. *H. pylori* interferes with microbiota compositions and impairs goblet cell function 83
5.3. *H. pylori* modulates the tumor environment 86
5.4. H. pylori induced phenotype is normalized upon eradication and is partly depending on the presence of microbiota 87
5.5. *H. pylori* affects immune, epithelial and microbial signatures in human colon 88
5.6. *H. pylori* induced colorectal carcinogenesis: a proposed model of underlying mechanisms 89
5.7. Conclusion and outlook 90
6. References 98

1. Introduction

1.1. Helicobacter pylori

Helicobacter pylori is a gram-negative, spiral shaped, microaerophilic bacterium that colonizes the gastric mucosa of more than half of the world's population. Infection prevalence ranges widely among different continents, with the highest prevalence in Africa (79.1%) and the lowest prevalence in Western Europe (34.3%) and Oceania (24.4%) (Figure 1.1) (1). The discovery of the bacterium's causative role in peptic ulcer disease in 1983 by Robin Warren and Barry Marshall was awarded with the Nobel Prize in 2005 and changed the perception from a life threatening into a curable disease (2). This milestone set the groundwork for an enormous amount of studies conducted on the molecular pathogenesis and clinical impact of *H. pylori* infection, concerning not only its effects on gastric disease but also on extragastric conditions.

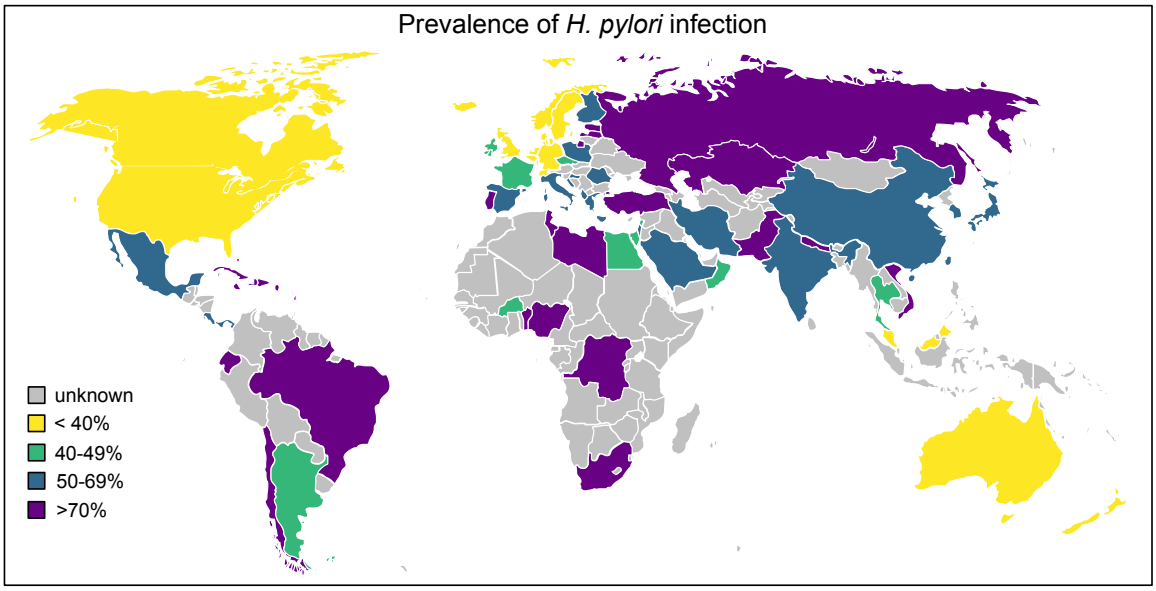

Figure 1.1: Percentages of *H. pylori* infected individuals worldwide. Distribution of *H. pylori* positive people in countries across the world, shown in % of the population (1).

1.1.1. Pathogenesis of *H. pylori* infection

Infection with *H. pylori* is typically acquired at early childhood and persists life-long. The transmission routes remain controversial, in most cases, however, transmission is intrafamilial, mostly from mother to child and between siblings (3). However, especially in developing countries, environmental contamination may also constitute a route of infection, which certainly contributes to the previously stated wide range of bacterial prevalence across continents (4). Furthermore, the overall trend towards lower prevalence

of *H. pylori* infection can be possibly related to rising socioeconomic status and urbanization (5).

H. pylori has evolved several mechanisms to survive within the hostile environment of the stomach. Upon entry, *H. pylori* encounters a highly acidic gastric lumen (pH 2), which is buffered by its urease activity, converting urea to ammonia and carbon dioxide (6). Subsequently, the bacterium has to overcome clearance by the host and therefore penetrate the gastric mucus to reach the epithelial cells. This is achieved by its morphological features, characterized by spiral shape, high motility and unipolar flagella. In addition, sensors for pH and bicarbonate ions enable the bacterium to navigate from the highly acidic gastric lumen to the almost pH neutral epithelial cell surface (7, 8). This pH sensing is likely also responsible for the almost exclusive colonization of the antrum and cardia, whereas the corpus is only colonized when acid secretion is decreased due to long-term medicinal acid suppression or when atrophy has developed (9-11). It has been shown that more than 80% of the bacterium reside within the mucus and the remaining fraction adheres to the surface of the gastric epithelium and resides within the glands (8). The close proximity to the gastric epithelial cells enables the bacterium to both extract nutrients and to deliver bacterial factors, which are crucial for persistent infection but that also imply the activation of the immune system.

Successful attachment to the stomach epithelium is the next decisive factor in the cascade of *H. pylori*-induced pathogenesis. Several bacterial cell surface proteins belonging to the outer membrane protein (OMP) family Hop, such as blood group antigen binding adhesin (BabA) and sialic acid-binding adhesin (SabA), AlpA and AlpB and HopQ mediate this process. Those Hop proteins use distinct epithelial host receptors and functionally contribute to the outcome of infection. BabA and SabA both use human blood group antigens, di-fucosilated Lewis^{b} and sialyl-dimeric-Lewis^{x} respectively, as receptors on human gastric epithelial cells (12-14). BabA positive *H. pylori* strains have shown to contribute to the virulence of *H. pylori*, especially when co-occurring with the virulence factors cytotoxin-associated gene A (CagA) and vacuolating cytotoxin gene A (VacA) as positive strains for these factors aggravate inflammatory responses in the stomach (15) and are associated with peptic ulcer disease and gastric adenocarcinoma development (16). BabA and SabA show a certain interdependency, as initial BabA-Lewis^{b} binding upregulates Lewis^{x}, therefore supporting SabA-mediated binding (17). Furthermore, it has been shown that in patients with rather low Lewis^{b} expression, SabA/ Lewis^{x} mediated binding enables similar densities of *H. pylori* colonization (18). Interestingly, the expression of BabA declines over the course of infection, whereas SabA binding is gaining importance with chronicity of the infection, as sialylated antigens are highly expressed in the inflamed,

but not in the healthy stomach (14). Adherence associated lipoproteins AlpA and AlpB use host laminin as receptor for binding and are also involved in host cell signaling and induction of cytokines, as interleukin (IL)-6 and IL-8 (19, 20). Infections of mice with AlpA/AlpB deficient strains led to sparse colonization and underline the importance of these OMPs in successful *H. pylori* infection (20). Furthermore, a study reported reduced adherence of *H. pylori* to human gastric tissue upon AlpA/AlpB (21). Recently, members of the carcinoembryonic antigen-related cell adhesion molecules (CEACAM) family have been identified as receptors for the OMP HopQ, in particular CEACAM1, CEACAM5 and CEACAM6. Binding occurs at the N-terminal sites via a protein-protein interaction and has shown to be a prerequisite for the translocation of the virulence factor CagA into gastric epithelial cells. Furthermore, deletion of HopQ resulted in lower bacterial adhesion and less cytokine response, suggesting a pivotal role of HopQ in *H. pylori* induced pathogenesis (22, 23).

1.1.2. Virulence factors of *H. pylori*

After successful attachment to the gastric epithelium, *H. pylori* induces a chronic inflammatory response, which is mediated by different virulence factors, including cag pathogenicity island (cagPAI) and CagA, peptidoglycan, VacA and γ-glutamyltranspeptidase (gGT). Those virulence factors are essential for *H. pylori*'s unique way to activate host signaling pathways and to manipulate distinct immune cell populations, with the effect to simultaneously maintain a chronic inflammatory state while avoiding clearance by the immune system.

CagPAI-encoded proteins build up a type IV secretion system (T4SS), which enables the translocation of bacterial factors, namely CagA, into the host cell by interacting with integrin $\alpha_5\beta_1$ (24). Once translocated, CagA is phosphorylated at distinct EPIYA motifs, first by c-Src kinase and at later stages of infection by c-Abl kinase (25) and drives the inflammatory response by activation of nuclear factor 'kappa-light-chain-enhancer' of activated B-cells (NF-κB) and induction of IL-8 (26). The site of phosphorylation at EPIYA motifs is specific for distinct *H. pylori* isolates and gives insight into their geographical distribution and correlation with clinical disease (27). Thus, EPIYA-A, EPIYA-B and EPIYA-C motifs are typical for Western strains, whereas Asian strains display EPIYA-A, EPIYA-B and EPIYA-D motifs (28, 29). The presence of a cagPAI in general is a marker of virulence, as it correlates with a symptomatic course of infection and therefore implies a greater risk for gastritis and eventually gastric cancer (30). Another virulence factor delivered via the T4SS into gastric epithelial cells is peptidoglycan (31), which activates nucleotide-binding oligomerization domain 1 (NOD1) and is involved in stimulating a pro-inflammatory environment, induced by MIP-2, ß-defensin and IL-8 mediated activation of

NF-κB, p38 and Erk signaling (32, 33). Moreover, studies indicate that structural changes in peptidoglycan leading to host immune evasion contribute to bacterial persistence (34).

The pore-forming toxin VacA enters the host cells by forming anion-selective channels and has been described to induce apoptosis and vacuolation in epithelial cells as well as autophagy (35, 36). Furthermore, it is involved in immune evasion of *H. pylori*, by infiltrating the lamina propria of the stomach through disruption of epithelial tight junctions and inhibition of T-cell proliferation and function (37). The *vacA* gene is present in all *H. pylori* strains and has two allelic variants in each region: s1/s2 in the signal, i1/i2 in the intermediate and m1/m2 in the mid-region. This genetic polymorphism is of clinical importance, as e.g. the s1 and i1 alleles are associated with increased risk for symptomatic disease and gastric adenocarcinoma (38, 39).

gGT is a highly conserved virulence factor expressed by all *H. pylori* strains. Its biochemical function consists of converting glutamine into glutamate and ammonia as well as glutathione into glutamate and cysteine-glycine (40). It has been shown that gGT is important for initial colonization in mouse models of infection and that it is involved in $CD8^+$ T-cell infiltration in a glutamine-dependent manner (41). In general, gGT seems to be a dominant player in *H. pylori* induced immune responses, as it not only contributes to gastric inflammation via H_2O_2 -triggered activation of NF-κB and upregulation of IL-8, but is also involved in immune tolerization and bacterial persistence (42, 43).

1.1.3. *H. pylori*-induced immune response

Even though *H. pylori* infection triggers a complex plethora of immune cascades leading to severe gastric inflammation, the bacterium has evolved mechanisms to persist lifelong in infected individuals. The previously described virulence factors CagA, VacA and gGT, but also adhesins like HopQ play a role in this immune evasion, which will be described in the following section.

When entering the host, bacteria are recognized at their pathogen associated molecular patterns (PAMPs) by specific receptors, such as toll-like receptors (TLRs), on immune and epithelial cells, which then lead to clearance of the infection. *H. pylori* has evolved several mechanisms to overcome this initial clearance (Figure 1.2).: Lipopolysaccharide (LPS) of gram-negative bacteria is usually recognized by TLR2 and TLR4. *H. pylori* avoids recognition of its LPS by two main mechanisms. First, its outer membrane lipid A is structurally modified via distinct phosphorylation patterns which decrease recognition by TLRs and reduce the sensitivity towards antimicrobial peptides. *H. pylori* lacking this dephosphorylation enzyme fail to establish successful infection in mice, showing the

importance of these modifications (44). Another mechanism contributing to evasion of TLR-mediated signaling is the variation of expression of *H. pylori's* LPS O-antigen. By structural modifications, this antigen mimics human Lewis and related blood group antigens and is therefore not recognized as a foreign but rather a host antigen (45). Besides LPS, *H. pylori* has also evolved to structurally modify the conserved domain D1 of its flagellin to overcome recognition by TLR5 and subsequent activation of NF-κB (46, 47).

Next to immune evasion, *H. pylori* is able to selectively activate TLR-signaling to induce a rather anti-inflammatory environment, such as in TLR2- mediated activation of Myd88, leading to IL-10 release or via the activation of TLR9. The knockout of these two TLRs lead to a more severe gastric inflammation, evident in upregulation of pro-inflammatory cytokines interferon-γ (IFNγ) and tumor necrosis factor-α (TNFα) and simultaneous downregulation of regulatory T-cell transcription factor forkhead box P3 (FoxP3) in mouse models of *H. pylori* infection (48-50).

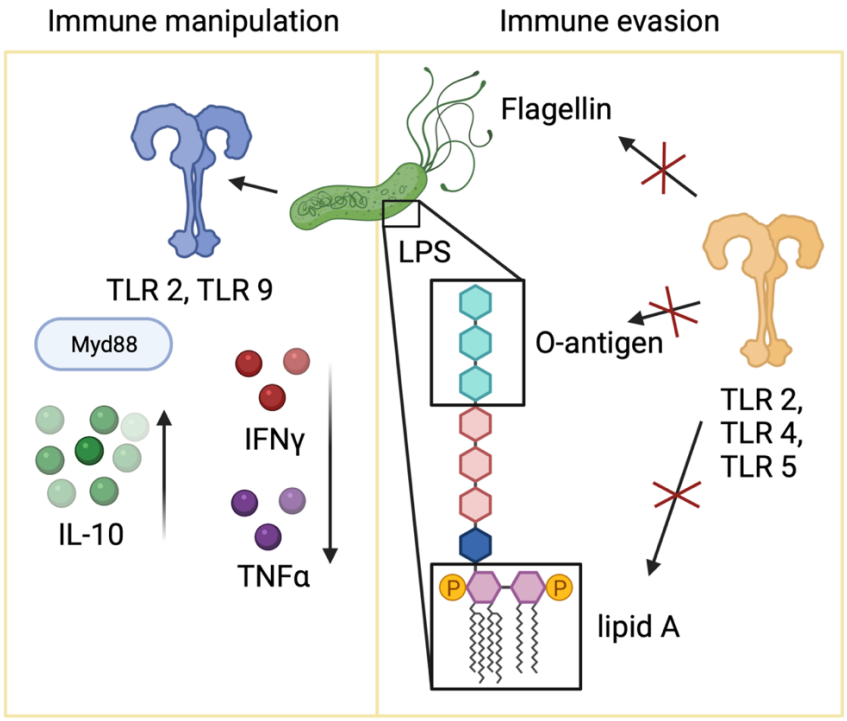

Figure 1.2: TLR-mediated signaling as paradigm of simultaneous manipulation and evasion of immune mechanisms by *H. pylori*. *H. pylori* distinctly activates TLR-signaling leading to a tolerogenic immune environment, characterized by induction of IL-10 release and inhibition of pro-inflammatory cytokines IFNγ and TNFα. Structural modifications in the O-antigen and lipid A of *H. pylori* LPS as well as modifications in flagellin lead to circumvention of TLR recognition and therefore contribute to immune evasion. Created with BioRender.com.

The function of dendritic cells (DCs) is to sense foreign antigens and orchestrate adaptive immune responses, which is why they are known as the bridge between innate and adaptive immunity. They play an important role in *H. pylori*-induced immune response, as they have been shown to reach the gastric mucus by traversing the epithelium, where they can take up virulence factors of *H. pylori* (51). However, the bacterium has developed mechanisms to manipulate DCs, in which virulence factors CagA, VacA and gGT are involved. CagA e.g. blocks the differentiation of $CD4^+$ T-cells into Th1 cells via the inhibition of interferon regulatory factor 3 (IRF-3), while it is also involved in inducing a tolerogenic environment via IL-10 dependent activation of signal transducer and activator of transcription 3 (STAT3), leading to expansion of regulatory T-cells (Tregs) (52, 53). VacA and gGT have been shown to be essential in reprogramming DCs towards a tolerogenic phenotype inducing Tregs (42). Mechanistically, it has been shown that the enzymatic activity of gGT leading to activation of glutamate receptors on human DCs results in the suppression of IL-6, which promotes Treg induction (54). Altogether, DCs play an eminent role in *H. pylori* pathogenesis, as they promote the induction of Tregs while simultaneously inhibiting T-cell differentiation. In addition, they are indispensable for persistent colonization of the stomach. Besides DCs, antigen presentation is also conducted by macrophages (55). However, *H. pylori* has been shown to modulate microRNAs, leading to alterations in expression of the immune receptor *CD300E* and thereby interferes with antigen-presentation abilities of macrophages (56). Next to classical antigen-presenting cells (APCs), antigen presentation occurs in gastric epithelial cells. They have been shown to upregulate major-histocompatibility complex molecule class II (MHCII) and costimulatory molecules CD80 and CD86 and via the release of IFNγ, contribute to the induction of a Th1 response (57, 58).

The uptake of bacterial antigens by APCs promotes the activation of specific immune responses. The initial priming of specific immune cells in response to *H. pylori* infection occurs at the Peyer's Patches and the mesenteric lymph nodes of the small intestine (59, 60), from where they then migrate to the stomach mucosa. Lymphocytes display the most important leucocyte subtype, being decisive in the outcome of infection. The cellular infiltrate of the gastric mucosa of infected patients consists of both $CD4^+$ and $CD8^+$ T-cells (61) and both subsets show antigen-specific responses towards *H. pylori* (62). The importance of T-cells to induce chronic inflammation and to keep the bacterial load in check was demonstrated in mouse models deficient in the T-cell receptor ß-chain (TCR-ß), thus almost completely lacking $CD4^+$ and $CD8^+$ T-cells. Infection with *H. pylori* in this model resulted in much less inflammation and higher colonization rates (63). The main inflammatory response against *H. pylori* is mediated by $CD4^+$ T-cells, in particular by Th1 and Th17 subsets. Th1- mediated effects are typically directed against intracellular

pathogens, however high production of Th1 cytokines IFNγ and TNFα was observed in response to the extracellular pathogen *H. pylori* in human gastric biopsies (64, 65). While infection of mice deficient in TNFα resulted in no changes in disease severity, the bacterial load was higher in those mice (66). In contrast to that, IFNγ knockout mice infected with *H. pylori* presented no gastric pathologies and similar or higher colonization compared to wild type mice (67-69). IL-17-producing Th17 cells have been extensively linked to *H. pylori*-induced immunopathology. It has been shown that this cytokine is highly upregulated in both human and murine stomach upon *H. pylori* infection (70, 71). Several studies report a pivotal role of Th17 cells in controlling bacterial load and inducing gastritis using mouse models devoid of IL-17 or antibodies neutralizing the cytokine (59, 70, 72). A study in humans showed, that IL-17 leads to induction of IL-8 and thereby promotes neutrophil infiltration and enhances inflammation (71).

These strong $CD4^+$ T-cell responses are kept in balance by Tregs, which allows the bacterium to persist life-long. A similar scenario occurs in the intestine, where gut microbiota and dietary antigens continuously stimulate the immune system, while Tregs control antigen-specific immune responses and thereby ensure a symbiotic balance between host and microbiota. Therefore, *H. pylori* is often referred to as commensal of the stomach microbiome. A study comparing responses of infected children with adults revealed, that the gastric immune infiltrate in children primarily consists of Tregs and high levels of regulatory cytokines IL-10 and transforming-growth-factor ß (*TGF-β*), resulting in reduced gastric pathology. In contrast, infected adults display rather proinflammatory responses and gastritis (73). However, *H. pylori*-induced gastritis is also associated with both recruitment of naturally occurring Tregs, defined as $CD4^+$, $CD25^{high}$, $FOXP3^+$, and with high bacterial colonization (74). The absolute requirement of Tregs for bacterial persistence has been shown in a study with IL-$10^{-/-}$ mice, which underwent a so-called natural course of infection: *H. pylori* infected mice displayed a transient, Th1-mediated gastritis with subsequent complete clearance of infection (75). Adoptive transfer of $CD4^+$, $CD25^{high}$ Tregs into $Rag^{-/-}$ mice, devoid of mature B- and T-cells, lead to less gastric pathology and higher bacterial colonization upon *H. pylori* infection. In contrast, wild type mice typically display a regulatory response, which contributes to the balanced inflammatory phenotype induced by *H. pylori* infection (68).

To summarize, it is widely accepted that the main triggered response upon *H. pylori* infection is predominantly $CD4^+$ T-cell mediated, consisting of a mixed Th1 and Th17 response. This is counterbalanced by a regulatory T-cell response, which blocks clearance and results in bacterial persistence. Furthermore, experimental evidence derived from

mouse models deficient in T-cell subsets or their surrogate cytokines indicate that precancerous lesions in the stomach are T-cell driven.

1.1.4. *H. pylori*-induced changes in microbiota

The crosstalk between host, microbiota and immune cells has been described extensively and plays a decisive role in the outcome of various diseases. It has been shown that upon *H. pylori* infection of C57BL/6 mice, the gastric as well as the distant microbiota of the intestine and caecum are affected (76) and that the expression of cytokines *Il1β*, *Il17a* and *Reg3γ* in the stomach vary depending on changes induced in gastric microbial communities (77). Furthermore, antibiotic treatment of mice before infection resulted in a lower inflammatory response, specifically in less CD4+ T-cell recruitment and lower expression of *Ifnγ* in the stomach compared to non-treated controls (78). The relevance of the microbiota in the development of *H. pylori*-induced gastric pathologies was highlighted in a study comparing *H. pylori* infected germ-free and specific pathogen free (SPF) insulin-gastrin (INS-GAS) mice, prone to develop spontaneous gastritis and gastrointestinal intraepithelial neoplasia (GIN). Germ-free mice showed a significantly delayed development of gastritis and GIN compared to SPF mice (79). In humans, the impact of *H. pylori* infection on the gastric microbiome is controversial. No significant differences between negative and positive individuals were reported in some studies (80), while others found distinct changes in relative abundances of *Proteobacteria* and *Acidobacteria* (81, 82). Interestingly, a study in Colombia revealed distinct gastric microbiota compositions between two villages sharing the same *H. pylori* prevalence but a 25-fold difference in the risk for gastric cancer development (83), indicating a decisive role of the microbiota in *H. pylori*-induced gastric cancer also in humans. In children, *H. pylori*-induced changes in microbiota have been linked to a tolerogenic environment in the stomach, consisting of higher levels of *FOXP3*, *TGF-β* and *IL-10* compared to adults and non-infected children (84, 85). In summary, there is much data that the microbiota and the impact of *H. pylori* on their composition are decisive players in bacterial pathogenesis and development of disease.

1.1.5. H. pylori-induced gastric and extragastric diseases

Residing within the gastric mucosa, *H. pylori* infection is known to result in superficial gastritis, which remains asymptomatic in most individuals (2, 86). Chronic infection, however, increases the risk for gastric and duodenal ulcers and is ultimately the main risk factor for development of gastric cancer and mucosa-associated lymphoid tissue (MALT) lymphoma (86, 87). This risk depends on a variety of factors. One determinant is the colonizing strain, as described in the previous section. Polymorphisms in the cagPAI – including distinct phosphorylation of EPIYA motifs, and VacA as well as expression of

BabA and OipA are associated with a higher risk of disease (30, 88-90). Other risk factors include host and environmental factors, such as male gender, specific *IL-1β* haplotypes, diet and presence of parasitic infections (91-93). A Japanese study including patients with ulcers, hyperplasia or non-ulcer dyspepsia showed that approximately 3% of infected individuals developed gastric cancer, compared to none of the *H. pylori* negative patients (94). Epidemiologically, the risk of gastric cancer attributed by *H. pylori* infection lays around 75% (87). This risk is significantly decreased upon eradication therapy in patients with and without premalignant lesions, pointing towards a role of *H. pylori* in the early carcinogenic process (95). Furthermore, a recently published long-term cohort study in Taiwan, a region with a high infection prevalence, reported a reduction of gastric cancer incidence by 53% upon mass eradication with no increase in likelihood of adverse effects (96).

Besides its prominent role in the involvement of gastric disease, *H. pylori* infection has been linked to and associated with a variety of extragastric diseases. Epidemiological and experimental evidence supports both positive and negative associations between the bacterium and various disease entities (Table 1.1) (97).

Table 1.1: *H. pylori*'s role in extragastric diseases

Disease	Association	Underlying mechanism	References
Coronary artery disease	Increased risk	– Systemic inflammatory processes – Molecular mimicry of bacterial heat shock protein 60	(98-100)
Stroke	Reduced mortality	Unknown	(101)
	Increased risk	Activation of platelets and coagulation	(102, 103)
Alzheimer's disease	Increased risk	Access to the brain via infected monocytes and increased TNFα production	(104, 105)
Multiple sclerosis	Protective role	Inhibition of Th1 and Th17 responses	(106)
	Increased risk	Molecular mimicry of bacterial and human anti-aquaporins	(101)
Parkinson's disease	Increased risk	Bioavailability of L-3,4 dihydroxyphenylalanine	(107-109)
Guillain-Barrè syndrome	Positive association	Molecular mimicry of bacterial LPS and peripheral nerve gangliosides	(110-112)
Rosacea	Positive association	Unknown	(113, 114)
Psoriasis	Controversial	Unknown	(115)

Iron deficiency anemia	Positive association	Upregulation of hepcidin levels, reduction of bioavailability of dietary iron	(116-118)
Vitamin B12 deficiency	Positive association	Impaired absorption due to gastritis	(119)
Idiopathic thrombocytopenic purpura	Positive association	– Genetic susceptibility (IL-1β polymorphism) – Modulation of Fcγ receptor balance – Molecular mimicry of bacterial virulence factors and platelet surface glycoproteins	(120, 121)
Diabetes mellitus and Insulin resistance	Positive association	Induction of hepatic insulin resistance via Jun/miR-203/suppressor of cytokine signaling 3 pathway	(122-124)
Allergic diseases	Protective	Induction of Tregs via DC derived IL-18	(125, 126)
Non-alcohol fatty liver disease	Positive association	– Access to the liver via increased mucosal permeability through portal vein – Pro-inflammatory cytokines	(127-129)
Hepatic fibrosis	Positive association	TGF-β1- mediated pro-inflammatory signaling	(130)
Primary biliary cirrhosis	Positive association	Molecular mimicry of bacterial urease and pyruvate dehydrogenase complex	(131, 132)
Hepatocellular carcinoma	Positive association	Proinflammatory processes	(133, 134)
Gastro-esophageal reflux disease (GERD)	Controversial	– Pangastritis resulting in lower acid-secretion and amelioration of GERD-associated symptoms – VacA mediated impairment of parietal cells leading to lower acid secretion (135)	(136-139)
Barett's esophagus	Protective		(140, 141)
Esophageal adenocarcinoma	Protective		(141)
Inflammatory Bowel Disease	Strong negative association	– Induction of IL-10 in mesenteric lymph nodes leading to suppression of Th17 response – TLR2/NLRP3/caspase-1/IL-18 signaling inducing immune tolerance	(49, 142-145)
Colorectal cancer	Positive association	unknown	(146, 147)

These diverging associations of *H. pylori* with extragastric diseases, on the one hand acting pathogenic and on the other immunomodulatory, and the fact that most individuals infected with *H. pylori* remain asymptomatic lifelong, contradict a solely pathogenic nature

of the bacterium and rather support the idea that the bacterium, shaped by years of coevolution within its human host, in most patients could also be carefully considered as a commensal. This underlines the necessity to stratify *H. pylori* positive patients with an increased risk to develop disease. In case of colorectal cancer (CRC), epidemiological studies have shown a nearly two-fold increased risk for *H. pylori* positive patients (146-151). Considering that 50% of the world's population are *H. pylori* positive and assuming that the relative risk of *H. pylori* positive patients to develop CRC accounts for 1.8, the population attributable risk (PAR) of CRC cases that could be attributed to *H. pylori* infection is 29%. This demands for investigation of the underlying mechanisms in order to appropriately screen those at risk with the possibility to subsequently intervene.

1.2. Colorectal Cancer

CRC is the second most frequently diagnosed cancer in women and the third most diagnosed in men. It is the third most common cause of cancer related deaths among both sexes with 9.5% for women and 9.3% for men (152).

1.2.1. Colorectal Carcinogenesis

Three pathways have been described to give rise to sporadic CRC: the adenoma-carcinoma sequence, the serrated pathway and the inflammatory pathway (153). The adenoma-carcinoma sequence accounts for 85-90% of all sporadic CRCs and starts with an aberrant crypt focus, developing to neoplastic precursor lesions, called adenomas, which eventually progress to colorectal cancer. This multistep process is characterized by mutations that lead to activation of oncogenes and inactivation of tumor-suppressor genes. Mutations in the tumor suppressor *APC*, found in 80-90% of CRC cases, lead to deregulation of Wnt/ß-Catenin signaling resulting in hyperproliferation and adenoma formation, whose growth is fueled by mutations in the oncogene *KRAS*, seen in 45% of all CRCs, and inactivating mutations of the tumor suppressor *TP53*, found in 54% of all cases (154-156). The mutation leading to *APC* inactivation has been attributed to be the initiating and maintaining event of carcinogenesis, as restoration of its function in mouse models has shown to reestablish normal cell homeostasis and differentiation (157). About 10-15% of CRC cases arise from the serrated pathway, which progress from normal cells over hyperplastic polyps and sessile serrated adenomas to cancer. This pathway is typically initiated by mutations in the oncogene *BRAF* (158, 159) and the tumor suppressor *RNF43* is found to be frequently co-mutated (160, 161). Finally, the remaining 1-2% of CRC cases have an inflammatory etiology, where chronic inflammation drives the progression from low- to high-grade dysplasia to the development of cancer (162). This is why patients with inflammatory bowel disease (IBD), in particular with ulcerative colitis, harbor a 2.4-fold increased risk to develop CRC (163). Within this pathway, mutations occur in reversed

order compared to the adenoma-carcinoma sequence: *TP53* mutations, found in 63% of patients, occur early and mutations in *APC*, observed in only 13% of cases, are found late in the carcinogenic process (164). Beyond those pathways, genetic and epigenetic aberrations play an important role in colorectal carcinogenesis, including CpG island methylator phenotype (CIMP), microsatellite instability (MSI) and somatic copy number alterations (SCNA) (165). Those genetic alterations accumulate throughout the course of colorectal carcinogenesis, overlap with each other and their occurrence across CRC cases are estimated to be 85% for SCNA, 20% for CIMP and 15% for MSI (166).

In 2015, a new subtyping of CRC was introduced based on gene expression, the so called four consensus molecular subtypes (CMS) (167):

1. CMS1 (MSI immune): characterized by MSI, CIMP high, hypermutations, mutations in *BRAF*, immune infiltration and activation and worse survival after relapse.
2. CMS2 (canonical): characterized by high SCNA and WNT as well as MYC activation.
3. CMS3 (metabolic): characterized by mixed MSI status, SCNA low, CIMP low, mutations in *KRAS* and metabolic deregulation
4. CMS4 (mesenchymal): SCNA high, stromal infiltration, *TGF-β* activation, angiogenesis and worse relapse-free and overall survival.

Those efforts in molecular subtyping are sought to facilitate drug development, extend therapeutic options, maximize personalized therapy and improve clinical outcomes of the very heterogenous cancer entity of colorectal cancer.

1.2.2. Inflammation and Colorectal Cancer

Chronic intestinal inflammation is a major risk factor for CRC and immune infiltration is known to not only dictate initiation and progression of disease, but also therapy response. This is supported by the fact that patients with long-term intake of anti-inflammatory aspirin exhibit a significantly lower risk of CRC development (168, 169). Furthermore, as already described in section 1.2.1, more than 20% of IBD patients develop colitis-associated cancer (CAC), resulting in a mortality of 50% (170). Inflammatory pathways, such as STAT3 and NF-kB, have been shown to be constitutively active in many CRC cases (171, 172), suggesting a strong contribution of immune cells and their cytokines to CRC development. Thereby, the type of infiltrating immune cells determines the effect on the prognosis. While the presence of Th1 cells and associated cytokine IFNγ in CRC tumors has been shown to beneficial, Th17 infiltrates have been shown to be less favorable (173). This is supported by experiments in animal models of colorectal cancer, which have shown that IL-17A induces a pro-tumorigenic environment, which is possibly driven by microbial triggers (174, 175).

1.2.3. Microbiota, intestinal homeostasis and Colorectal Cancer

Microbial compositions and functions have been proposed to impact development, progression and treatment response of CRC (176, 177). Both distinct bacterial species and microbiota- associated mechanisms have been linked to colorectal carcinogenesis and will be introduced in the following section.

Several bacterial species are known to contribute to and promote CRC. *Fusobacterium nucleatum* was found to be 79-fold overabundant in CRC tumor tissue compared to healthy tissue (178) and has been proposed to drive carcinogenesis by induction of proinflammatory NF-kB and induction of IL-6 as well as epithelial-mesenchymal transition, a precursor of metastasis (179, 180). Similarly, pathogenic strains of *Escherichia coli* have been described to promote CRC via the induction of DNA damage in consequence to translocation of its genotoxin colibactin (181, 182). Enterotoxigenic *Bacteroides fragilis* and its toxin Bacteroides Fragilis Toxin has been shown to drive both colitis and CRC via Th17 mediated inflammation and tissue injury leading to increased permeability (183-186). Next to those direct effects of distinct species on tumorigenesis, bacterial metabolites, such as short chain fatty acids (SCFA) and bile acids play a role in the development and progression of CRC. Those are highly dependent on dietary patterns and play an important role in an individual's risk for CRC, as e.g. a high-fiber diet has been shown to decrease the progression from adenoma to carcinoma (187), while high-fat diet was found in populations with increased CRC risk (188). A study in mice fed a high-fat Western diet revealed increased tumor formation compared to mice on a control diet, which resulted from inactivation of nuclear bile acid receptor farnesoid X, leading to increased proliferation and deregulation of bile acid metabolism (189). Furthermore, the microbial modulation of both innate and adaptive immune cells within the tumor and in the tumor microenvironment is a major mechanism by which the microbiota impact cancer. Also here, sensing of microbe-associated molecular patterns (MAMPs) via TLR and NOD-like receptors form the basis of microbe-immune interactions and can result in both pro- and anti-inflammatory environments (177).

Intestinal homeostasis requires an elaborate balance between microbiota, the intestinal immune system and the epithelial compartment. An intact intestinal barrier is crucial for intestinal homeostasis and defects have shown to greatly contribute to intestinal inflammation and CRC (190, 191). From base to top, this barrier consists of the lamina propria, containing both innate and adaptive immune cells, epithelial cells, which are connected via tight junctions that ensure permeability for selective nutrient uptake while simultaneously providing a barrier for invading pathogens and the mucus layer, often referred to as the first layer of defense protecting the intestinal epithelium (190). The

intestinal mucus layer is composed of highly glycosylated mucus proteins and is replenished by goblet cells (191). MUC-2 constitutes the major intestinal mucin and the fact that mouse models bearing a knockout in *Muc2* (Muc2$^{-/-}$ mice) are prone to develop colitis and spontaneous CRC (192, 193) underlines the importance of an intact intestinal mucus layer for a balanced gut homeostasis.

1.2.4. Mouse models of Colorectal Cancer

Despite remarkable advances in screening and treatment of CRC, *in vivo* models are still indispensable to study the full aspects of colorectal tumorigenesis, including the tumor microenvironment and systemic effects of immune responses and microbiota. The ideal mouse model of CRC would allow to study the progression from premalignant precursors to invasive carcinomas with the ultimate possibility to metastasize, while simultaneously mirroring the genetic heterogeneity and involving the tumor microenvironment of colon tumors. However, to date no such mouse model exists. Categorically, 3 types of CRC mouse models are currently used: carcinogen-induced, genetically engineered and transplant models. Selected models are summarized in Table 1.2 (194, 195).

Table 1.2: Selected mouse models of colorectal cancer

Mouse model	Tumor location	Invasion/ Metastasis	Characteristics	References
Carcinogen induced				
AOM	Colon	No	Sporadic tumorigenesis, widely used for dietary studies	(196)
AOM/DSS	Colon	No	Inflammation driven tumorigenesis	(197)
Genetically engineered				
Apc$^{+/min}$	Small Intestine	No	• Multiple intestinal adenomas already at relatively young age (3-4 months) • Only few adenomas in the colon • high mortality with increasing age	(198)
Apc$^{+/1638N}$	Small Intestine	No	• Adenomas proceeding to carcinomas with advanced age • More tumors develop in the colon compared to Apc+/min mice	(199)
KRAS^{V12G} /*Apc*$^{+/1638N}$	Small Intestine and Colon	Yes	• Increase in tumor numbers, size and progression to invasive carcinomas • Tumors develop also in the colon	(200)
Apc$^{lox/lox}$ /*Trp53*$^{lox/lox}$ /Tet-O-LSL-*Kras*^{G12D} /VillinCre^{ERT2}	Small Intestine and Colon	Yes	• Recapitulates tumor progression from adenoma to carcinoma • Invasive and metastatic disease	(201)

Transplantation				
Xenograft models	Injected s.c. into flanks of mice	Yes	• Cell-derived and patient-derived models available • Incomplete tumor microenvironment (only stromal cells, not immune cells) • Used for drug testing	(202)
Organoids	Colon	Yes	• Mouse- and patient-derived organoids • Genetically engineered mouse models can be transplanted • Whole spectrum of tumor progression and metastasis can be studied • Complete tumor microenvironment	(203)

1.2.5. Risk factors

All subtypes of CRC described in section 1.2.1 share the notion of a window of opportunity for early intervention. Arising from premalignant precursor lesions, which are detectable by means of screening, and the sometimes more than 10-year time-gap between those precursors and the progression to cancer, allow for the possibility to reduce cancer incidence and mortality by means of secondary prevention (204). In line with that, next to the individual risk determined by genetic and epigenetic factors, modifiable risk and protective factors play a decisive role in CRC and in patient risk-stratification for primary prevention (Figure 1.3).

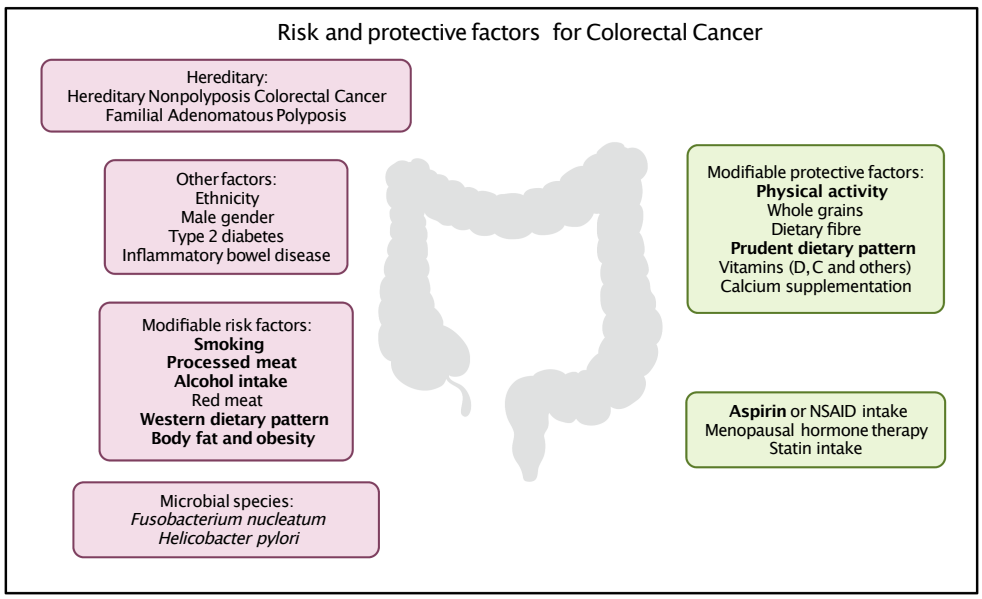

Figure 1.3: Summary of risk and protective factors of CRC. Risk factors for CRC are shown in red boxes and protective factors in green boxes. Convincing risk factors with a high level of evidence are depicted in bold (153, 205). Created with BioRender.com.

Compelling epidemiological evidence suggests *H. pylori* as a strong risk factor for CRC, however experimental and mechanistic evidence conferring this risk are missing and would allow for improved patient risk stratification and intervention.

2. Aims

Emerging epidemiological evidence supports a strong association of *H. pylori* infection with an increased risk for CRC development. The causal nature of this association, and the underlying mechanisms however are yet to be elucidated. The strong immune response elicited upon infection, consisting of an intricate balance between a mixed Th1/Th17 response and a compensatory regulatory component, might be one of the mechanisms involved. Second, signaling pathways, activated upon chronic inflammatory stimuli and contributing to epithelial transformation, might play a crucial role in the progression from non-malignant precursors to cancer. Finally, the microbiota, which have been shown to not only be affected by *H. pylori* locally in the stomach, but also in the distant intestine, and are known to contribute to the development and progression of CRC, could contribute to the cancer promoting effects of *H. pylori* in the distant colon.

The aims of this thesis are to identify those underlying mechanisms. Therefore, a comprehensive analysis of the effects of *H. pylori* infection on intestinal and colonic tissue of C57BL/6 mice will be conducted, with particular focus on T-cell response, immune signaling, epithelial response, including proliferation and activation of pro-inflammatory and potentially carcinogenic signaling pathways. Furthermore, *H. pylori* induced microbial signatures, including both luminal and mucosa-adherent microbiota of the gastrointestinal tract, will be evaluated. To assess direct effects on colorectal carcinogenesis, two tumor mouse models bearing mutations in the *Apc* gene, prone to develop intestinal and colonic adenomas and carcinomas, will be infected with *H. pylori*: $Apc^{+/1638N}$ and $Apc^{+/min}$ mice. Additionally, transcriptomic signatures of immune and epithelial cells upon *H. pylori* infection will be assessed on a single cell level. As a proof of concept, eradication experiments of *H. pylori* infected C57BL/6 and $Apc^{+/1638N}$ mice will be performed. To evaluate the role and the necessity of the microbiota, germ-free $Apc^{+/1638N}$ mice will be infected and stool transfer experiments will be performed.

Finally, colon biopsies of a human cohort, comprising *H. pylori* positive, eradicated and negative patients, will be evaluated in order to confirm that the observed effects in mouse models are transferable to humans.

3. Material and Methods

3.1. Material

Table 3.1: Instruments used within this study

Instrument	Company
Agarose Gel chamber	Bio-Rad Laboratories
Biofuge Fresco Refrigerated Microliter Centrifuge	Thermo Fisher Scientific
Biophotometer, 6131 Spectrophotometer	Eppendorf
Bioanalyzer 2100	Agilent
C1000 Touch Thermal Cycler	Bio-Rad Laboratories
CFX384 Touch Real-Time PCR Detection System	Bio-Rad Laboratories
Chromium Controller	10x genomics
Cooling Plate COP 30	Medite
Cryotome Leica CM3050S Cryostat	Leica Biosystems
Fine Balance (max: 120g, d~0.0001g)	ScalTec
Flow cytometer CytoFlex S	Beckman Coulter
Forma Series II Water Jacket CO2 incubator, bacteria incubator	Thermo Fisher Scientific
Heating plate/magnetic stirrer	ARE VELP Scientifica
Hera Safe Bio-Flow cell culture	Hera Instruments
Heraeus Megafuge 40R	Thermo Fisher Scientific
Ice machine CoolNat	Ziegra Eismaschinen
Maxwell RSC 48	Promega
Microtome Leica RM2245	Leica Biosystems
Mini shaking oven, hybridisation oven; OV3	Biometra
MoFlo Astrios Cell Sorter	Beckman Coulter
NanoDrop 1000	Thermo Fisher Scientific
Precellys 24 Tissue Homogenizer	Bertin Technologies
Qubit 4 Fluorometer	Thermo Fisher Scientific
Tissue Flotation Bath TFB 35	Medite
ZellScanner One	Zellkraftwerk

Table 3.2: Consumables used within this study

Consumables	Company
6-well plate	Corning
12-well plate	Corning
24-well plate	Corning
96-well plate U-Bottom	Corning
96-well plate V-Bottom	Kuhnle
Adhesion slides, Menzel Gläser, SuperFrost Plus	Thermo Fisher Scientific
CapLock microtubes 0.5ml, 1.0ml, 2.0ml	Trefflab
Centrifuge Tube 15/ 50ml	Corning
Cell Strainer 70/100µm	Corning
CellSafe Chips	Zellkraftwerk
Clarithromycin	Eberth
Combitips Advanced	Eppendorf AG

Feather Microtome Blades A35	pfm medical
Filtertips 10/20µl, 20µl, 200µl, 1000µl	
FrameStar 384 Well Skirted PCR Plate	4titude
Inoculation loop, 10µl	
Microscope Cover Glasses	VWR
PCR tube stripes with lid (8 tubes)	Kisker Biotech
Precellys Lysing Kit CKMix	VWR
qPCR Seal	4titude
Sapphire PCR tubes	Greiner Bio-One
Sealing film, self-adhesive, OV96	A. Hartenstein
Serological Pipettes 10ml, 25ml	Greiner Bio-One
Spreaders, L-shaped, disposable	VWR
Superfrost Plus Adhesion Microscope Slides	Gerhard Menzel
ZellSafe tissue chips	Zellkraftwerk

Table 3.3: Chemicals used within this study

Product	**Company**
30 % (w/w) H_2O_2	Sigma-Aldrich
100 % molecular grade ethanol (EtOH)	AppliChem
Agarose	Sigma-Aldrich
Albumin (BSA) Fraction V	AppliChem
AMPure XP beads	Beckman-Coulter
BD GolgiPlug Protein Transport Inhibitor	BD Life Sciences
BenchTop 100 bp DNA ladder	Promega
Collagenase Type II and IV from Clostridium histolyticum	Sigma-Aldrich
Dimethyl sulfoxide (DMSO)	AppliChem
DNAse	AppliChem
Eosin 1 %, aqueous	MORPHISTO
Fixation Buffer	Zellkraftwerk
Formaldehyd Lösung 3.5 – 3.7 %	Otto Fischar
Goat anti-rabbit IgG (HRP)	Promega
Hematoxylin (Hemalum solution acc. to Mayer)	Carl Roth
Histosette I biopsy processing/embedding cassettes	Simport
Hydrochloric acid (HCl)	Carl Roth
Hydroxy-propyl-methyl-cellulose	Sigma-Aldrich
Tissue-Tek O.C.T. Compound	A. Hartenstein
Tissue-Tek Cryomold	A. Hartenstein
Metronidazole	Carl Roth
Normal goat serum	Abcam
Nuclease-free water	Promega
Omeprazole	Carl Roth
PBS, pH 7.4	Thermo Fisher Scientific
Percoll	VWR
Periodic acid 1 %	Carl Roth
Phenol-chloroform-isoamyl alcohol (PCI), 25:24:1	Sigma-Aldrich
Random primers	Promega

ROTI Mount mounting medium	Carl Roth
RPMI 1640 Medium	Thermo Fisher Scientific
Schiffs reagent	Carl Roth
SignalStain Antibody Diluent	Cell Signaling
Sodium hydroxide (NaOH)	Sigma-Aldrich
Storage Buffer	Zellkraftwerk
Washing Buffer	Zellkraftwerk
Xylol Roticlear	Carl Roth
Fetal Calve Serum	Sigma-Aldrich
P/S	
NEAA	
Glutamine	

Table 3.4: Buffers and solutions used within this study

Buffer	Ingredients	Company
0,5 M EDTA buffer	18.61 g Ethylenediaminetetraacetic acid disodium salt dihydrate (Na_2EDTA) (M= 372,24 g/mol), dissolved in 100 mL dH_2O, pH8	Carl Roth
1 mM EDTA buffer	0.744 g Ethylenediamine tetraacetic acid disodium salt dihydrate (Na_2EDTA) (M= 372,24 g/mol), dissolved in 2 L dH_2O, pH 8	Carl Roth
1M HEPES	23.84 g HEPES (M= 238,31 g/mol), dissolved in 100 mL dH_2O, pH 7.5	Carl Roth
20 % SDS	40 g Dodecylsulphate sodium salt (SDS), ultra pure (M= 288,38 g/mol), dissolved in 200 mL dH_2O	Carl Roth
3 M Sodium acetate	24.61 g Sodium acetate, anhydrous (M= 82.03 g/mol), dissolved in 100 mL dH_2O, pH 5.2	Carl Roth
1 M Sodium citrate buffer	5.88 g tri-Sodium citrate dihydrate, dissolved in 2 L dH_2O, pH 6	Carl Roth
10x TBS	50 mM Tris-ultra-pure (60.5 g) 150 mM NaCl (87.6 g), dissolved in 1 L dH_2O, pH 7.5	AppliChem Carl Roth
1x TBS + 0.1 % Tween (TBS-T)	100 mL 10x TBS, 1 mL Tween, 900 mL dH_2O	
1x Tris-acetate-EDTA (TAE) buffer	250 mL 50x TAE buffer dissolved in 1 L dH_2O	
DNA extraction buffer	2 mL 0.2 M NaCl 2 mL 0.2 M Tris, pH 8.0 2 mL 20 mM EDTA, pH 8.0 5 mL NFW	
Flow cytometry buffer	500 mL PBS + 0.5 % BSA	
Percoll 100 %	Percoll + 10 % 10x PBS	

Percoll 40 %	40 % Percoll 100 % +60 % RPMI	
Percoll 80 %	80 % Percoll 100 % + 20 % RPMI	

Table 3.5: Assays and kits used within this study

Name	Company
3' Feature Barcode Kit, 16 rxns	10x genomics
BD Cytofix/CytopermFixation/Permeablization Kit	BD Life Sciences
BCA Protein Assay Kit	Thermo Fisher Scientific
Chromium Next GEM Chip G Single Cell Kit, 16 rxns	10x genomics
Chromium Next GEM Single Cell 3' Kit v3.1, 4 rxns	10x genomics
Dual Index Kit TT Set A 96 rxns	10x genomics
Dual Index Kit NT Set A, 96 rxn	10x genomics
eBioscience Foxp3 / Transcription Factor Staining Buffer Set	Thermo Fisher Scientific
GoTaq qPCR Master Mix	Promega
High sensitive DNA kit	Agilent
Illumina MiSeq Reagent Kit v3	Ilumina
KAPA Library Quantification Kit Illumina Platforms	KAPA Biosystems
Maxwell RSC – simplyRNA Tissue Kit	Promega
Moloney Murine Leukemia Virus Reverse Transcriptase Kit	Promega
Nextera XT Index Kit	Ilumina
recomwell Helicobacter IgG kit	Mikrogen
recomline Helicobacter IgG kit	Mikrogen
SignalStain DAB Substrate Kit	Cell Signaling
Qubit dsDNA HS assay kit	Life technologies
Zombie aqua Fixation and Viability Kit	Biolegend

Table 3.6: Softwares and Packages used within this study

Software	Company/Developer
Affinity Designer	Serif
Affinity Photo	Serif
Aperio eSlide Manager	Leica Biosystems
Aperio ImageScope	Leica Biosystems
CFX Manager Software	Bio-Rad Laboratories
FlowJo v10.7	FlowJo LCC
GraphPad Prism 8	GraphPad Software
Python	Python Software Foundation
R	R Core Team
RStudio	RStudio
ZellExplorer Software	Zellkraftwerk
CellRanger v1.6	10x genomics
SCANPY v5.0.0	(206)
velocyto	(207)
scvelo	(208)
qiime2 v2021.4	QIIME2 development team
FastQC v0.11.9	Babraham Bioinformatics

3.2. Methods

3.2.1. Animal experiments

3.2.1.1. Mouse models

Female C57BL/6 mice were purchased from Envigo RMS GmbH at an age of 6 weeks and acclimatized to our animal facility for 1-2 weeks prior infection. Tumor mouse models *Apc*$^{+/min}$, initially obtained from Jackson Laboratories, and *Apc*$^{+/1638N}$ mice, provided by Prof. Klaus-Peter Janssen (Klinikum rechts der Isar, München) (200), were bred under specific pathogen-free conditions at our animal facility at the Institute for Medical Microbiology, Immunology and Hygiene, TUM. Both female and male mice were co-housed with wild type littermates, which served as controls in experiments.

Apc$^{+/1638N}$ mice and wild type littermates were re-derived germ-free from conventional mice by Prof. Bleich and Dr. Basic (Hannover medical school, Hannover).

Mice were fed with a standard diet and water ad libitum and maintained under a 12-hour light-dark cycle. DNA extracted from mouse tails was used for genotyping. All animal experiments were conducted in compliance with European guidelines for the care and use of laboratory animals and were approved by the Bavarian Government (Regierung von Oberbayern, Az.55.2-1-54-2532-161-2017).

3.2.1.2. *H. pylori* infection

H. pylori pre-mouse Sidney Strain 1 (PMSS1) was cultured on Wilkins-Chalgren (WC) Dent (containing vancomycin, trimethoprim, cefsoludin and amphotericin) agar plates in a microaerophilic atmosphere (5% O2, 10% CO2). Mice were infected aged 6–8-weeks by oral gavage, twice within 72 hours, with 2 × 10^8 *H. pylori* PMSS1 in 200 µl brain-heart-infusion (BHI) medium containing 20% fetal calve serum (FCS) for distinct timepoints (Figure 3.1). Proof of infection was assessed by plating homogenized stomach tissue on WC Dent plates supplemented with 200 g/ml bacitracin, 10 g/ml nalidixic acid and 3 g/ml polymycin B, and counting colony-forming units (CFU) per mg stomach.

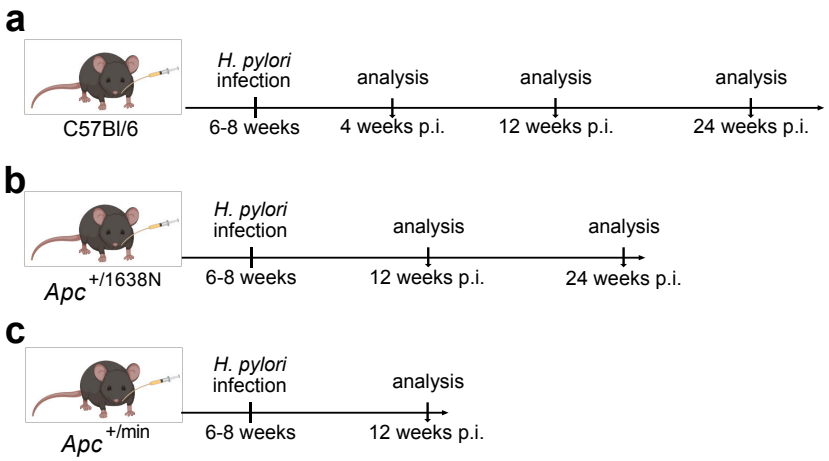

Figure 3.1: *H. pylori* infection setup.

3.2.1.3. *H. pylori* eradication

Mice infected for 4 weeks with *H. pylori* PMSS1 were eradicated according to the "Italian triple therapy", consisting of the antibiotics clarithromycin (Eberth) (7.15 mg/kg/day) and metronidazole (Carl Roth) (14.2 mg/kg/day) and the proton-pump inhibitor omeprazole (Carl Roth) (400 µmol/kg/day). Omeprazole was dissolved in 200µl 2.5% Hydroxy-propyl-methyl-cellulose (Sigma-Aldrich) with pH adjusted to 9 and antibiotics were dissolved in 200µl PBS. Mice were orally gavaged twice daily for 7 consecutive days, whereas the antibiotics were administered 45 minutes after omeprazole (209). Mice were analyzed 4, 12 or 24 weeks after eradication therapy (Figure 3.2).

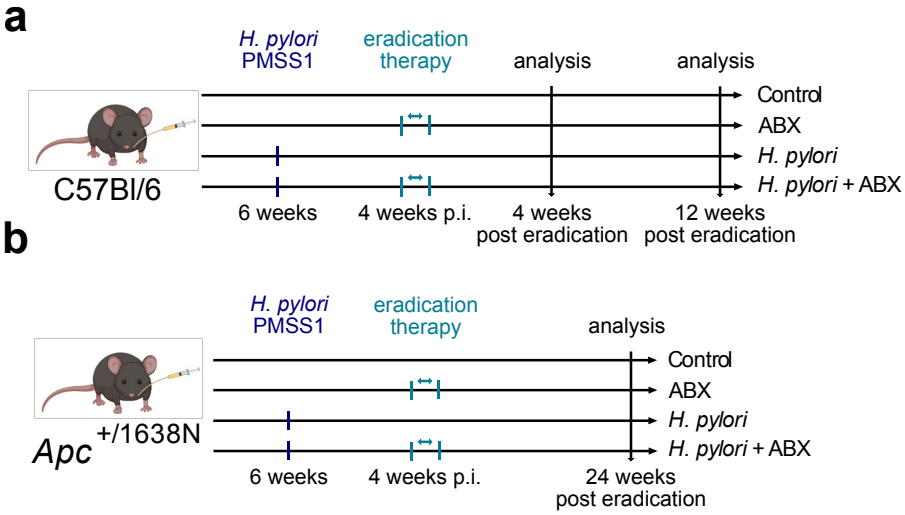

Figure 3.2: Eradication of *H. pylori* infection.

3.2.1.4. Stool transfer

For stool transfer experiments, stool was obtained from SPF mice and transferred into germ-free $Apc^{+/1638N}$ mice. Therefore, $Apc^{+/1638N}$ mice and $Apc^{+/+}$ littermates were infected at an age of 6-8 weeks and after 24 weeks of infection, stool pellets were collected from "donor" mice, dissolved in 0.1ml PBS/g stool, and administered via oral gavage to germ-free $Apc^{+/1638N}$ "recipient" mice.

3.2.2. Histological evaluation

3.2.2.1. Preparation of tissue

Stomach tissue was opened along the great curvature after removing the front stomach and flushed with phosphate-buffered saline (PBS). Intestine and colon were longitudinally opened, flushed with PBS and a cross-section as well as a swiss roll was collected. Dissected tissue was fixed in approximately 4% formaldehyde for at least 48 hours and subsequently dehydrated and embedded in paraffin. 4µm thick sections were cut on a microtome (Leica).

3.2.2.2. HE staining

Hematoxylin Eosin staining was performed to assess histopathological changes. To melt the paraffin, slides were incubated at 60°C for 30 min. After deparaffinization and rehydration (Table 3.7, steps 1-6), slides were treated with Mayer's hematoxylin (Carl Roth) and Eosin (Morphisto). Stained and dehydrated slides (Table 3.7, steps 11-15) were mounted with mounting medium (Carl Roth) and covered with cover glass.

Table 3.7: HE staining

Step	Reagent	Incubation	Step	Reagent	Incubation
1	Xylene	3 x 10 min.	**9**	Eosin	6 min.
2	100 % EtOH	2 x 10 min.	**10**	dH20	rinse
3	90 % EtOH	5 min.	**11**	50 % EtOH	5 min.
4	70 % EtOH	5 min.	**12**	70 % EtOH	5 min.
5	50 % EtOH	5 min.	**13**	90 % EtOH	5 min.
6	dH20	rinse	**14**	100 % EtOH	2 x 5 min.
7	Hematoxylin	6 min.	**15**	Xylene	3 x 10 min.
8	Tap water	rinse			

3.2.2.3. Immunohistochemical staining

For immunohistochemical staining, FFPE slides were incubated at 60°C for 30 min., deparaffinized and rehydrated as described in Table 3.7 (steps 1-6). Antigen retrieval was achieved with 10 mM sodium citrate (pH 6) for surface antibodies or 1 mM EDTA (pH 8) for antibodies detecting intranuclear signals. Slides were blocked with 5% goat serum and primary antibodies were diluted in Antibody Diluent (CellSignaling) and applied overnight at 4°C (Table 3.8). Horseradish peroxidase (HRP) coupled secondary antibodies (Promega) and diaminobenzidine (DAB) (CellSignaling) were used to detect signal. Slides were counterstained with hematoxylin, dehydrated (Table 3.7, steps 10-15) and mounted.

Table 3.8: Antibodies used for immunohistochemical evaluation

Target	Clone	Origin/Target	Antigen retrieval	Dilution	Company
CD3	SP7	Rabbit mAB	sodium citrate	1:150	Thermo Fisher Scientific
Ki67	D3B5	Rabbit mAB	sodium citrate	1:400	Cell Signaling
pSTAT3	D3A7	Rabbit mAB	EDTA	1:200	Cell Signaling

3.2.2.4. PAS staining

Periodic acid Schiff (PAS) staining was performed to detect proteoglycans (mucins) and to assess the quantity of mucus producing goblet cells, using Schiff's reagent (Carl Roth)

and 1% perjodic acid (Carl Roth). Slides were deparaffinized and rehydrated as described in Table 3.7 (steps 1-6). PAS staining was performed as described in Table 3.9. Stained slides were dehydrated (Table 3.7, steps 10-15) and mounted.

Table 3.9: PAS staining

Step	Reagent	Incubation
1	1% periodic acid	5 min.
2	dH20	rinse
3	Schiff's reagent	15 min.
4	luke warm tap water	5 min.
5	Hematoxylin	1 min.
6	tap water	5 min.

3.2.2.5. Imaging and Quantification

Slides were scanned at a magnification of 20 by the Institute of General and Surgical Pathology, TUM. Stomach, intestinal and colonic sections were blindly quantified by two independent researchers by measuring the area of a functional unit (stomach gland, intestinal crypt/villus unit or colonic crypt) and counting positive cells per mm^2, using Aperio ImageScope (Leica BioSystems).

3.2.3. Quantitative PCR

3.2.3.1. RNA Isolation

Stomach, intestine and colon tissue was snap frozen in liquid nitrogen upon sacrifice. For RNA Isolation, tissue was thawed on ice and homogenized with Precellys 24 homogeniser (Avantor) and RNA subsequently isolated with a Maxwell 48 RSC simply RNA Tissue Kit, including DNase treatment, on a Maxwell RSC Instrument (Promega) according to manufacturer's instructions. RNA concentration was measured on a NanoDrop (Thermo Fisher Scientific).

3.2.3.2. cDNA synthesis

RNA concentration was adjusted to 1µg/µl with nuclease-free water (NFW) (Promega) and incubated with random primers at 70° for 5 minutes. cDNA was synthesized with Moloney Murine Leukemia Virus Reverse Transcriptase RNase H- Point Mutant (Promega) under the following conditions (Table 3.10 and Table 3.11):

Table 3.10: cDNA master mix

Reagent	Volume	Volume Negative Control
Nuclease free water	3,75 µl	4,75 µl
dNTPs	1,25 µl	1,25 µl
M-MLV Reverse Transcriptase	1 µl	-
M-MLV 5x RT buffer	5 µl	5 µl

Table 3.11: cDNA cycling conditions

Temperature	Time
22°	10:00
50°	50:00
70°	15:00
12°	∞

3.2.3.3. qPCR

Gene expression was assessed with GoTaq qPCR Mastermix (Promega) on a CFX384 system (Bio-Rad), with cDNA diluted 1:5 and primers 1:10 in NFW. The following conditions were applied (Table 3.12 and Table 3.13):

Table 3.12: qPCR master mix

Reagent	Volume
Diluted cDNA	4 µl
GoTaq qPCR Master Mix	5 µl
Diluted forward primer	0,5 µl
Diluted forward primer	0,5 µl

Table 3.13: qPCR cycling conditions

Step	Temperature	Time
1	95°	5:00
2	95°	0:10
3	60°	0:30
4	Go to step 2	39x
5	65°	0:05
6	95°	0.5°/cycle
7	12°	∞

According to the ΔΔCT method, CT values were normalized to *Gapdh* and to uninfected controls, in order to determine fold changes in gene expression. The sequences of primers used within this study are summarized in Table 3.14.

Table 3.14: Primer sequences used for qPCR

Target gene	Forward sequence	Reverse sequence
Gapdh	GCCTTCTCCATGGTGGTGAA	GCACAGTCAAGGCCGAGAAT
KC (Cxcl)	AATGAGCTGCGCTGTCAGTG	CGCGACCATTCTTGAGTGTG
Tnfα	CGATGGGTTGTACCTTGTC	CGGACTCCGCAAAGTCTAAG
Foxp3	AGGAGCCGCAAGCTAAAAGC	TGCCTTCGTGCCCACTGT
Il17a	GCTCCAGAAGGCCCTCAGA	AGCTTTCCCTCCGCATTGA
Il6	AGTTGCCTTCTTGGGACT	CAGAATTGCCATTGCACAAC
Il11	CGATTCCCTAAGCTGCGG	AGTAGCTGCAGCTAGAGC
Lgr5	GGGAGCGTTCACGGGCCTTC	GGTTGGCATCTAGGCGCAGGG
RegIIIγ	TTCCTGTCCTCCATGATCAAAA	CATCCACCTCTGTTGGGTTCA
Muc2	TTCTCTTCCTCGTCG	TGAAGGCTGGATTTC

3.2.4. ChipCytometry and automatic image quantification

ChipCytometry and automatic image quantification was performed as described previously (210). Murine intestinal and colonic cross-sections were preserved with O.C.T. compound (Tissue Tek) in cryomolds (Tissue Tek) and kept frozen at -80°C. For ChipCytometry, 7µm thick sections were cut on a Cryotome (Leica), fixed in Fixation Buffer (Zellkraftwerk) for 45 minutes and subsequently transferred to CellSafe Chips (Zellkraftwerk). ChipCytometry on human FFPE biopsies was performed according to the procedure described in Jarosch, Köhlen et al. (211). Briefly, tissue sections were rehydrated on coverslips and antigen retrieval was performed using TRIS-EDTA buffer (pH 8.5) and then transferred to CellSafe Chips. Alternating cycles of staining, immunofluorescence detection and photobleaching were performed for various markers (Table 3.15). Automated image processing was performed as described in Jarosch, Köhlen et al., which includes segmentation of cells, removing of outliers and spatial spill over correction (211). The resulting cell – marker matrix was analyzed using FlowJo software, which enabled absolute quantification of cells.

Table 3.15: Antibodies used for ChipCytometry (as described in 210)

Epitope	Fluorochrome	Clone	Dilution	Company	Catalog #
anti-mouse CD3	PerCP/Cy5.5	17A2	1:200	BioLegend	100218
anti-mouse CD4	eFluor450	RM4-5	1:80	BioLegend	100531
anti-mouse CD45	FITC	30-F11	1:100	BioLegend	103108
anti-mouse Foxp3	PE	FJK-16s	1:80	eBioscience	14-5773-82
Pan-cytokeratin	AlexaFluor 488	C-11	1:100	BioLegend	628602
Hoechst	BUV395	-	1:50.000	ThermoScientific	H3570
α-SMA	eFluor570	1A4	1:750	eBioscience	41-9760-80
anti-human CD3	unconjugated	SP7	1:150	ThermoScientific	RM-9107-S1
anti-human CD4	AlexaFluor 488	polyclonal	1:50	R&D Systems	FAB8165G
anti-human CD45	PerCP/Cy5.5	HI30	1:80	BioLegend	304028
anti-human Foxp3	PE	236A/E7	1:30	eBioscience	563791
2nd anti-rabbit	PE	Polyclonal	1:300	BioLegend	406421

3.2.5. Flow Cytometry

3.2.5.1. Lamina propria lymphocyte isolation

Harvested intestinal tissue was cut open longitudinally after removing Peyer's Patches and adjacent tissue. Subsequently, tissue was treated with 30mM EDTA and digested with 0.5mg/mL collagenase from Clostridium histolyticum Type IV (Sigma Aldrich) and 10µg/mL DNase I (Applichem), until the tissue dissociated. Filtered and centrifuged cell suspensions were density separated using a Percoll gradient (Thermo Fisher).

Fresh human biopsies were collected in Hank's Balanced Salt Solution w/o Mg^{2+}/Ca^{2+} (HBSS) and digested with 0.1% collagenase from Clostridium histolyticum Type IV (Sigma Aldrich) for 30 min. at 37°C. Digestion was stopped by adding 20 mL HBSS and

centrifugation twice. Isolated lymphocytes were frozen in Dimethyl sulfoxide (Applichem) + 20 % FCS at -80° C.

3.2.5.2. *H. pylori* lysate

Frozen stocks of *H. pylori* PMSS1 were plated on WC Dent plates and split after 2 days. Bacteria were collected with inoculation loops and sonicated 3 times for 10 seconds. Protein concentration was determined with BCA protein assay kit (Thermofisher) according to manufacturer's instructions.

For stimulation with whole *H. pylori* lysate, cells were stimulated for 12 hours with 20µg/mL PMSS1 lysate at 37° C and protein transport inhibitor Golgi Plug (BD Biosciences) added 1:1000 after 7 hours for a total of 5 hours.

3.2.5.3. Antibody staining

For staining of intestinal single cell suspensions, unspecific binding was minimized by applying Fc block and applying live/dead staining. After 3 washing cycles with Flow Cytometry buffer, cells were stained with surface antibodies, which were diluted according to titration experiments (Table 3.3). For transcription factors, cells were permeabilized and blocked with Foxp3 Transcription Factor Staining Buffer Set (eBioscience) according to manufacturer's instructions. Stimulated cells were permeabilized and blocked with intracellular cytokine staining kit according manufacturer's instructions (BD Biosciences). After 3 washing cycles, primary transcription and cytokine antibodies (Table 3.16) were diluted according to titration experiments and cells stained for 30 min at 4° C. Stained single cell suspensions were acquired on a CytoFlex S (Beckman Coulter) and analyzed with FlowJo software.

Table 3.16: Antibodies used for flow cytometry

Epitope	Fluorochrome	Clone	Dilution	Catalog #	Company
anti-mouse CD16/CD32	-	93	1:500	14-0161-86	eBioscience
anti-mouse CD45	AlexaFluor 700	30-F11	1:400	103128	BioLegend
anti-mouse CD3ε	FITC	500A2	1:200	152304	BioLegend
anit-mouse CD4	BV605	RM4-5	1:250	100548	BioLegend
anti-mouse CD4	eFluor450	RM4-5	1:250	48-0042-82	eBioscience
anti-mouse CD8a	APC-H7	53.6-7	1:250	560182	BD Biosciences
anti-mouse FoxP3	eFluor450	FJKL-16s	1:200	45-5773-82	eBioscience
anti-mouse IL-17A	APC	eBio17B7	1:150	17-7177-81	eBioscience
anti-human CD45	AlexaFluor 700	2D1	1:50	368514	BioLegend
anti-human CD3	FITC	OKT3	1:300	317306	BioLegend
anti-human CD4	PB450	SK3	1:30	344620	BioLegend
anti-human CD8	APC-H7	SK1(RUO)	1:150	560179	BD Biosciences
anti-human FoxP3	PerCP/Cy5.5	PCH101		35-4776-42	eBioscience
Human TruStain FcX	-	-	1:500	422302	BioLegend

3.2.5.4. Gating strategy

In the forward scatter (FSC) and sideward scatter (SSC) gate, an initial lymphocyte gate was set based on their known size and granularity. Doublets were excluded by plotting area and height within the forward scatter. After excluding dead cells, $CD45^+$ and $CD3^+$ cells were determined. T-cells were distinguished into $CD4^+$ and $CD8^+$ cells, on which transcription factors as well as cytokines were finally gated (Figure 3.3).

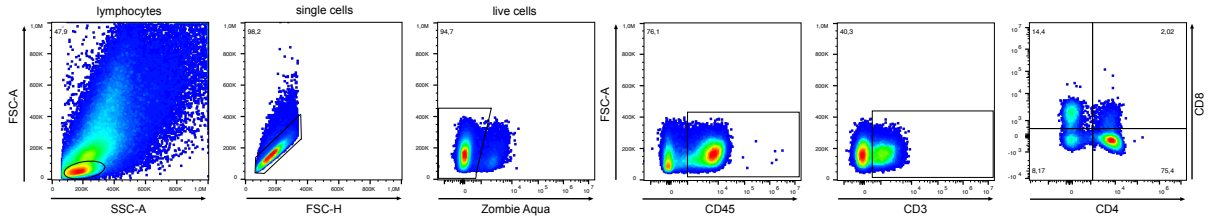

Figure 3.3: Gating strategy

3.2.6. 16S rRNA Sequencing

16S rRNA Sequencing was performed as described in Ralser et al. 2022 (210).

3.2.6.1. DNA extraction and 16S rRNA Sequencing

Genomic DNA was extracted from stomach, proximal and distal as well as colon tissue and caecum including content as well as stool from *H. pylori* infected mice and controls. Sequencing was partly performed by the Core Facility Microbiome of the ZIEL Institute for Food & Health (Technical University of Munich) as described previously (212, 213). Otherwise, phenol chloroform DNA isolation and ethanol precipitation were performed following modified protocols of P.J. Turnbaugh et al., 2009 and E. G. Zoetendal et al. 2006 (214, 215). Briefly, samples were lysed with a Precellys 24 homogeniser (Avantor) in a mixture of DNA extraction buffer, 20% SDS and phenol-chloroform-isoamyl alcohol (PCI). After 2-3 rounds of purification with DNA extraction buffer and PCI, DNA precipitation was performed with pre-cooled 100% EtOH and 3M sodium acetate. Subsequently, the V3/V4 region of the *16S rRNA* gene was amplified with the KAPA Library Quantification Kit and double indexed using barcoding primers modeled after Kozich et al. (216) (Table 3.17) under the conditions stated in Table 3.12.

Table 3.17: 16S rRNA primer sequence

	Sequence
Forward	TCGTCGGCAGCGTCAGATGTGTATAAGAGACAGCCTACGGGNGGCWGCAG
Reverse	GTCTCGTGGGCTCGGAGATGTGTATAAGAGACAGGACTACHVGGGTATCTAATCC

Table 3.18: PCR conditions for amplification of 16S rRNA gene

Step	Temperature	Time
1	95°	3:00
2	95°	0:30
3	55°	0:30
4	72°	0:30
5	Go to step 2	25x
6	72°	5:00
7	12°	∞

PCR fragments were purified using magnetic AMPure XP beads (Beckman Coulter, USA) according to manufacturer's instructions (216) and indexing was performed with the Nextera XT Index Kit (Illumina). The final pooled library was sequenced on an Illumina MiSeq with Reagent Kit v3 (Illumina) for 600 cycles of paired-end reads.

1.1.1.1. Bioinformatic analysis

Quality of raw sequences were checked with FastQC (v0.11.9) and analyzed using the Qiime2 platform (v2021.4) (217). In detail, denoising, removing of chimeras and generation of Amplicon Sequence Variants (ASVs) was performed with dada2. Subsequently, a phylogenetic tree was generated and diversity measures were calculated. Chao1 and Shannon index were used to determine community alpha diversity. Taxonomic classification was performed with a qiime2 feature classifier trained on the SILVA132 99% OTUs, specifically targeting the V3 region. Linear discriminant analysis effect size (LEfSe) determining differentially abundant features was performed on the online interface at http://huttenhower.sph.harvard.edu/lefse/, developed by Segata et al. (218).

3.2.7. Single cell RNA sequencing

Single cell RNA sequencing was performed as described in Ralser et al. 2022 (210). Thereby, cells were isolated as described in section "Lamina propria lymphocyte isolation and Flow cytometry". Single cell suspensions were stained with anti-mouse CD45 PB450 (Clone: 30-F11, BioLegend, #103126), anti-mouse EPCAM APC (Clone: G8.8, BioLegend, #118214) and Propidium Iodide (PI). CD45+ PI- and EPCAM+ PI- cells were sorted.

Single cell RNA Sequencing was performed with 10X Genomics, according to manufacturer's instructions (Chromium™ Single Cell 3' GEM v3 kit). Briefly, sorted cells were centrifuged and resuspended in mastermix and 37.8 µl of water, before 70 µl of the cell suspension was transferred to the chip. QC was performed with a high sensitivity DNA Kit (Agilent) on a Bioanalyzer 2100, and libraries were quantified with the Qubit dsDNA HS assay kit (life technologies).

Libraries were pooled according to their minimal required read counts (20.000 reads/cell for gene expression libraries). Illumina paired end sequencing was performed with 150 cycles on a NovaSeq 6000.

Annotation was performed using cellranger (V5.0.0, 10X genomics) against the murine reference genome GRCm38 (mm10-2020-A). All subsequent analysis was performed using SCANPY V1.6 (206). Preprocessing was performed following the guidelines of best practice in single-cell RNA-seq analysis (219) and involved less than 15% mitochondrial genes, regressing out cell cycle, mitochondrial genes and total counts. The data was normalized per cell count and logarithmized.

RNA velocities were calculated using velocyto (207) and analyzed with scVelo (V 0.2.3) (208).

3.2.8. Human studies

As described previously (210), 87 fresh colonoscopy biopsies were collected within the framework of the COLOBAC study of the CRC1371 (Dept. of Surgery and II. Medical Dept. Klinikum rechts der Isar, Technical University of Munich, Germany) and 67 FFPE colon biopsies were obtained from the Klinikum Bayreuth. Both studies were approved by the respective ethics committees (Klinikum rechts der Isar #322/18, Klinikum Bayreuth #241_20Bc).

H. pylori status of colonoscopy biopsies was determined in serum samples using the recomwell Helicobacter IgG kit (Mikrogen) according to manufacturer's instructions. Additionally, strain specific virulence factors were assessed recomline Helicobacter IgG kit (Mikrogen), which revealed the current infection status of these patients. *H. pylori* status of FFPE biopsies was determined histologically in corresponding gastric biopsies by Prof. Michael Vieth.

3.2.9. Statistical analysis

Statistical analysis was carried out using Prism 8 (GraphPad Software) and conducted on biological replicates of 1-3 independent infection experiments. Depending on Gaussian distribution, statistical significance between two groups was determined with unpaired student's t-test or Mann-Whitney-U test and for analysis among more than two groups, one-way ANOVA with Tukey's multiple-comparisons test was used in case of normal distribution, otherwise Kruskal-Wallis-test with Dunn's multiple-comparisons test. Values below 0.05 were considered significant.

Figures were constructed with Affinity Photo and Affinity Designer (Serif).

4. Results

4.1. Characterization of the influence of *H. pylori* infection on intestinal/colonic inflammation and signaling pathways

To assess the impact of *H. pylori* infection on homeostasis in the lower gastrointestinal tract, C57Bl/6 mice (WT mice) were infected and an extensive analysis of the elicited immune response, the activation of signaling pathways and changes in epithelial cell compartments and microbial compositions was conducted.

4.1.1. *H. pylori*-infected mice exhibit a pro-inflammatory T-cell response in intestine and colon

WT mice were infected with the pathogenic *H. pylori* strain PMSS1 for 4, 12 and 24 weeks (Figure 4.1a). The infection status of each mouse was detected by counting of CFU, which revealed stable infection over time (Figure 4.1b). To confirm the infection status on a molecular level, typical markers of *H. pylori*-induced immune response in the stomach were assessed. This revealed increased T-cell infiltration (Figure 4.1c), upregulated *Cxcl1* and *Il17a* levels as well as a tendency towards more *Foxp3* expression in stomach tissue upon *H. pylori* infection (Figure 4.1d).

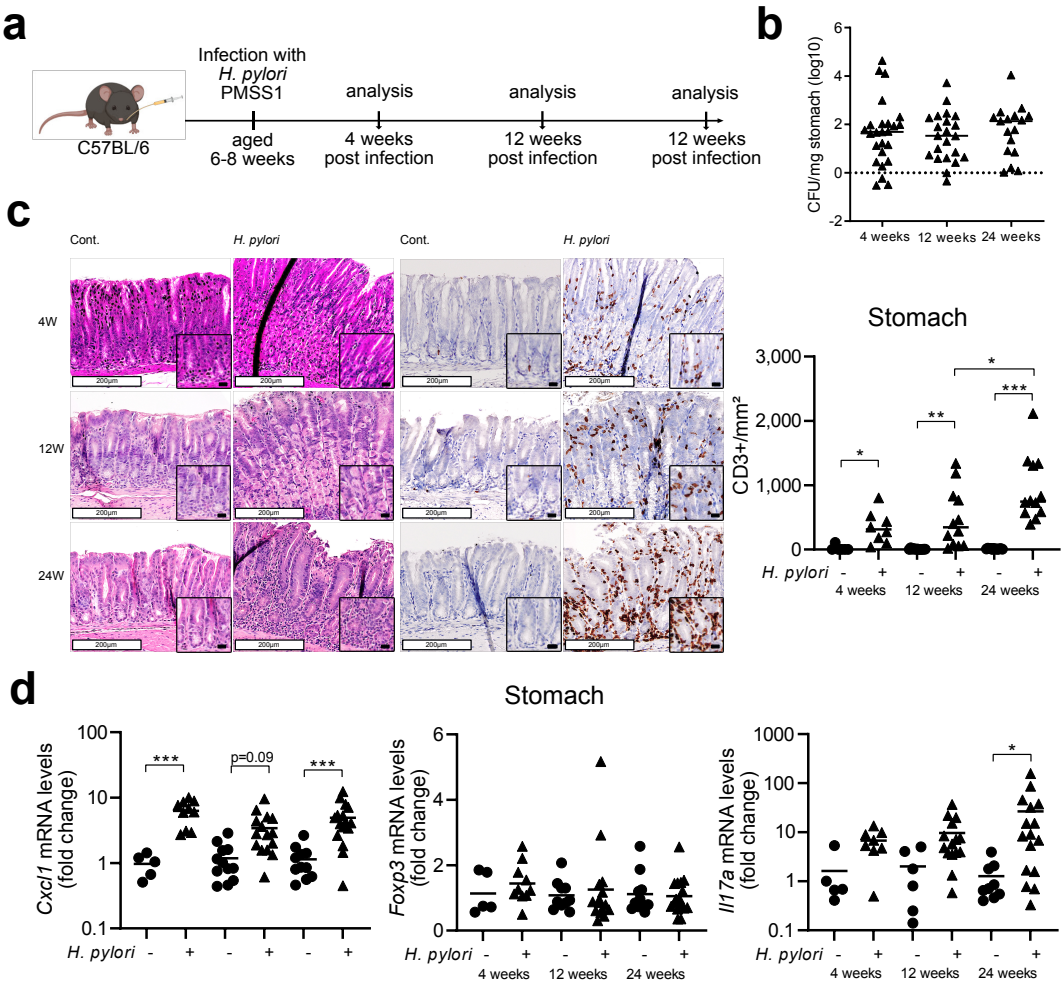

Figure 4.1: WT mice were successfully infected with *H. pylori* strain PMSS1 for 4, 12 and 24 weeks. (a) Experimental setup of *H. pylori* infection experiments is shown. (b) Colony forming units after 4, 12 and 24 weeks of infection were counted. (c) T cell infiltration into stomach epithelium determined via $CD3^+$ immunohistochemical staining. Representative images of HE and $CD3^+$ staining are shown. White scale bar corresponds to 200µm, small scale bar to 20µm. (d) Gene expression of *Cxcl1*, *Il17a* and *Foxp3* in stomach tissue was assessed by qPCR. Fold change in expression is depicted as $2^{\Delta\Delta CT}$ value, normalized to *Gapdh* and control mice. Dots represent data of individual mice from 3 independent experiments. Horizontal bars indicate medians. Statistical significance was determined with one-way ANOVA with Tukey's multiple comparisons in case of normal distribution, otherwise with Kruskal Wallis test with Dunn's multiple comparisons. *p<0. 05, **p<0.01, ***p<0.001.

In summary, C57Bl/6 mice were successfully infected with *H. pylori* for 3 time points and showed robust CFU as well as known characteristic inflammatory responses in the stomach upon *H. pylori* infection.

In the stomach, *H. pylori* infection leads to a strong T cell response. This response consists of an intricate balance between proinflammatory Th1 and Th17 cells and Tregs. We hypothesized that such inflammatory response my not be restricted to the stomach, but may also extend to the lower gastrointestinal tract. To explore such immune response in intestine and colon upon *H. pylori* infection, intraepithelial $CD3^+$ T-cells of the intestine and colon were first assessed by immunohistochemistry. This revealed an increased recruitment of $CD3^+$ T cells into the epithelium of proximal and distal intestine as well as

colon after 4, 12 and 24 weeks of infection (Figure 4.2a). Furthermore, the abundance and phenotype of lamina propria lymphocytes in the intestine was assessed via flow cytometry. A shift towards less $CD4^+$ and more $CD8^+$ T cells upon *H. pylori* infection (Figure 4.2b) was detected. In this context, the number of $FoxP3^+$ regulatory T cells was evaluated, which were reduced in *H. pylori*-infected compared to non-infected mice (Figure 4.2c). Remarkably, a *H. pylori* specific $CD4^+$ T cell response was observed in lymphocytes isolated from intestines of infected mice after in vitro culture and restimulation with whole *H. pylori* lysate, showing significant IFNγ and IL-17 release (Figure 4.2d). This indicated that immune cells primed to *H. pylori* were homing to the gut lamina propria.

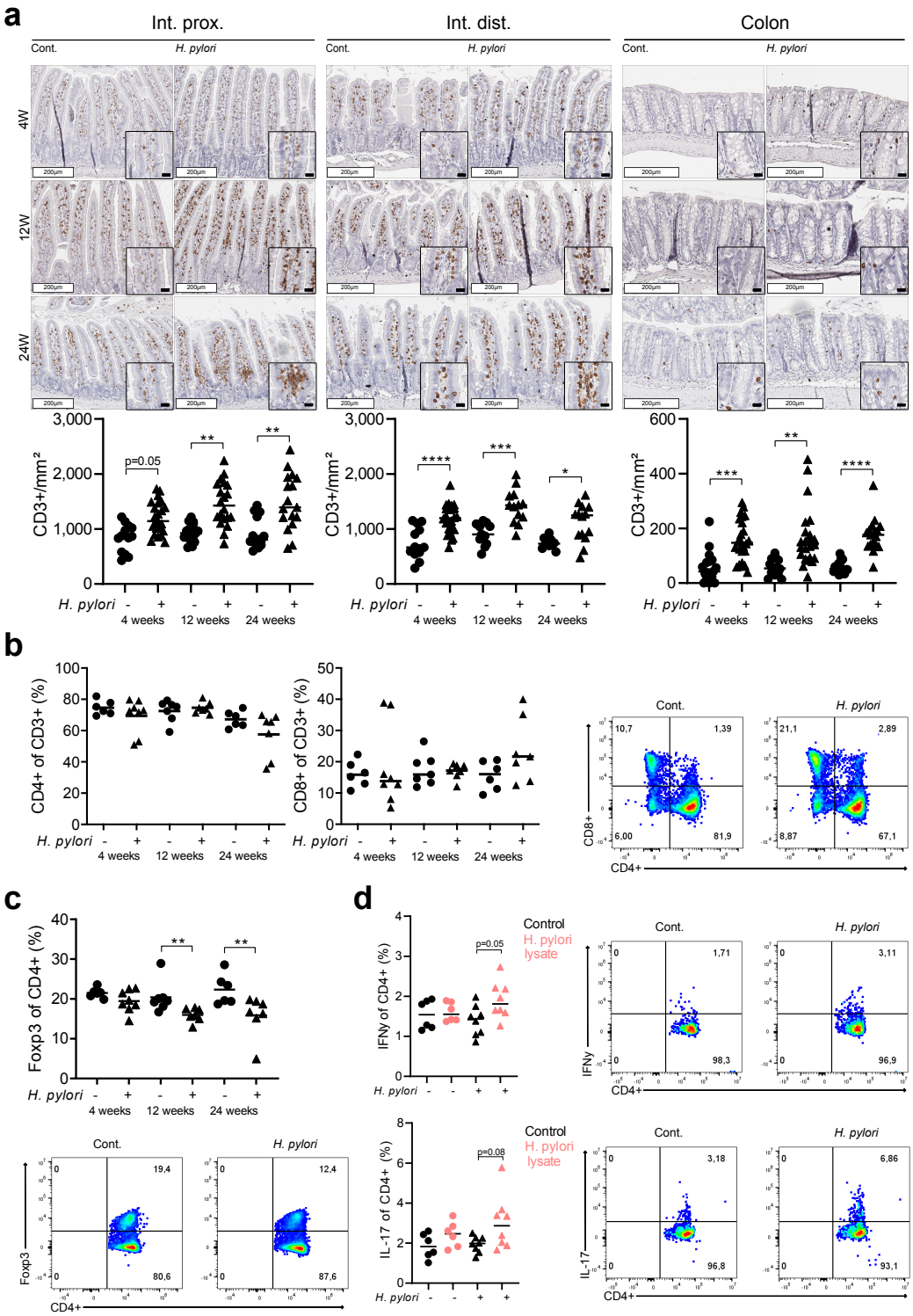

Figure 4.2: *H. pylori* infection induces pro-inflammatory T-cell responses in intestine and colon.
(a) T cell infiltration into intestinal and colon epithelia determined via CD3⁺ immunohistochemical staining. Representative images of CD3⁺ staining are shown. White scale bar corresponds to 200µm, small scale bar to 20µm. Dots represent data of individual mice of 3 independent experiments. Horizontal bars indicate medians. (b) CD4⁺ and CD8⁺ T cell properties in intestinal lamina propria lymphocytes are depicted. Cells are gated on single cells, live, CD45⁺ and CD3⁺. Representative pseudocolor plots are shown. (c) FoxP3⁺ regulatory T cells frequencies are shown, gated on single cells, live, CD45⁺, CD3⁺ and CD4⁺. Cells are shown as percentages of CD4⁺ cells with representative pseudocolor plots. (d) Overnight stimulation with whole *H. pylori* lysate and subsequent intracellular cytokine staining for IFNγ (upper graphs) and I17a (lower graphs), shown as percentages of CD4⁺ cells. Cells are gated on single cells, live, CD45⁺, CD3⁺ and CD4⁺ and shown with representative pseudocolor plots. One representative flow cytometry experiment out of 3 is shown. Statistical significance was determined with one-way ANOVA with Tukey's multiple comparisons in case of normal distribution, otherwise with Kruskal Wallis test with Dunn's multiple comparisons or with Mann-Whitney U test, *p<0.05, **p<0.01, ***p>0.001, ****p<0.001.

The immune response elicited upon *H. pylori* infection in the gastrointestinal tract was further characterized by examining the expression of innate, regulatory and proinflammatory cytokines and transcription factors. As shown in Figure 4.1, the immune response in the stomach upon *H. pylori* infection is characterized by a strong innate response, marked by *Cxcl1* and *Tnfα*, as well as a strong Th17 response, marked by the key cytokine *Il17a*. In the stomach, this strong proinflammatory response is normally counteracted by a high regulatory response. In the intestine and colon, a tendency towards more *Cxcl1* and *Tnfα* in both acute and chronic infection settings was observed. The *Il17a* expression showed a tendency towards upregulation, however not significant. In contrast to the findings in the stomach, *Foxp3* expression showed a trend towards downregulation after 12 weeks of infection (Figure 4.3).

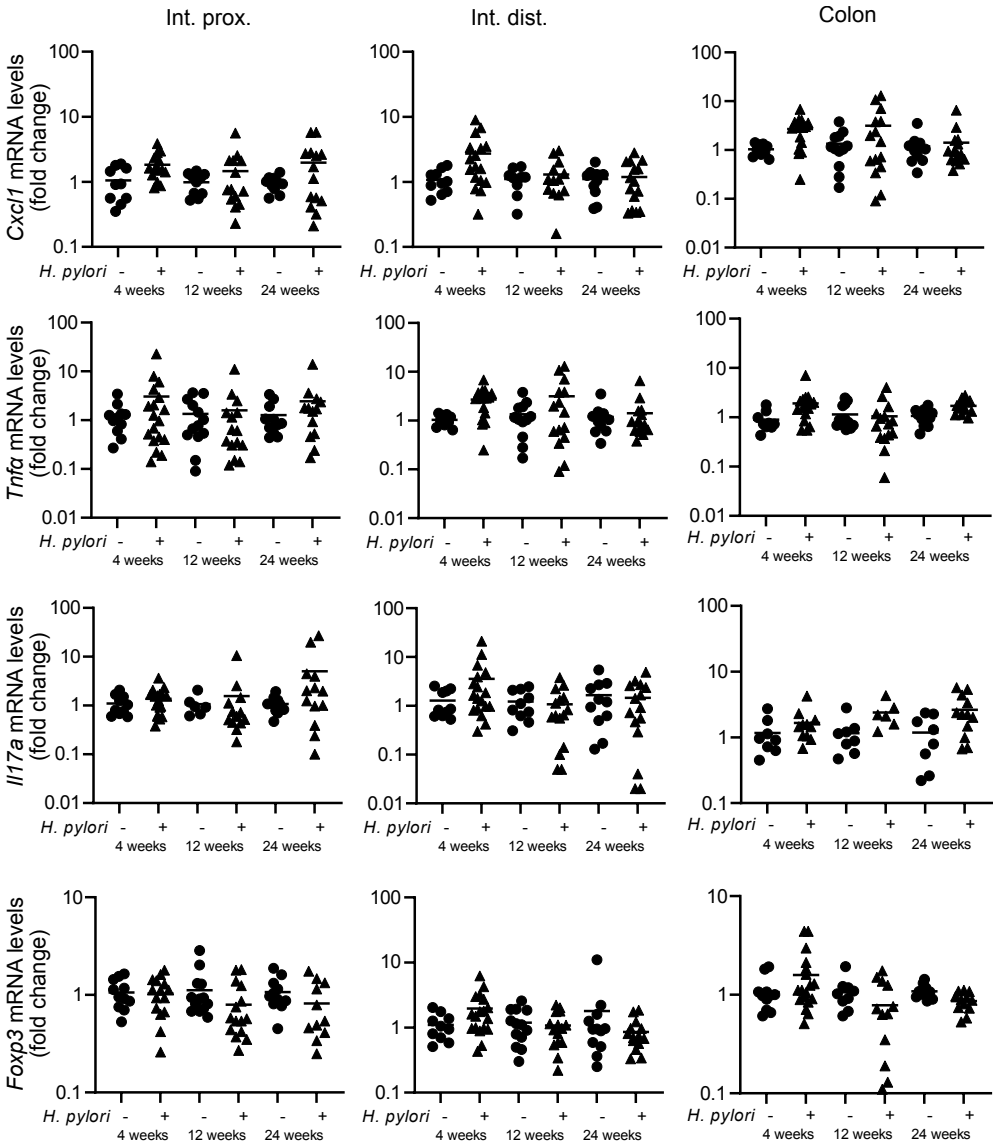

Figure 4.3: Immune response elicited upon *H. pylori* infection in intestinal and colonic tissue.
Gene expression of Cxcl1, Tnfα, Il17a and *Foxp3* in proximal and distal intestine as well as colon tissue assessed by qPCR. Fold change in expression is depicted as $2^{\Delta\Delta CT}$ value, normalized to Gapdh and control mice. Dots represent data of individual mice of 3 independent experiments. Horizontal bars indicate medians. Statistical significance was determined with one-way ANOVA with Tukey's multiple comparisons in case of normal distribution, otherwise with Kruskal Wallis test with Dunn's multiple comparisons.

To characterize Tregs in further detail, chip cytometry was performed to assess localization and distribution of cells in colon tissue on a single cell level. Regulatory T cells were identified by $^{+}$ CD45^{+}, CD4^{+}, CD3^{+}and intranuclear FoxP3staining and quantified via automated image processing (Figure 4.4a). This confirmed that *H. pylori* infection leads to a higher CD3^{+} T cell infiltration and a reduction of FoxP3^{+} regulatory T cells in the colon (Figure 4.4b). Furthermore, cytokeratin staining enabled distinguishing between intraepithelial and lamina propria location of regulatory T cells and revealed, that in *H. pylori* infected mice, FoxP3^{+} regulatory T cells completely lose their intraepithelial localization (Figure 4.4b).

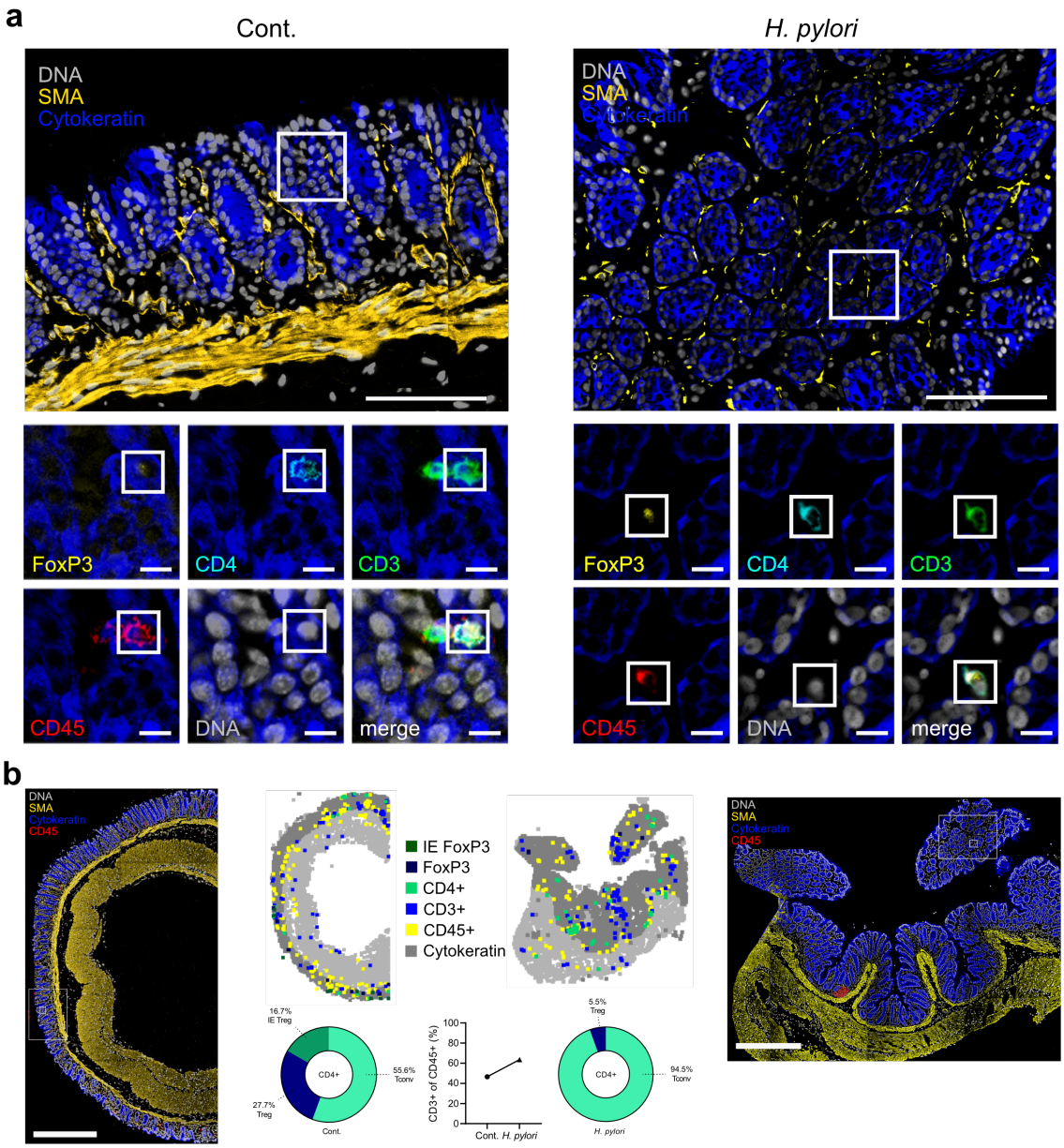

Figure 4.4: *H. pylori* infection leads to loss of intraepithelial regulatory T cells in colon tissue.
(a) Representative picture of colon tissue stained with multiplexed chip cytometry. FoxP3^{+} cell, defined by intranuclear FoxP3^{+}, CD4^{+} CD3^{+} and CD45^{+} staining. Large scale bar corresponds to 100µm, small scale bar to 10µm. (b) Whole colonic transection tissue stained with multiplexed chip cytometry. Automatic image processing of multiplexed chip cytometry on colon tissue identifies CD3^{+} T-cell infiltration and CD4^{+} T-cell properties in H. pylori positive and negative C57BL/6 mice: frequencies of conventional T-cells (Tconv), regulatory T-cells (Treg) and intraepithelial regulatory T-cells (IE Treg) are shown. Scale bar corresponds to 500µm.

Thus, *H. pylori* was found to induce a proinflammatory, antigen-specific T-cell response and an overall as well as intraepithelial reduction of Tregs in intestine and colon.

4.1.2. *H. pylori* infection activates STAT3 signaling, enhances proliferation and reduces mucus producing goblet cells in intestine and colon

The STAT3 signaling pathway is known to be induced upon inflammatory processes and has been described to contribute to gastric and colon carcinogenesis. Against this background, the activation of STAT3 signaling in *H. pylori* infected mice was investigated. Immunohistochemical staining for phosphorylated STAT3 (pSTAT3), which is a marker for active STAT3 signaling, revealed stronger activation of this pathway in the intestinal and colonic epithelium of *H. pylori* infected mice compared to non-infected controls (Figure 4.5a). Next, *Il6* and *Il11*, cytokines known to induce STAT3 signaling, were assessed in *H. pylori* infected mice. This revealed a tendency towards more *Il6* expression in the intestine, however not in the colon. The expression levels of *Il11* did not show any consistent changes. (Figure 4.5b)

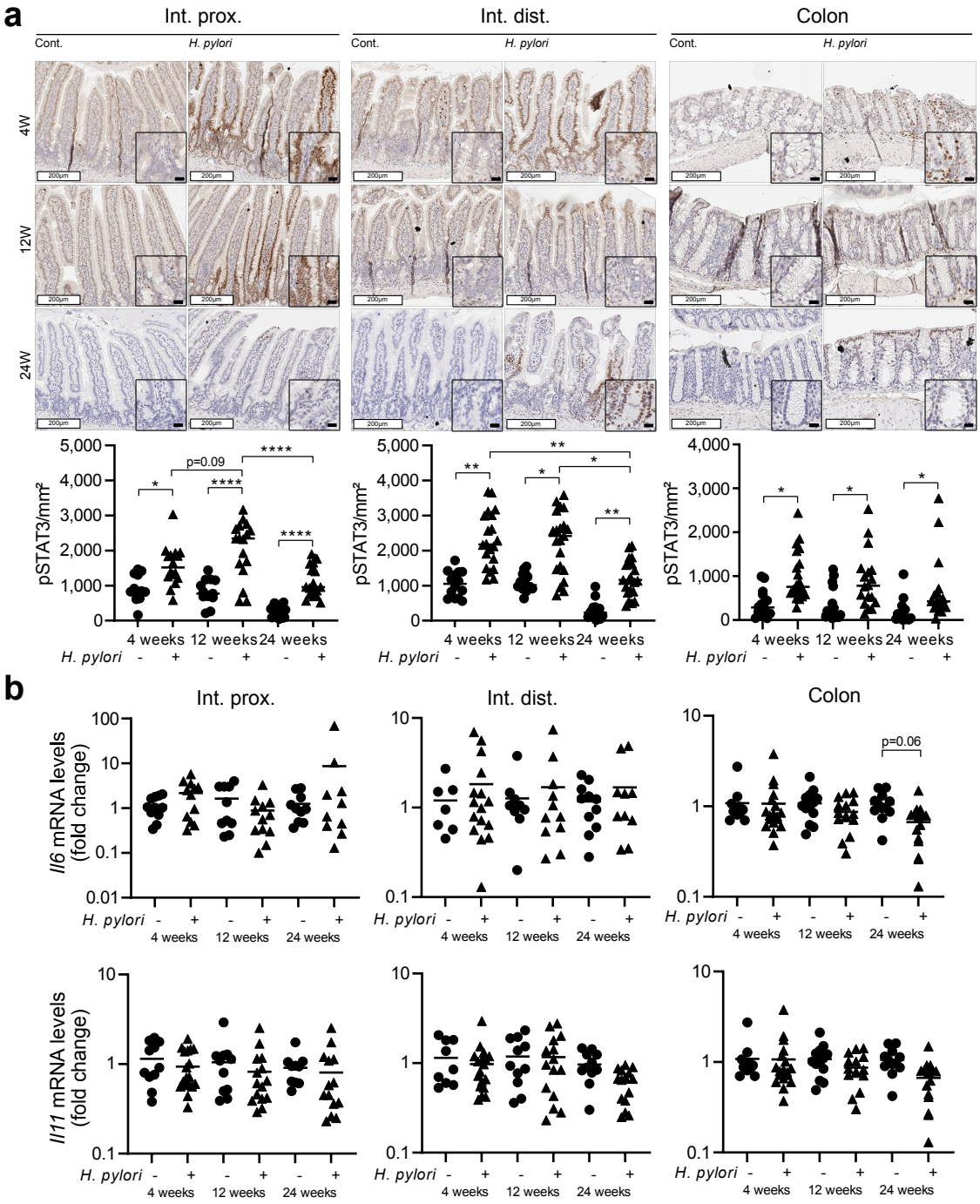

Figure 4.5: *H. pylori* infection activates STAT3 signaling in intestine and colon.
(a) Number of active STAT3 epithelial cells in proximal and distal intestine as well as colon was assessed by immunohistochemical staining of phosphorylated STAT3. Representative pictures are shown. White scale bar corresponds to 200µm, small scale bar to 20µm. (b) Gene expression levels of *Il6* and *Il11* in proximal and distal intestine as well as colon tissue was assessed by qPCR. Fold change in expression is depicted as $2^{\Delta\Delta CT}$ value, normalized to Gapdh and control mice. Dots represent data of individual mice of 3 independent experiments. Horizontal bars indicate medians. Statistical significance was determined with one-way ANOVA with Tukey's multiple comparisons in case of normal distribution, otherwise with Kruskal Wallis test with Dunn's multiple comparisons, *p<0.05, **p<0.01, ***p>0.001, ****p<0.001.

Intestinal homeostasis is important to sustain the functionality of distinct intestinal cell types and to prevent disease. An optimal balance between proliferation and apoptosis is

a crucial aspect to ensure a healthy intestinal epithelium and to prevent the development of cancer.

To assess the impact of *H. pylori* infection on intestinal and colonic proliferation, we first assessed proliferating cells via Ki67 immunohistochemical staining and changes in gene expression of the stem cell marker *Lgr5*, in order to assess possible effects of *H. pylori* infection on stemness. We characterized both proliferating cells per mm^2 tissue (Figure 4.6a) and measured the proportion of the proliferating zone in relation to the whole crypt-villus - or in case of the colon crypt only – length (Figure 4.6b). This analysis revealed increased proliferation in intestinal and colonic tissue of *H. pylori* infected mice. However, no significant changes in the expression of *Lgr5* were detected (Figure 4.6c).

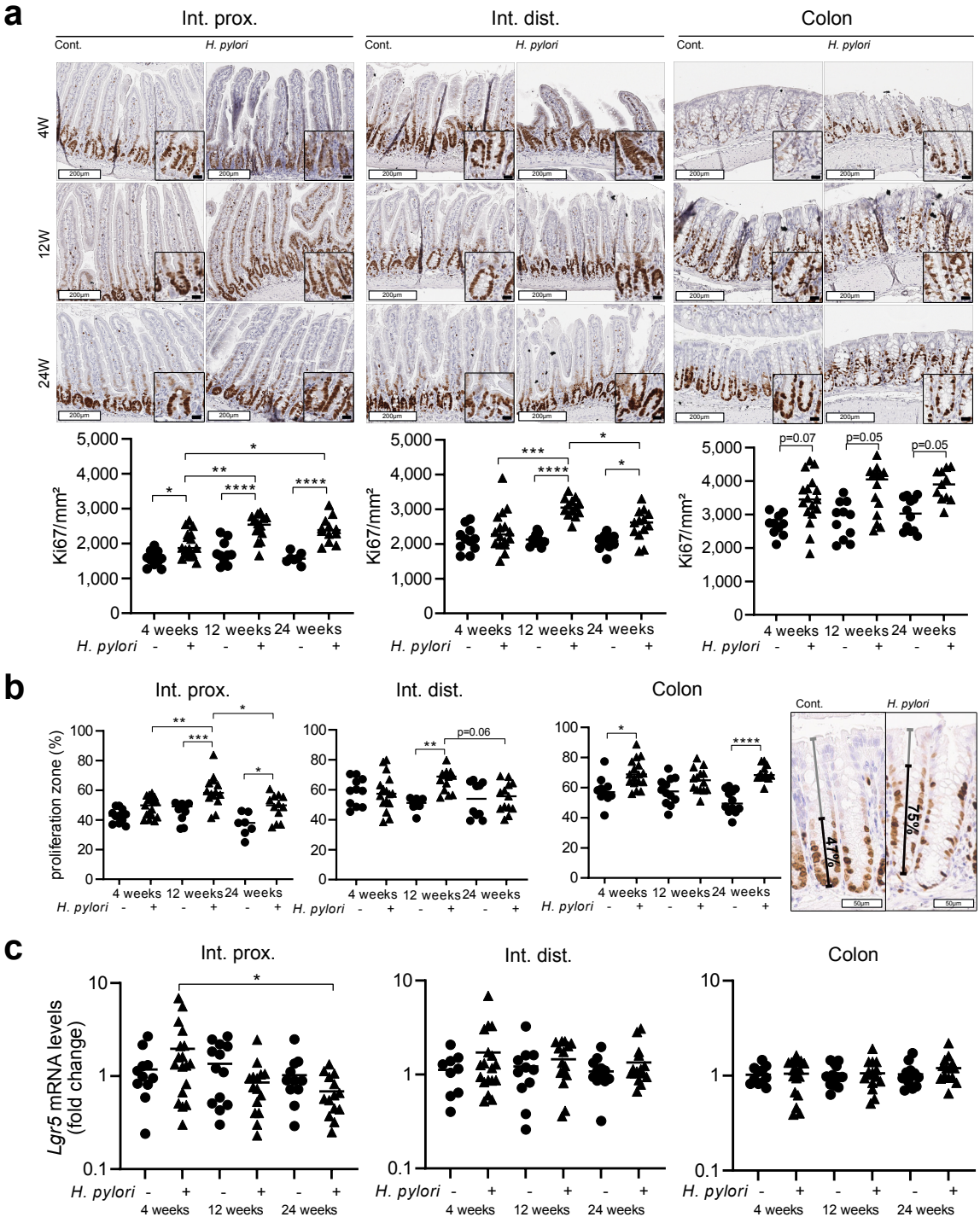

Figure 4.6: *H. pylori* infection drives proliferation in intestinal and colonic tissue.
(a) Number of proliferating epithelial cells in proximal and distal intestine as well as colon was assessed by immunohistochemical staining of Ki67. Representative pictures and quantifications per mm^2 tissue are shown. White scale bar corresponds to 200µm, small scale bar to 20µm. (b) Proportions of proliferating cells in relation to whole crypt-villus/crypt length is shown in %. Representative picture of proliferation zone measured in colon is depicted. White scale bar corresponds to 50µm. (c) Gene expression of *Lgr5* in proximal and distal intestine as well as colon tissue was assessed by qPCR. Fold change in expression is depicted as $2^{\Delta\Delta CT}$ value, normalized to Gapdh and control mice. Dots represent data of individual mice of 3 independent experiments. Horizontal bars indicate medians. Statistical significance was determined with one-way ANOVA with Tukey's multiple comparisons in case of normal distribution, otherwise with Kruskal Wallis test with Dunn's multiple comparisons, *p<0.05, **p<0.01, ***p>0.001, ****p<0.001.

The mucus constitutes a protective layer separating the gastrointestinal epithelium from the lumen and is known as the first line of defense against invading pathogens. Therefore,

the number of mucus producing goblet cells and constituent genes as well as genes involved in antimicrobial defense were assessed upon *H. pylori* infection. *H. pylori* infection was found to lead to a decreased number of goblet cells (Figure 4.7a) and to a downregulation of mucin *Muc2* in proximal intestine and colon (Figure 4.7b). The antimicrobial peptide *RegIIIγ* showed trends towards downregulation in the proximal intestine and colon after chronic infection with *H. pylori* (Figure 4.7b).

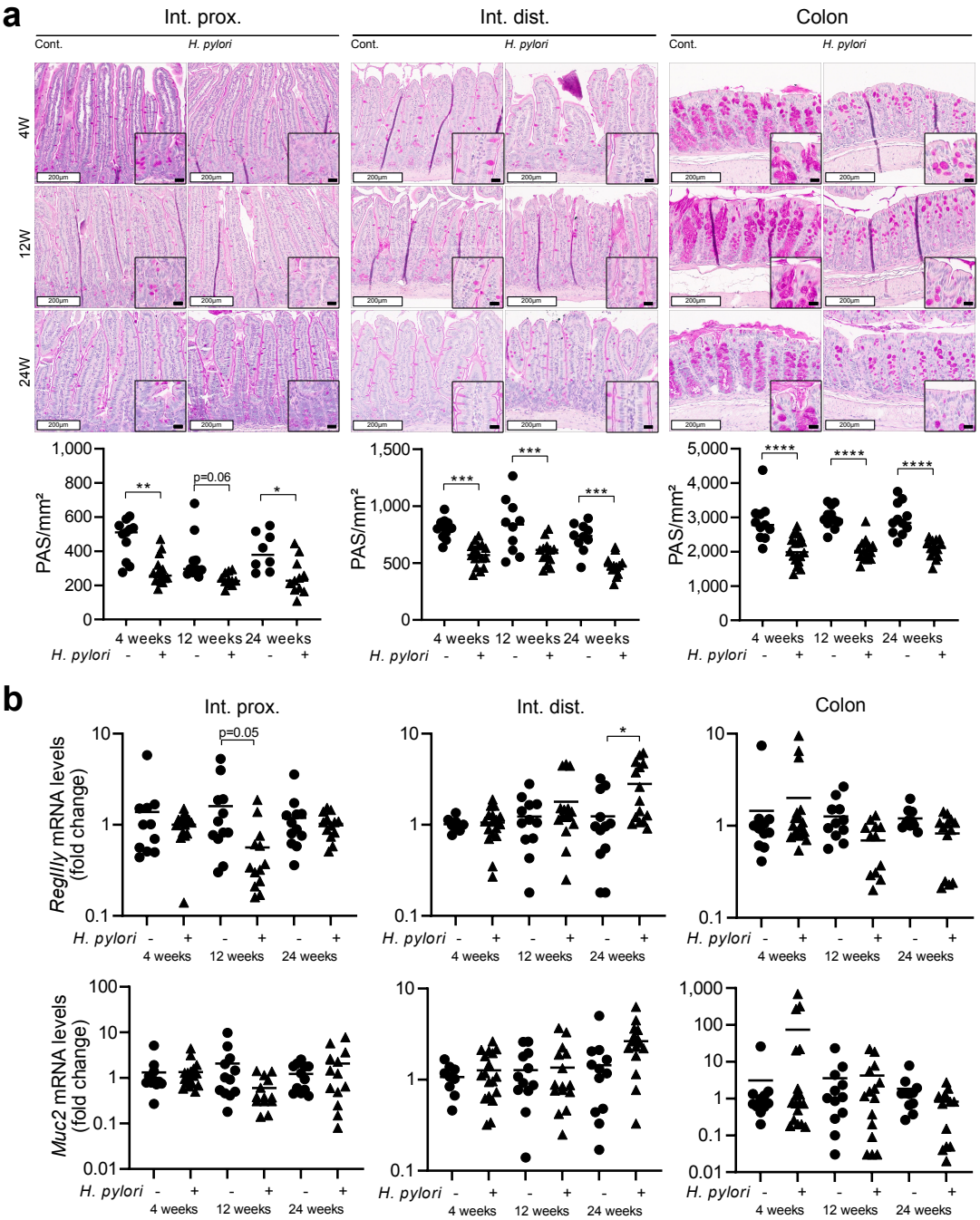

Figure 4.7: *H. pylori* reduces mucus producing cells in intestine and colon.
(a) Number of mucus producing cells in proximal and distal intestine as well as colon was assessed by PAS staining. Representative pictures and quantifications per mm^2 tissue are shown. White scale bar corresponds to 200µm, small scale bar to 20µm. (b) Expression levels of *Muc2* and *RegIIIγ* in proximal and distal intestine as well as colon tissue was assessed by qPCR. Fold change in expression is depicted as $2^{\Delta\Delta CT}$ value, normalized to *Gapdh* and control mice. Dots represent data of individual mice of 2 independent experiments. Horizontal bars indicate medians. Statistical significance was determined with one-way ANOVA with Tukey's multiple comparisons in case of normal distribution, otherwise with Kruskal Wallis test with Dunn's multiple comparisons, *p<0.05, **p<0.01, ***p>0.001, ****p<0.001.

In summary, we detected activation of pro-inflammatory and carcinogenic STAT3 signaling pathway, increased proliferation of epithelial cells and a reduction of mucus producing goblet cells in proximal and distal intestine as well as colon tissue upon *H. pylori* infection.

4.1.3. *H. pylori* infection shapes gut microbiota towards mucus-degradation

Host-microbiota interactions and balanced gut microbiota are important for gut intestinal health, a functional immune system and gut homeostasis, and can therefore be decisive players in the development and outcome of disease. Literature reports an effect of *H. pylori* infection not only on local gastric, but also on distant microbiota (76). To analyze the effects of *H. pylori* infection on the gut microbiome, 16S rRNA sequencing of the gastrointestinal tract of *H. pylori* infected WT mice was performed. Thereby, stomach, intestinal and colonic tissue as well as caecum including content and stool were analyzed, which allowed to assess both luminal and mucosa-associated microbiota. This revealed changes in alpha-diversity (depicted as Chao1 index) based on infection status (Figure 4.8a). *H. pylori* infection markedly affected microbiota compositions, assessed by relative taxonomic abundances at phyla level (Figure 4.8b) and clustering according to infection status in the Bray-Curtis dissimilarity index (Figure 4.8c). To determine differentially abundant features upon infection LEfSe analysis was performed (Figure 4.8d). To point out a few remarkable features, increased abundance of *Akkermansia* spp., a mucus degrading bacterium, in caecum, stool and colon was detected. Another interesting finding was the decrease in beneficial *Roseburia* spp. detected in caecum and intestine, which has been described to promote regulatory T-cells while simultaneously reducing Th17 responses (220). As a proof of concept, the abundance of *Helicobacter* spp. was assessed, which was highly abundant in stomach and detectable in single samples of intestine and colon (Figure 4.8e). On genera level, the abundance of mucus degrading *Akkermansia* and *Ruminococcus species* was confirmed to be increased throughout the intestinal tract upon *H. pylori* infection (Figure 4.8e).

Figure 4.8: *H. pylori* infection affects gastrointestinal microbiota.

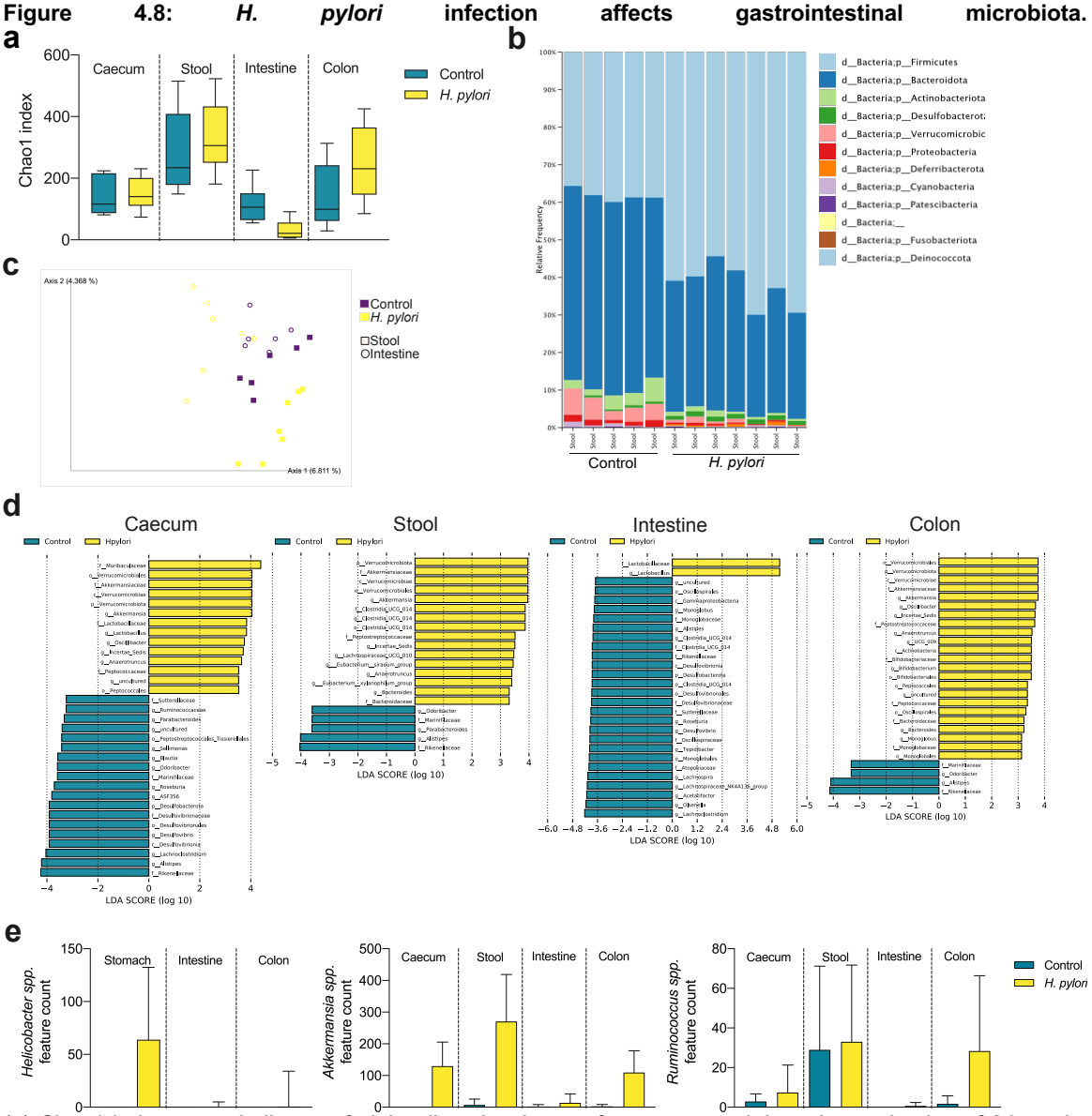

(a) Chao1 index as an indicator of alpha-diversity shown of caecum, stool, intestine and colon of 24 weeks infected WT mice and aged matched, non-infected controls. (b) Taxonomic binning showing relative frequencies at phyla level in stool of non-infected and infected WT mice. (c) Bray Curtis emperor plot as an indicator of beta-diversity of intestine and stool of non-infected and infected WT mice. (d) LEfSe analysis of caecum, stool, intestine and colon, depicting differentially abundant features upon *H. pylori* infection. (e) Feature counts of Helicobacter species (spp.), *Akkermansia* spp. and *Ruminococcus* spp. in ceacum, stool, intestine and colon of non-infected and infected WT mice. Chao1 index depicted as box and whiskers, from min to max. Feature counts shown as bar plots, indicating mean with standard deviation.

In summary, *H. pylori* infection induced distinct changes in microbiota composition throughout the gastrointestinal tract with evident effects on both luminal and tissue-adherent microbiota, pointing towards signatures of inflammation and mucus degradation.

4.1.4. Eradication therapy reverses *H. pylori* induced phenotype to levels of non-infected controls

In order to proof that the observed effects were specifically attributable to *H. pylori* infection, *H. pylori* infected WT mice were eradicated. Thereby, mice infected for 4 weeks

were treated with a therapy regimen consisting of the proton pump inhibitor omeprazole and two antibiotics clarithromycin and metronidazole, resembling the “Italian triple therapy”, a gold-standard therapy to eradicate *H. pylori* in humans. To monitor the effects of the treatment itself, one group was administered with the eradication therapy alone (‘ABX’). Mice were analyzed after a short and a longer recovery time of 4 and 12 weeks, respectively (Figure 4.9a). This approach resulted in successful eradication of *H. pylori*, confirmed by absent CFU counts after antibiotic treatment (Figure 4.9b) as well as significantly reduced T-cell infiltration into the stomach epithelium (Figure 4.9c).

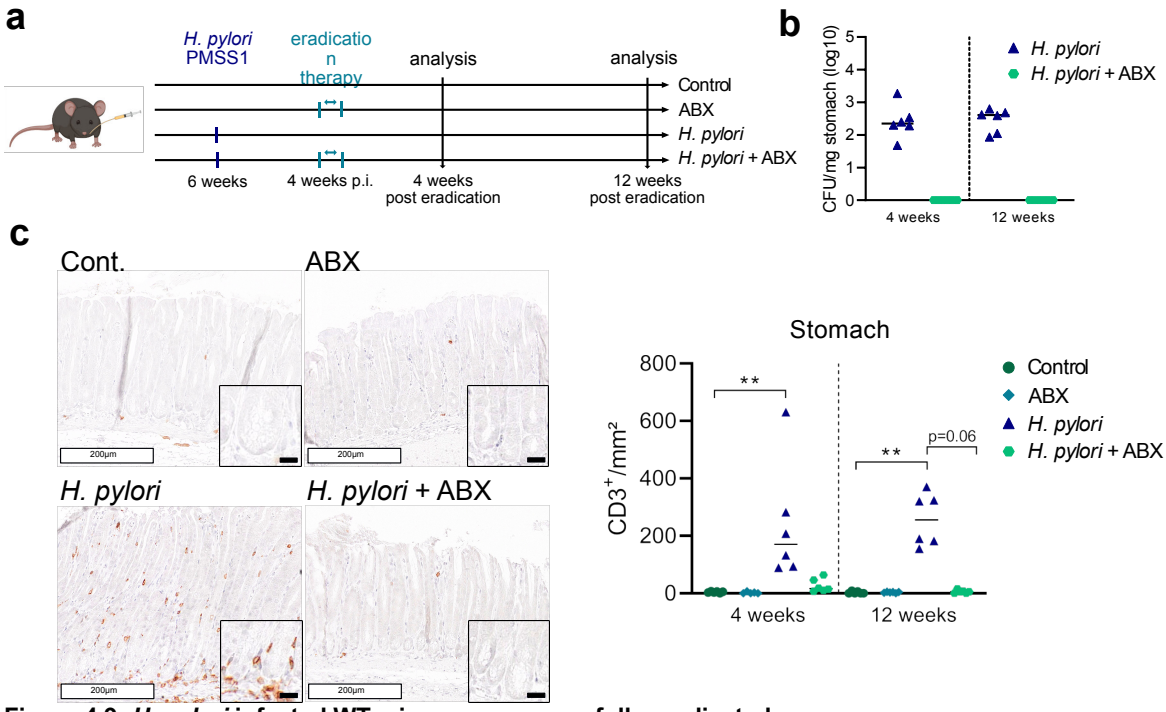

Figure 4.9: *H. pylori* infected WT mice were successfully eradicated.
(a) Experimental setup for eradication therapy of *H. pylori* infected WT mice. (b) CFU counts per mg stomach 4 weeks and 12 weeks after eradication are shown. (c) Representative pictures of $CD3^+$ immunohistochemistry staining of stomach tissue of control, antibiotically treated, infected and eradicated mice are shown. White scale bar corresponds to 200µm, small scale bar to 20µm. Quantification of positive cells per mm^2 tissue. Dots represent data of individual mice. Horizontal bars indicate medians. Statistical significance was determined with one-way ANOVA with Tukey’s multiple comparisons in case of normal distribution, otherwise with Kruskal Wallis test with Dunn’s multiple comparisons. *p<0. 05, **p<0.01.

When assessing the effect of eradication on the previously described phenotype, the enhanced immune cell infiltration as well as the higher activation of STAT3 signaling in intestinal and colonic epithelia upon *H. pylori* infection was normalized to the level of non-infected controls already 4 weeks after eradication and remained stable throughout 12 weeks after treatment (Figure 4.10a). The regulatory T-cell response was severely affected by antibiotic treatment, as observable in the reduction of Tregs in the ABX group at 4 weeks. This was followed by a delayed recovery of Tregs 12 weeks after eradication to the level of non-infected controls (Figure 4.10b). Given the availability of initial antigen priming and reencounter for a specific immune response, it was assumed that the previously described *H. pylori* specific T-cell response would not be affected by eradication. This held true only after a longer recovery from the antibiotic treatment, which

underlines again the impact of antibiotic treatment on immune cells (Figure 4.10c). Finally, when looking at the status of mucus producing cells, normalization of levels was depending on the recovery time after eradication therapy, eventually leading to number of goblet cells leveling with control mice 12 weeks after treatment (Figure 4.10a).

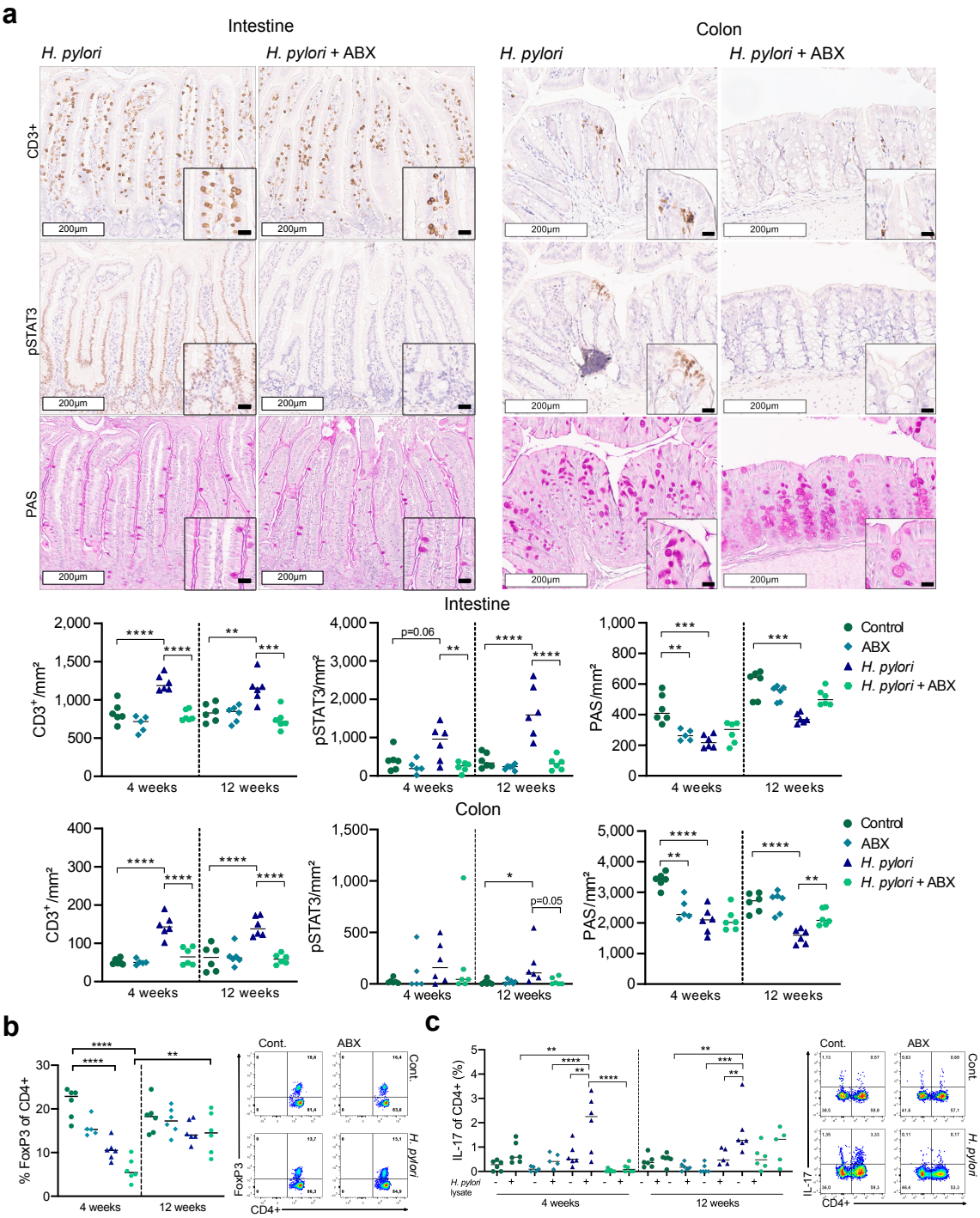

Figure 4.10: Eradication therapy reverses *H. pylori* induced phenotype in C57Bl/6 mice.
(a) Representative pictures of $CD3^+$, pSTAT3 and PAS staining of intestinal and colonic tissue of control, antibiotically treated, infected and eradicated mice are shown. White scale bar corresponds to 200µm, small scale bar to 20µm. Quantification of positive cells per mm^2 tissue is shown. (b) $FoxP3^+$ regulatory T cells frequencies are shown, gated on single cells, live, $CD45^+$, $CD3^+$ and $CD4^+$. Cells are shown as percentages of $CD4^+$ T-cells with representative pseudocolor plots. (d) Frequencies of I17a positive cells, shown as percentages of $CD4^+$ cells. Cells are gated on single cells, live, $CD45^+$, $CD3^+$ and $CD4^+$ and shown with representative pseudocolor plots. Dots represent data of individual mice. Horizontal bars indicate medians. Statistical significance was determined with one-way ANOVA with Tukey's multiple comparisons in case of normal distribution, otherwise with Kruskal Wallis test with Dunn's multiple comparisons. *p<0. 05, **p<0.01.

In summary, the eradication therapy resulted in a normalization of the *H. pylori* induced phenotype to the level of non-infected controls and simultaneously revealed a detrimental effect of antibiotics included in the eradication regimen on certain immune as well as epithelial cell populations.

Overall, an extensive analysis of the effects of *H. pylori* infection on the immune system, epithelial compartment and microbiota of the small and large intestine of WT mice revealed antigen specific, proinflammatory T-cell responses accompanied by reduction of Tregs, activation of STAT3 signaling, triggering of proliferation and shaping of microbiota towards mucus degradation as defined effects of *H. pylori* infection on intestinal and colonic tissue. *H. pylori* eradication experiments confirmed that those observed effects can be specifically attributed to *H. pylori* infection.

4.2. Characterization of the influence of H. pylori infection on intestinal/colonic carcinogenesis

To assess the carcinogenic potential of *H. pylori* in the colon, colon cancer mouse models, $Apc^{+/1638N}$ and $Apc^{+/min}$ mice were infected. Homozygous *Apc* wild type littermates ($Apc^{+/+}$) were used as controls. Those mouse models are resembling the human disease of familial adenomatous polyposis coli (FAP) and are known to develop multiple polyps and tumors in the intestine and colon. $Apc^{+/1638N}$ mice have been described extensively and develop tumors in both intestine and colon, often progressing to carcinomas with increasing age (199). In contrast, $Apc^{+/min}$ mice are known to develop high numbers of polyps in the intestine already at an earlier age, but tumors are only seldomly located in the colon and do not progress to carcinomas (198).

4.2.1. *H. pylori* drives tumor development in $Apc^{+/1638N}$ and $Apc^{+/min}$ mice

$Apc^{+/1638N}$ mice were infected for 12 and 24 weeks, in order to assess the effect of infection in both early and late stages of tumor development (Figure 4.11a and 4.11b). This revealed an increased tumor burden and tumor size in $Apc^{+/1638N}$ mice after 12 and 24 weeks of infection, compared to non-infected animals (Figure 4.11c). $Apc^{+/min}$ mice were analyzed after 12 weeks of infection (Figure 4.11d and 4.11e), as only 60% of the mice survived 12 weeks of infection (Figure 4.11f). Also in this mouse model an increased tumor number in both intestine and colon, compared to non-infected controls was found (Figure 4.11g).

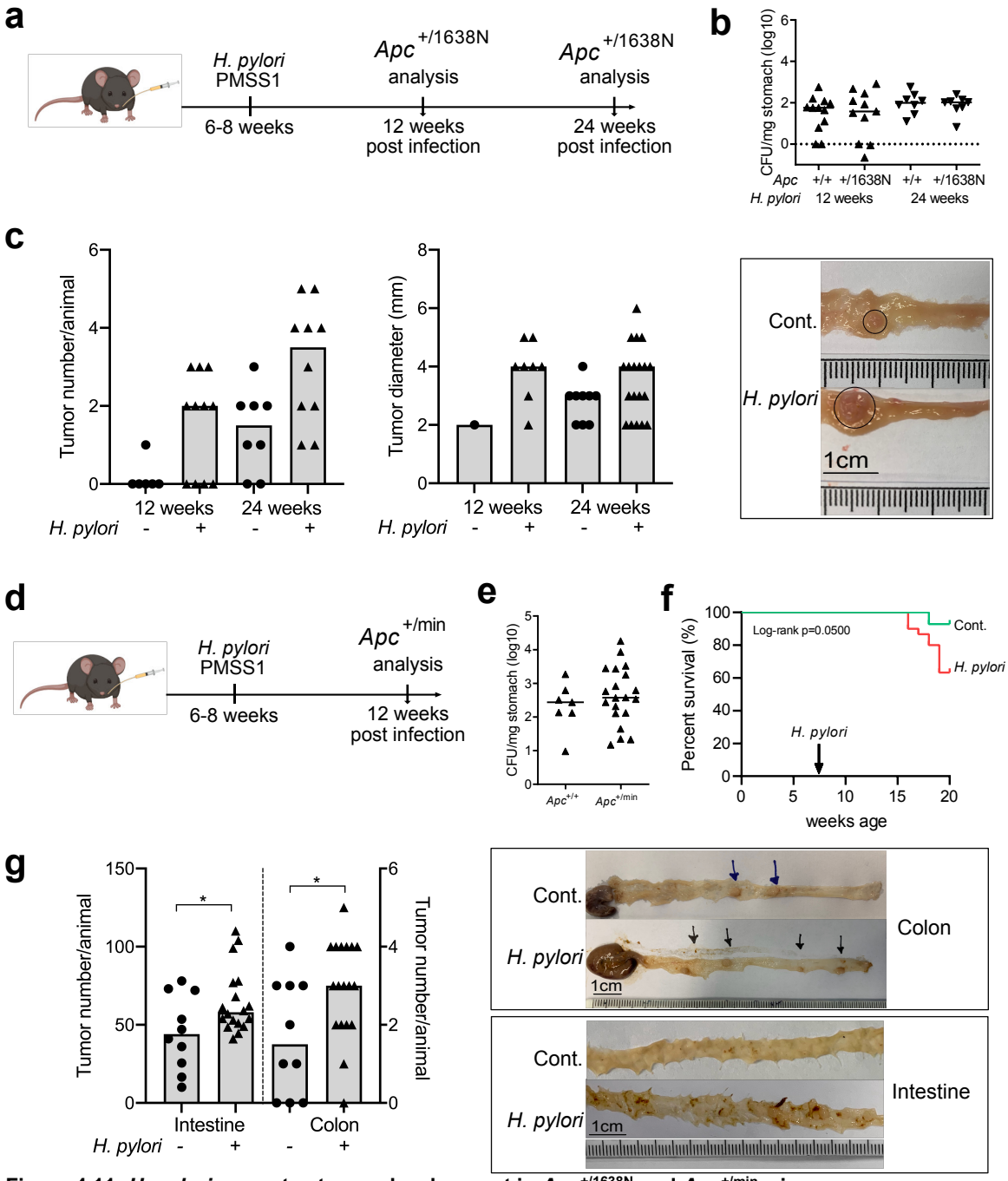

Figure 4.11: *H. pylori* promotes tumor development in *Apc*$^{+/1638N}$ and *Apc*$^{+/min}$ mice.
(a) Experimental setup for infection of *Apc*$^{+/1638N}$ mice. (b) CFU counts per mg stomach 12 weeks and 24 weeks after infection from *Apc*$^{+/1638N}$ mice and littermate controls (*Apc*$^{+/+}$) are shown. (c) Tumor number and diameter (in mm) as well as representative pictures of non-infected (Cont.) and infected *Apc*$^{+/1638N}$ mice are shown. (d) Experimental setup for infection of *Apc*$^{+/min}$ mice. (e) CFU counts per mg stomach 12 weeks after infection from *Apc*$^{+/min}$ mice and littermate controls (*Apc*$^{+/+}$) are shown. (f) Kaplan-Meier survival curve comparing *H. pylori* infected and non-infected *Apc*$^{+/min}$ mice. (g) Tumor counts of *H. pylori* infected and non-infected *Apc*$^{+/min}$ mice in intestine and colon and representative pictures of non-infected (Cont.) and infected (*H. pylori*) animals are shown. Each symbol represents one animal, from 2-3 independent experiments. Bars denote median. Statistical significance was determined with Mann-Whitney-U test or unpaired t-test, *p < 0.05.

4.2.2. *H. pylori* infection induces pro-inflammatory T-cell response in Apc$^{+/1638N}$ and Apc$^{+/min}$ mice

To identify underlying mechanisms of the tumor-promoting effect of *H. pylori* in *Apc* mouse models, the T-cell response in those mice was characterized, as this response was found

to be altered upon *H. pylori* infection in WT mice. The increased T-cell infiltration into the stomach upon infection was confirmed, however, no significant changes between mutant mice and littermate wildtype controls were detected (Figure 4.12a). Furthermore, significantly higher $CD3^+$ T-cell infiltration upon *H. pylori* infection in $Apc^{+/1638N}$ and $Apc^{+/min}$ mice compared to non-infected controls in both proximal and distal intestine (Figure 4.12b) as well as colon (Figure 4.12c) were observed. Similarly as in WT mice, a reduction of Tregs in *H. pylori* infected mice (Figure 4.12d) was found, which is remarkable, as it is known that especially in the $Apc^{+/min}$ mouse model, Tregs are increased and are important for tumor immune evasion (221). Also in those mice, an antigen-specific IL-17 response was detected upon restimulation of intestinal lymphocytes with whole *H. pylori* lysate (Figure 4.12e).

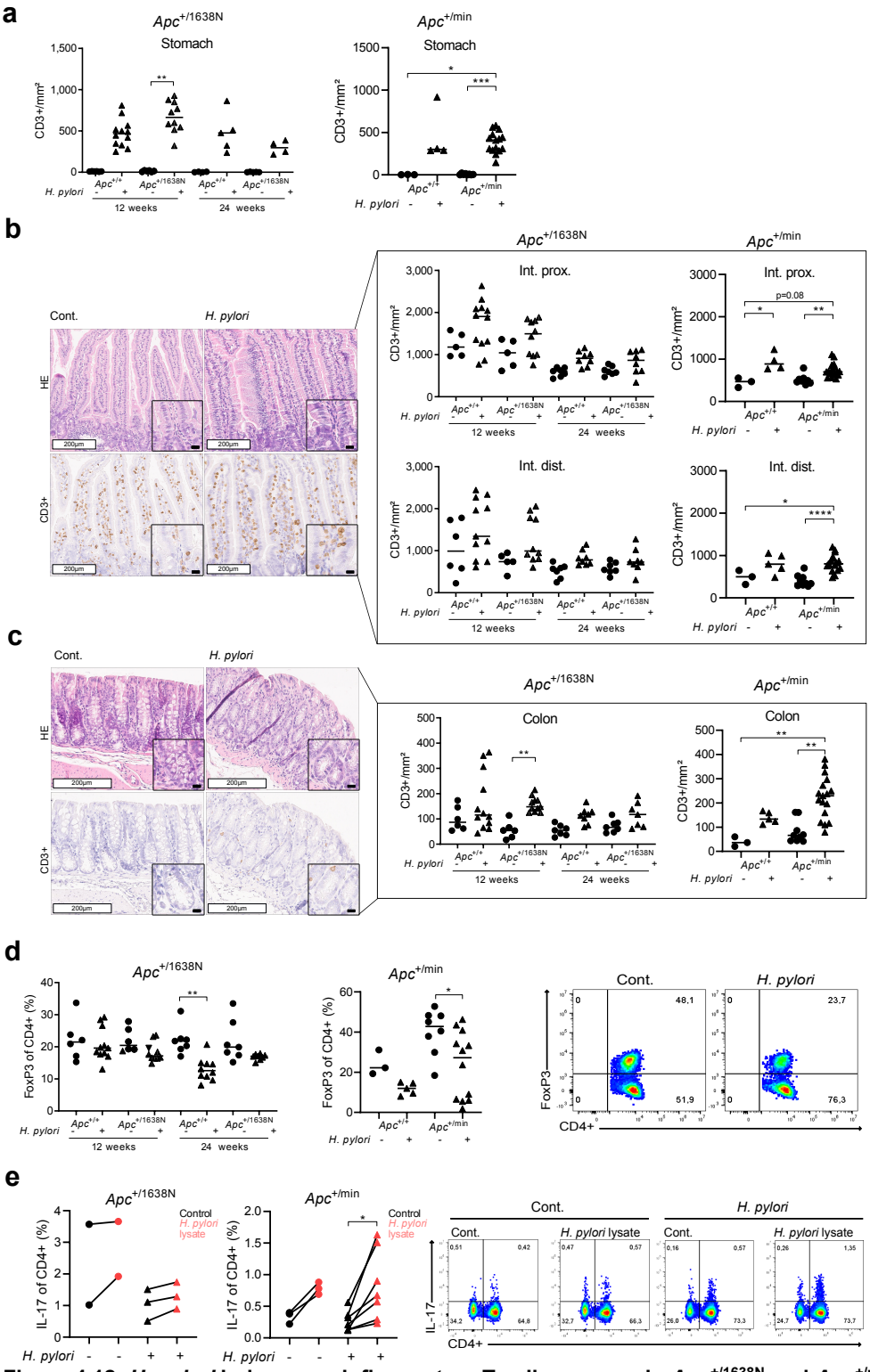

Figure 4.12: *H. pylori* induces proinflammatory T-cell response in *Apc*$^{+/1638N}$ and *Apc*$^{+/min}$ mice.
(a) Quantifications of intraepithelial CD3$^+$ cells per mm^2 stomach tissue of *Apc*$^{+/1638N}$ and of *Apc*$^{+/min}$ mice are shown. (b) Representative images of HE and CD3$^+$ staining of intestinal epithelium and quantifications of intraepithelial CD3$^+$ cells per mm^2 are shown. White scale bar corresponds to 200µm, small scale bar to 20µm. (c) Representative images of HE and CD3$^+$ staining of colonic epithelium and quantifications of intraepithelial CD3$^+$ cells per mm^2 are shown. White scale bar corresponds to 200µm, small scale bar to 20µm. (d) FoxP3$^+$ Tregs are shown, gated on single cells, live, CD45$^+$, CD3$^+$ and CD4$^+$. Cells are shown as percentages of CD4$^+$ T-cells with representative pseudocolor plots. (e) Frequencies of IL-17 releasing CD4$^+$ T-cells are shown, gated on live, CD45$^+$, CD3$^+$ and CD4$^+$. Cells are shown as percentages of CD4$^+$ T-cells with representative pseudocolor plots. Dots represent data of individual mice. Horizontal bars indicate medians. Statistical significance was determined with one-way ANOVA with Tukey's multiple comparisons in case of normal distribution, otherwise with Kruskal Wallis test with Dunn's multiple comparisons, *p<0.05, **p<0.01, ***p>0.001, ****p<0.001.

4.2.3. *H. pylori* infection activates STAT3 signaling, enhances proliferation and reduces mucus producing goblet cells in Apc$^{+/1638N}$ and Apc$^{+/min}$ mice

Given that disturbance of intestinal tissue homeostasis contributes to tumor formation and progression and against the background that effects of *H. pylori* infection on epithelial cell homeostasis have been observed in WT mice, the influence of infection on the epithelial cells in *Apc* tumor mouse models were evaluated. First, the activation of pro-inflammatory STAT3 signaling was assessed, which indeed was significantly higher in *H. pylori* infected mice, in both proximal and distal intestine (Figure 4.13a) as well as in colon (Figure 4.13b). As expected, the baseline activation of STAT3 signaling was higher in *Apc* mutant mice compared to the littermate controls, which was further increased by infection.

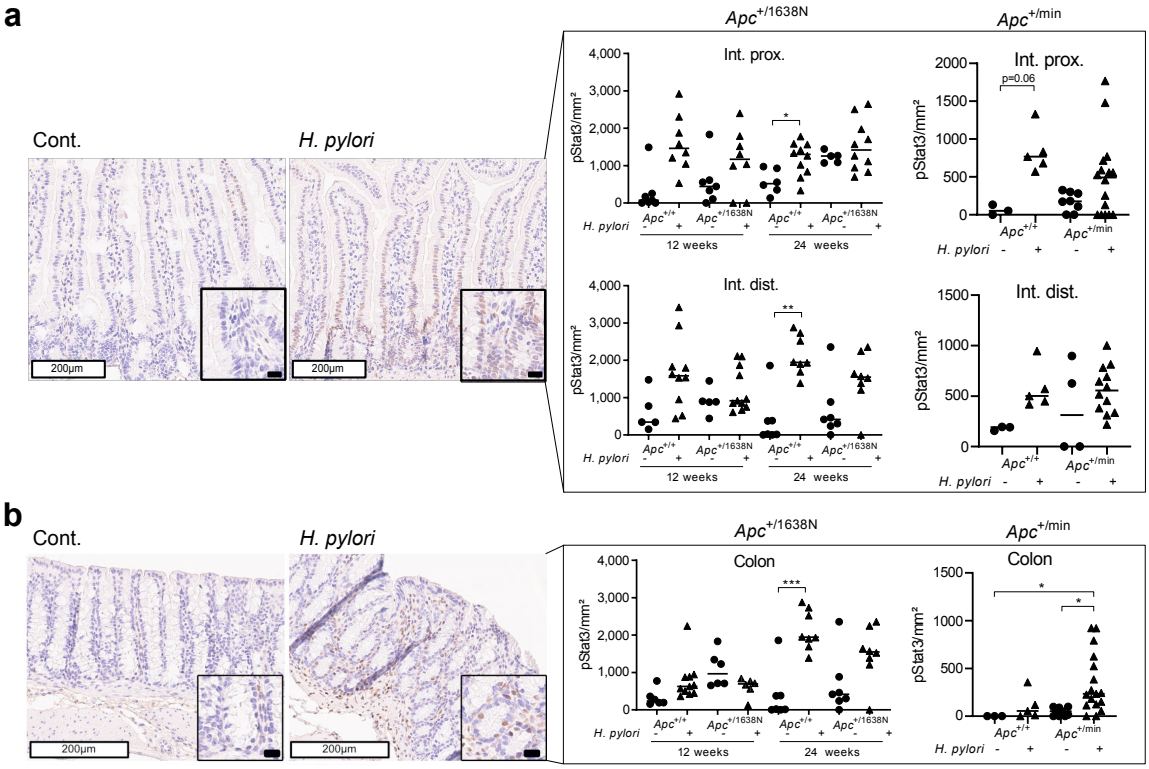

Figure 4.13: *H. pylori* enhances activation of STAT3 signaling in *Apc*$^{+/1638N}$ and *Apc*$^{+/min}$ mice.
(a) Representative pictures of pSTAT3 staining of intestinal tissue of of *Apc*$^{+/1638N}$ and of *Apc*$^{+/min}$ mice are shown. White scale bar corresponds to 200µm, small scale bar to 20µm. Quantification of positive cells per mm^2 proximal and distal intestinal tissue is shown. (b) Representative pictures of pSTAT3 staining of colon tissue of of *Apc*$^{+/1638N}$ and of *Apc*$^{+/min}$ mice are shown. White scale bar corresponds to 200µm, small scale bar to 20µm. Quantification of positive cells per mm^2 colon tissue is shown. Dots represent data of individual mice. Horizontal bars indicate medians. Statistical significance was determined with one-way ANOVA with Tukey's multiple comparisons in case of normal distribution, otherwise with Kruskal Wallis test with Dunn's multiple comparisons, *p<0.05, **p<0.01, ***p>0.001, ****p<0.001.

Next, the impact of *H. pylori* infection on mucus producing cells in *Apc* mouse models was investigated. PAS staining revealed a loss of mucus producing cells in both *Apc*$^{+/1638N}$ *and* *Apc*$^{+/min}$ mice, which was evident in the proximal and distal intestine (Figure 4.14a) as well as the colon (Figure 4.14b)

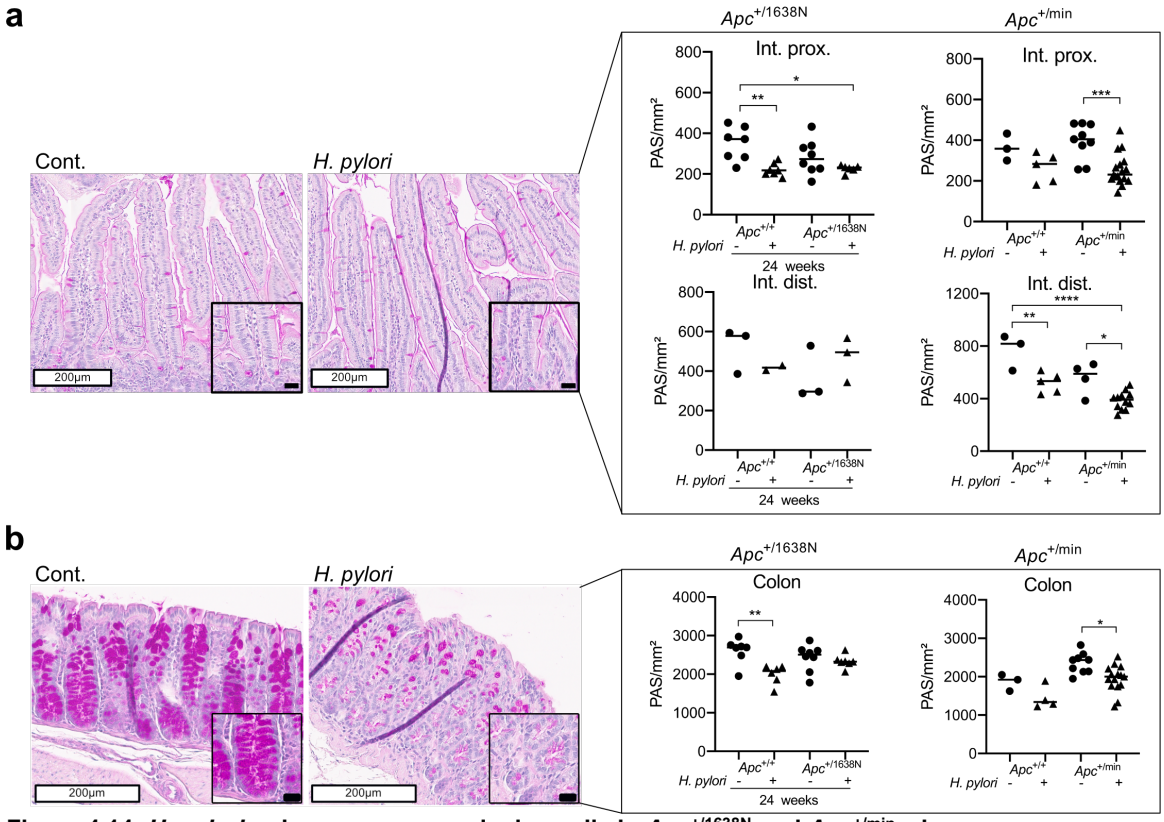

Figure 4.14: *H. pylori* reduces mucus producing cells in *Apc*$^{+/1638N}$ and *Apc*$^{+/min}$ mice.
(a) Representative pictures of PAS staining of intestinal tissue of of *Apc*$^{+/1638N}$ and of *Apc*$^{+/min}$ mice are shown. White scale bar corresponds to 200µm, small scale bar to 20µm. Quantification of positive cells per mm^2 proximal and distal intestinal tissue is shown. (b) Representative pictures of PAS staining of colon tissue of of *Apc*$^{+/1638N}$ and of *Apc*$^{+/min}$ mice are shown. White scale bar corresponds to 200µm, small scale bar to 20µm. Quantification of positive cells per mm^2 colon tissue is shown. Dots represent data of individual mice. Horizontal bars indicate medians. Statistical significance was determined with one-way ANOVA with Tukey's multiple comparisons in case of normal distribution, otherwise with Kruskal Wallis test with Dunn's multiple comparisons, *p<0.05, **p<0.01, ***p>0.001, ****p<0.001.

Those data confirm the phenotype that was previously observed in WT mice upon *H. pylori* infection and suggest that *H. pylori*-induced changes in epithelial signatures, namely the activation of proinflammatory STAT3 signaling in epithelial cells, as well as the loss of mucus producing goblet cells, might contribute to colon carcinogenesis.

4.2.4. *H. pylori* infection shapes gut microbiota in Apc$^{+/1638N}$ and Apc$^{+/min}$ mice

Increasing amount of literature highlights that disturbances in gut microbiota and certain microbiome compositions are contributing to development and progression of CRC (176, 177). To assess distinct changes in gut microbiota of *Apc*$^{+/1638N}$ *and Apc*$^{+/min}$ mice and whether *H. pylori* infection is further shaping the composition, 16S rRNA sequencing was performed analogously to the previously described for WT mice, assessing both luminal and tissue-adherent microbiota throughout the gastrointestinal tract.

H. pylori infection resulted in changes in alpha-diversity in both *Apc*$^{+/1638N}$ *and Apc*$^{+/min}$ mice (Figure 4.15a and Figure 4.16a). Furthermore, distinct taxonomic profiles were detectable

in *Apc*$^{+/1638N}$ *and* *Apc*$^{+/min}$ mice in comparison to WT littermates, which was further influenced by infection (Figure 4.15b, Figure 4.16b). Given the previously observed increase in mucus-degrading bacteria upon *H. pylori* infection in WT mice (Figure 4.8d), their frequency in *Apc* mutant mice was evaluated. Indeed, predominantly *Akkermansia spp.* was found to be increased in infected *Apc*$^{+/1638N}$ mice and *Ruminococcus spp.* in infected *Apc*$^{+/min}$ mice (Figure 4.15c and Figure 4.16c).

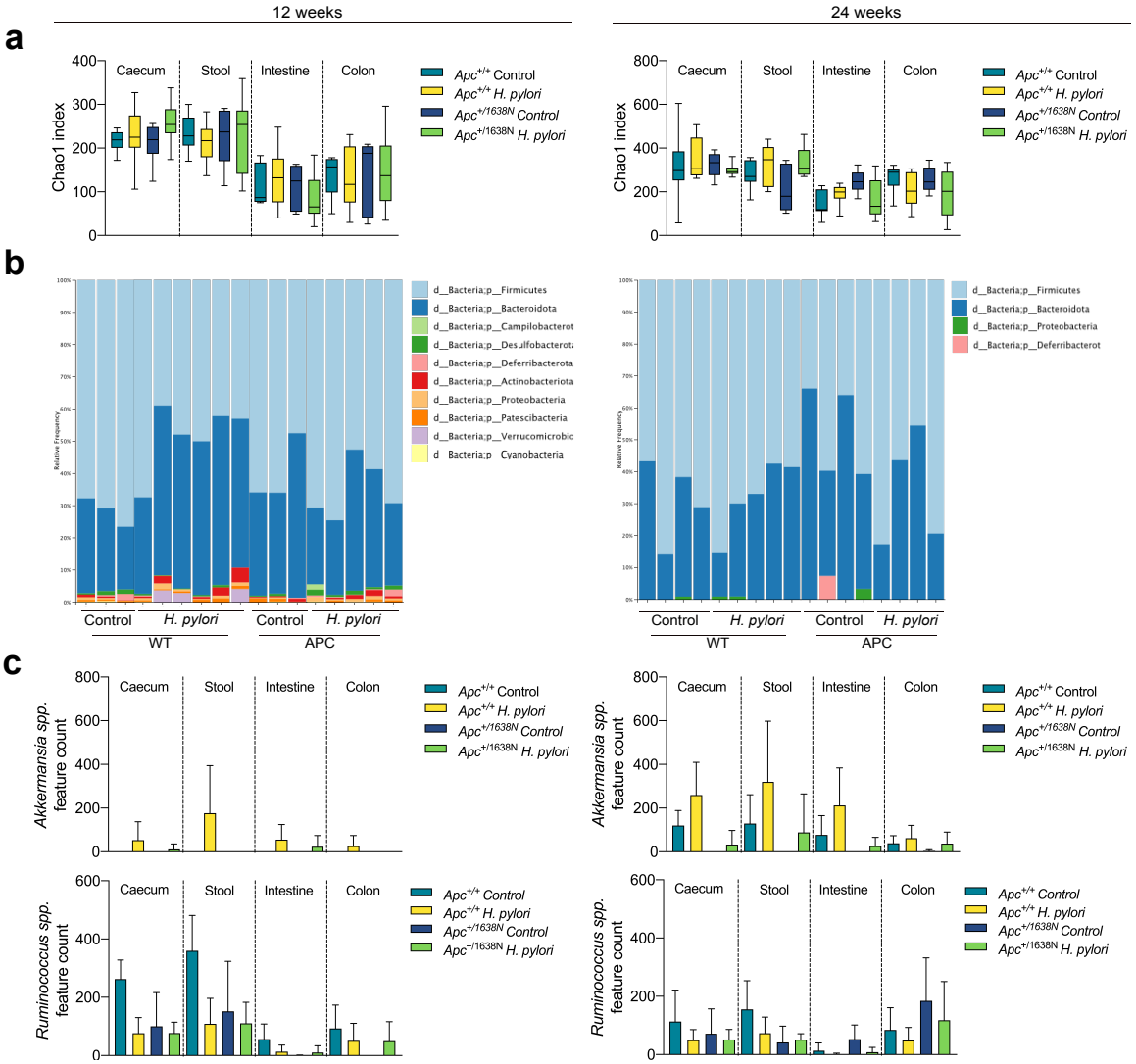

Figure 4.15: *H. pylori* infection shapes gastrointestinal microbiota of Apc$^{+/1638N}$ mice.
(a) Chao1 index as an indicator of alpha-diversity shown for caecum, stool, intestine and colon of Apc$^{+/1638N}$ and Apc$^{+/+}$ (WT) littermates infected for 12 and 24 weeks and non-infected controls. (b) Taxonomic binning showing relative frequencies at phyla level in stool of non-infected and infected Apc$^{+/1638N}$ and WT mice after 12 weeks and 24 weeks of infection. (c) Feature counts of *Akkermansia* species (spp.) and *Ruminococcus* spp. in ceacum, stool, intestine and colon of non-infected and infected Apc$^{+/1638N}$ and WT mice after 12 weeks and 24 weeks of infection. Chao1 index is depicted as box and whiskers, from min to max. Feature counts shown as bar plots, indicating mean with standard deviation.

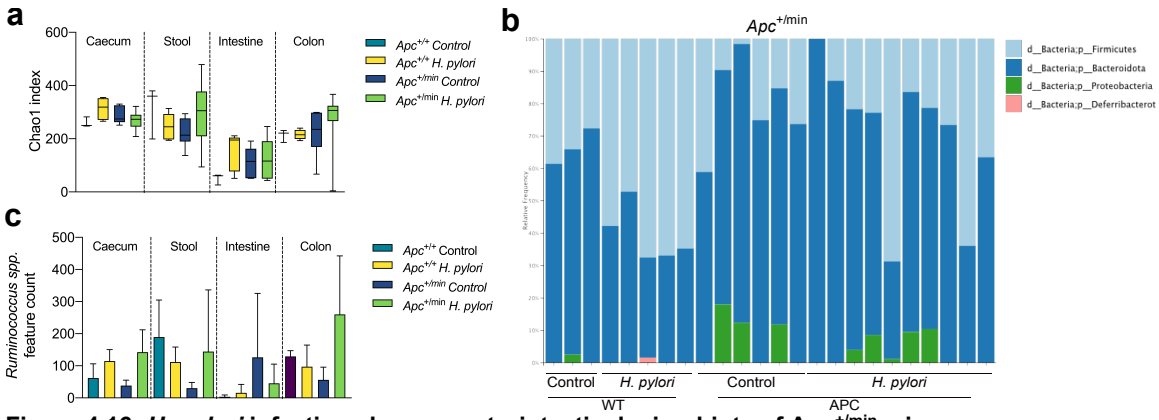

Figure 4.16: *H. pylori* infection shapes gastrointestinal microbiota of Apc$^{+/min}$ mice.
(a) Chao1 index as an indicator of alpha-diversity shown for caecum, stool, intestine and colon of Apc$^{+/min}$ and Apc$^{+/+}$ littermates (WT) infected for 12 weeks and non-infected controls. (b) Taxonomic binning showing relative frequencies at phyla level in stool of non-infected and infected Apc$^{+/min}$ and WT mice after 12 weeks of infection. (c) Feature counts of *Ruminococcus spp.* in ceacum, stool, intestine and colon of non-infected and infected Apc$^{+/min}$ and WT mice after 12 weeks of infection. Chao1 index is depicted as box and whiskers, from min to max. Feature counts shown as bar plots, indicating mean with standard deviation.

In summary, *H. pylori* infection was found to alter microbiota in *Apc* mouse models and, similarly as in WT mice, infection induced a mucus-degrading signature. When looking at the effect of *Apc* muation, by comparing *Apc* mutant and WT mice, changes could be observed in alpha-diversity and relative abundances, however these differences were not as pronounced as the effects upon infection with *H. pylori*.

4.2.5. *H. pylori*-induced immune and epithelial signatures depend on the presence of gut microbiota and level to non-infected controls upon eradication therapy.

Considering the known contribution of gut microbiota to carcinogenic processes and the observed effects of *H. pylori* infection on gut microbiota compositions in WT and *APC* mutant mice, germ-free *Apc*$^{+/1638N}$ mice were infected with *H. pylori* in order to determine the relevance of *H. pylori* induced microbiota signatures in the mechanism by which *H. pylori* contributes to CRC (Figure 4.17a and 4.17b). This revealed only slightly enhanced tumor number and normalization of tumor diameter to the levels of non-infected *Apc*$^{+/1638N}$ mice, indicating that the tumor-promoting effects of *H. pylori* infection were particularly lower in germ-free mice (Figure 4.17c). When evaluating the immune response in germ-free mice, *H. pylori* infection was still inducing a pro-inflammatory environment with an increased T-cell infiltration into stomach, intestine and colon (Figure 4.17d) and a reduction of regulatory T-cells (Figure 4.17e). Additionally, a *H. pylori* specific IL-17 response upon restimulation of lymphocytes derived from germ-free mice with *H. pylori* lysate was observed (Figure 4.17f). In contrast, neither significant activation of STAT3 signaling in intestine and colon (Figure 4.17g), nor a reduction of mucus producing goblet cells were identified in *H. pylori* infected germ-free mice (Figure 4.17h).

To ultimately assess the contribution of *H. pylori* induced changes in microbiota to intestinal carcinogenesis, a stool transfer experiment was performed. Therefore, stool was

obtained from 4 different groups, namely SPF non-infected and *H. pylori* infected Apc$^{+/1638N}$ and Apc$^{+/+}$ mice, respectively, and transferred into germ-free Apc$^{+/1638N}$ mice (Figure 4.17i). Higher tumor numbers in stool recipients from H. pylori infected mice were found, which was already evident in Apc$^{+/+}$ mice and further enhanced in an Apc$^{+/1638N}$ background (Figure 4.17j). This indicates a strong contribution of *H. pylori*-induced changes in microbiota to the tumor phenotype.

Altogether, these results show that *H. pylori* induced tumorigenesis in *Apc$^{+/1638N}$* mice depends on the presence of gut microbiota and that the combined alterations of immune and epithelial components elicited by *H. pylori* is required for its tumor promoting effects.

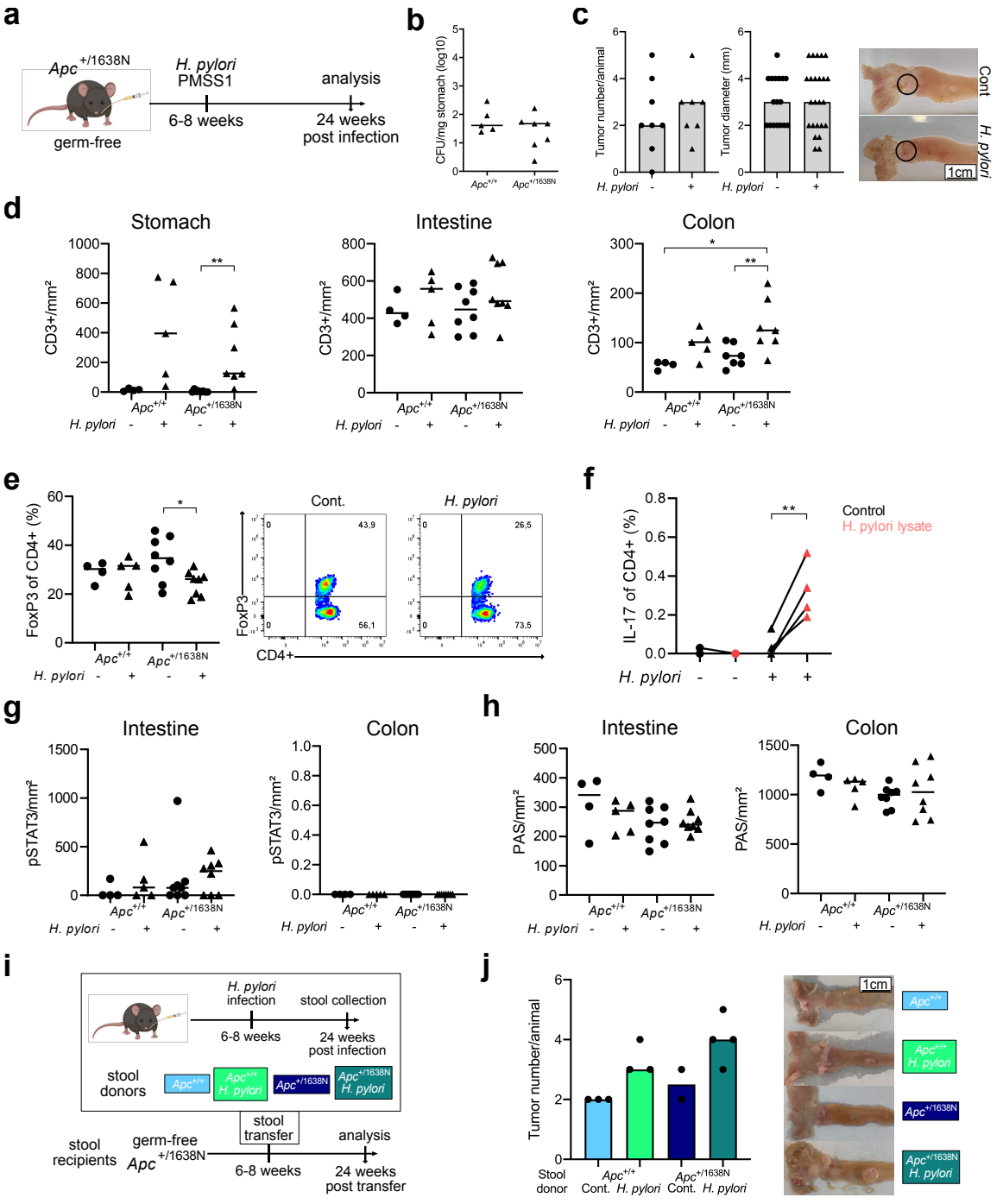

Figure 4.17: *H. pylori*'s cancer promoting effects are depending on the presence of gut microbiota.
(a) Experimental setup of infection of germ-free *Apc*$^{+/1638N}$ mice. (b) CFU counts per mg stomach 24 weeks after infection from *Apc*$^{+/1638N}$ mice and littermate controls (*Apc*$^{+/+}$) (WT) are shown. (c) Tumor number and diameter (in mm) as well as representative pictures of non-infected (Cont.) and infected germ-free mice are shown. (d) CD3^{+} T-cell infiltration into gastric, intestinal and colonic epithelium of germ-free mice are shown as quantification of positive cells per mm^2. (e) Regulatory T-cells of *H. pylori* infected and non-infected germ-free *Apc*$^{+/1638N}$ and WT mice are shown as frequencies of FoxP3^{+} CD4^{+} cells, gated on single, live, CD45 and CD3^{+} cells with representative pseudocolor plots. (f) Paired frequency of IL-17 releasing CD4^{+} cells are shown of *H. pylori* infected and non-infected germ-free *Apc*$^{+/1638N}$ mice, not stimulated and restimulated with *H. pylori* lysate (red). (g) Quantification of epithelial pSTAT3 positive cells per mm^2 intestine and colon tissue of *H. pylori* infected and non-infected germ-free *Apc*$^{+/1638N}$ and WT mice is shown. (h) Quantification of PAS positive cells per mm^2 intestine and colon tissue of *H. pylori* infected and non-infected germ-free *Apc*$^{+/1638N}$ and WT mice is shown. (i) Experimental setup for stool transfer from specific-pathogen free mice (non-infected and *H. pylori* infected Apc$^{+/+}$ or Apc$^{+/1638N}$ mice, respectively, (stool donors)) to germ-free Apc$^{+/1638N}$ mice (stool recipients). (j) Intestinal tumor counts of stool transfer experiments are shown. Statistical significance was determined with one-way ANOVA with Tukey's multiple comparisons in case of normal distribution, otherwise with Kruskal Wallis test with Dunn's multiple comparisons, *p<0.05, **p<0.01.

To ultimately confirm that *H. pylori* is responsible for the observed phenotype, *H. pylori* infected *Apc*$^{+/1638N}$ mice were next treated with the same eradication regimen as described in section 1.1.4, which successfully eradicated *H. pylori* in those mice (Figure 4.18a and 4.18b). Indeed, the tumor load of eradicated *Apc*$^{+/1638N}$ mice was reduced to the level of non-infected mice, while it was significantly increased in non-eradicated mice (Figure 4.19c). Next, the intestinal and colonic immune response was assessed and revealed that T-cell infiltration normalizied upon eradication (Figure 4.18d), whereas the reduction of regulatory T-cells did not reach baseline levels (Figure 4.18e). Furthermore, the elicited T-cell response was detected to be antigen-specific in *H. pylori* infected as well as eradicated *Apc*$^{+/1638N}$ mice (Figure 4.18f). The activation of STAT3 signaling normalized to non-infected controls in intestinal epithelium upon eradication (Figure 4.19g), as did the number of mucus producing goblet cells in both intestine and colon of *Apc*$^{+/1638N}$ mice (Figure 4.19h).

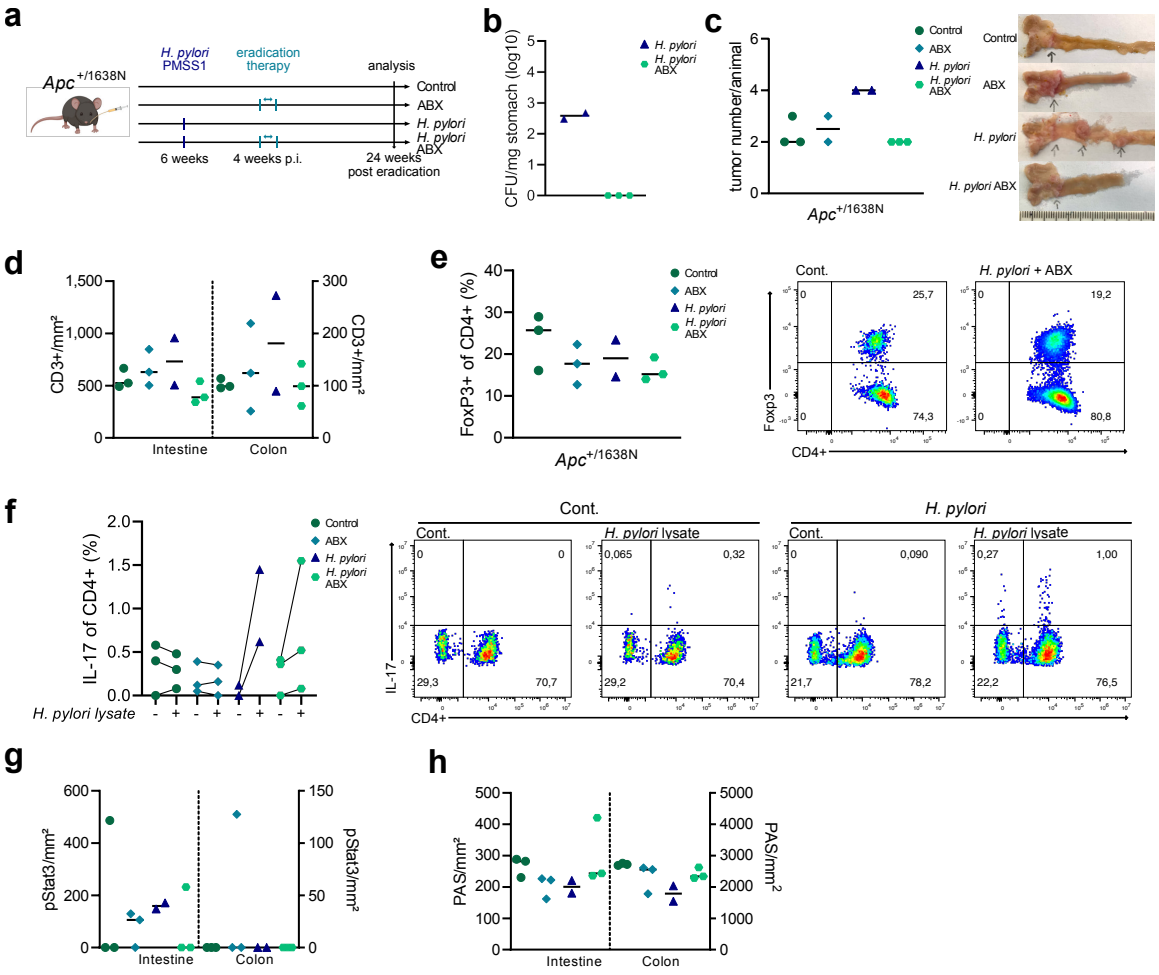

Figure 4.18: *H. pylori*'s cancer promoting effects are reversible upon eradication.
(a) Experimental setup of infection and eradication of *Apc*$^{+/1638N}$ mice. (b) CFU counts per mg stomach 24 weeks after eradication of *Apc*$^{+/1638N}$ mice are shown. (c) Tumor number as well as representative pictures of non-infected (Control), eradicated (ABX), infected (*H. pylori*) and infected and eradicated (*H. pylori* ABX) *Apc*$^{+/1638N}$ mice are shown. (d) CD3^{+} T-cell infiltration into intestinal and colonic epithelium are shown as quantification of positive cells per mm^2. (e) Regulatory T-cells are shown as frequencies of FoxP3^{+} CD4^{+} cells, gated on single, live, CD45^{+} and CD3^{+} cells with representative pseudocolor plots. (f) Paired frequency of IL-17 releasing CD4^{+} cells are shown from not stimulated and with *H. pylori* lysate restimulated lamina propria lymphocytes, gated on single, live, CD45^{+} and CD3^{+} cells with representative pseudocolor plots. (g) Quantification of epithelial pSTAT3 positive cells per mm^2 intestine and colon tissue is shown. (h) Quantification of PAS positive cells per mm^2 intestine and colon tissue is shown.

4.2.6. Single cell RNA Sequencing reveals molecular mechanisms in *H. pylori*-induced colon carcinogenesis

To identify detailed molecular pathways involved in the tumor promoting properties of *H. pylori*, the immune and epithelial cell compartments were investigated on a single cell level by single-cell RNA sequencing using the 10X genomics platform. Therefore, CD45^{+} immune cells and EPCAM^{+} epithelial cells isolated from the intraepithelial and lamina propria compartments of intestinal and colonic tissue from *Apc*$^{+/min}$ (APC) mice and littermate controls (WT) that had been infected for 12 weeks were sorted and compared to non-infected controls (Fig. 4.19a). Unsupervised clustering identified 16 clusters of CD45^{+} cells and 15 clusters of EPCAM^{+} cells according to their transcriptional profiles, which were visualized using Uniform Manifold Approximation and Projection (UMAP) (222)

(Figure 4.19b) and annotated based on known marker genes (Figure 4.19d and 4.19e). The overall frequencies of annotated CD45$^+$ cell clusters showed distinct differences in intestine and colon and were influenced by genotype and infection (Figure 4.19f). In epithelial cells, organ specific clusters of stem cells and enterocytes were detected, leading to different clusters in intestine and colon. Also here, the overall frequencies of annotated EPCAM$^+$ cell clusters were influenced by genotype and infection (Figure 4.19g).

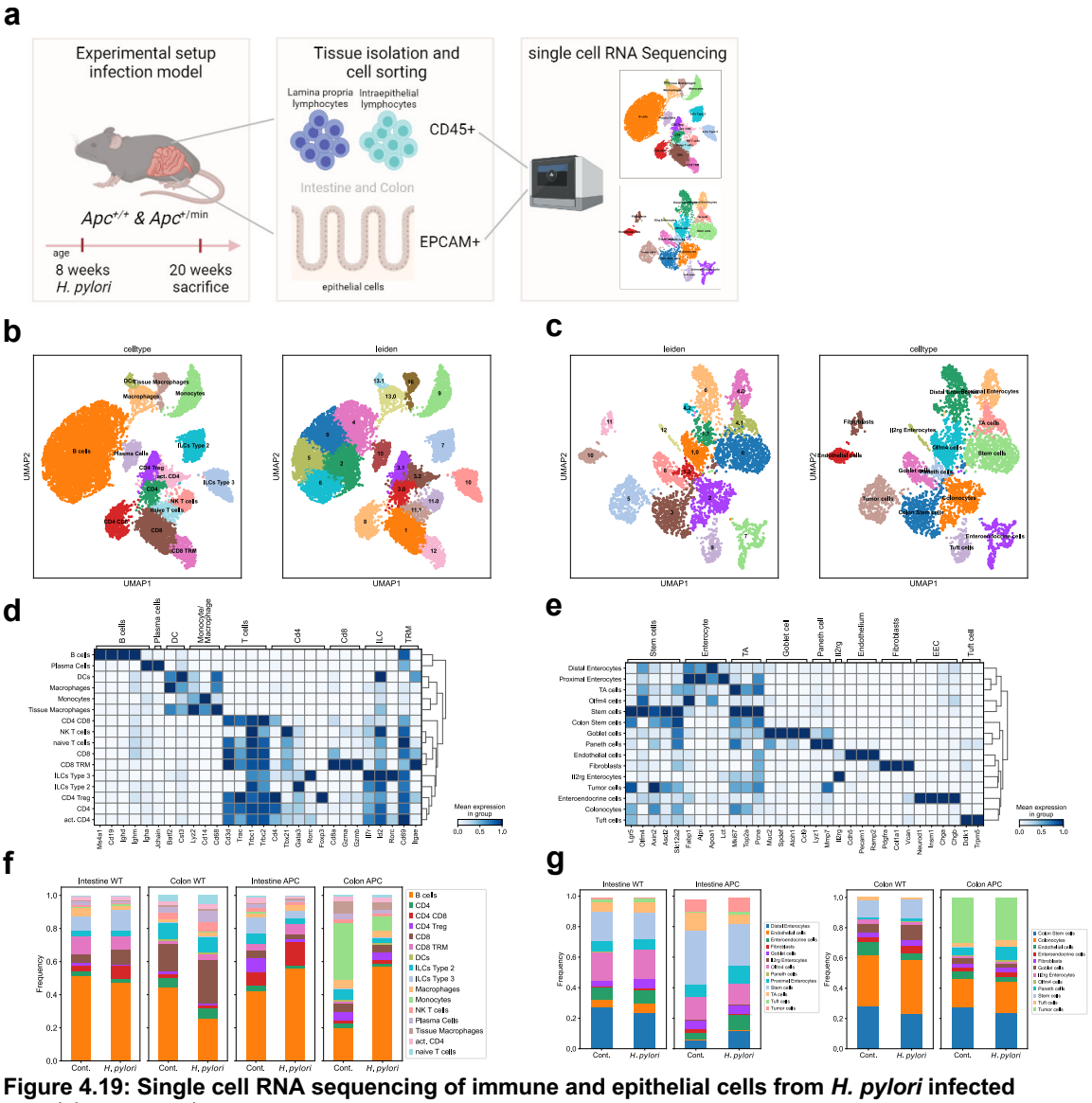

Figure 4.19: Single cell RNA sequencing of immune and epithelial cells from *H. pylori* infected *Apc$^{+/min}$* and *Apc$^{+/+}$* mice.
(a) Experimental setup of single cell RNA sequencing of CD45$^+$ and EPCAM$^+$ cells isolated from intestine and colon of *H. pylori* infected and non-infected A*pc*$^{+/min}$ and A*pc*$^{+/+}$ mice. (b) Annotated immune cells after unsupervised clustering plotted as uniform manifold approximation and projection (UMAP), n=2 mice per group, n= 11407 cells. (c) Annotated epithelial cells after unsupervised clustering plotted as UMAP, n=2 mice per group, n= 4249 cells. (d) Gene matrix of marker genes used for annotation of CD45$^+$ clusters. (e) Gene matrix of marker genes used for annotation of EPCAM$^+$ clusters. (f) Relative frequency of CD45$^+$ cell types in intestine and colon of A*pc*$^{+/+}$ (WT) and A*pc*$^{+/min}$ (APC) mice, grouped by infection. (g) Relative frequency of EPCAM$^+$ cell types in intestine and colon of WT and APC mice, grouped by infection.

Within this study, a strong and consistent effect of *H. pylori* infection on Tregs were observed, which is why this cluster was subclustered and annotated based on published

marker genes, resulting in three subclusters: activated Tregs (act. Tregs), peripherally induced Tregs (iTregs), characterized by high RORyt^{+} expression, and thymus-derived Tregs (nTregs), characterized by GATA3^{+} expression (223, 224) (Figure 4.20a and 4.20b). When looking into the distribution of these subclusters across organ and genotype upon infection, an increase of act. Tregs in APC mutant mice (Figure 4.20c) was observed. To get insight into their functionality, a Treg effector score (225) identified that act. Tregs and nTregs showed a tendency towards reduced effector properties (Figure 4.20d). This led to the assumption, that *H. pylori* infection might reprogram Tregs. Indeed, significantly increased Th17 differentiation genes in infected act. Tregs were identified (Figure 4.20e). CD8^{+} T-cells are known to play an important role in tumor immune surveillance. Next, CD8 and CD8 tissue resident memory (TRM) clusters were subclustered and annotated based on known marker genes (226). This resulted in four CD8 clusters: effector, memory, progenitor exhausted and terminally exhausted CD8 T-cells (Figure 4.20f and 4.20g). In the intestine, *H. pylori* led to a reduction of effector CD8 T-cells and an increase in terminally exhausted T-cells (Figure 4.20h). In order to assess their functionality, a gene score from genes upregulated in exhausted versus effector CD8^{+} T-cells was derived (227), which revealed a higher score in the terminally exhausted cluster of *H. pylori* infected cells, suggesting a more severe exhaustion phenotype upon *H. pylori* infection (Figure 4.20i). To understand cell dynamics of T-cells in APC mutant mice, RNA velocity vectors were identified, which predict future states of individual cells based on ratios of spliced and unspliced mRNAs. This revealed a strong directionality from the CD8 to the CD8 TRM cluster, which consisted mostly of terminally exhausted T-cells (Figure 4.20e).

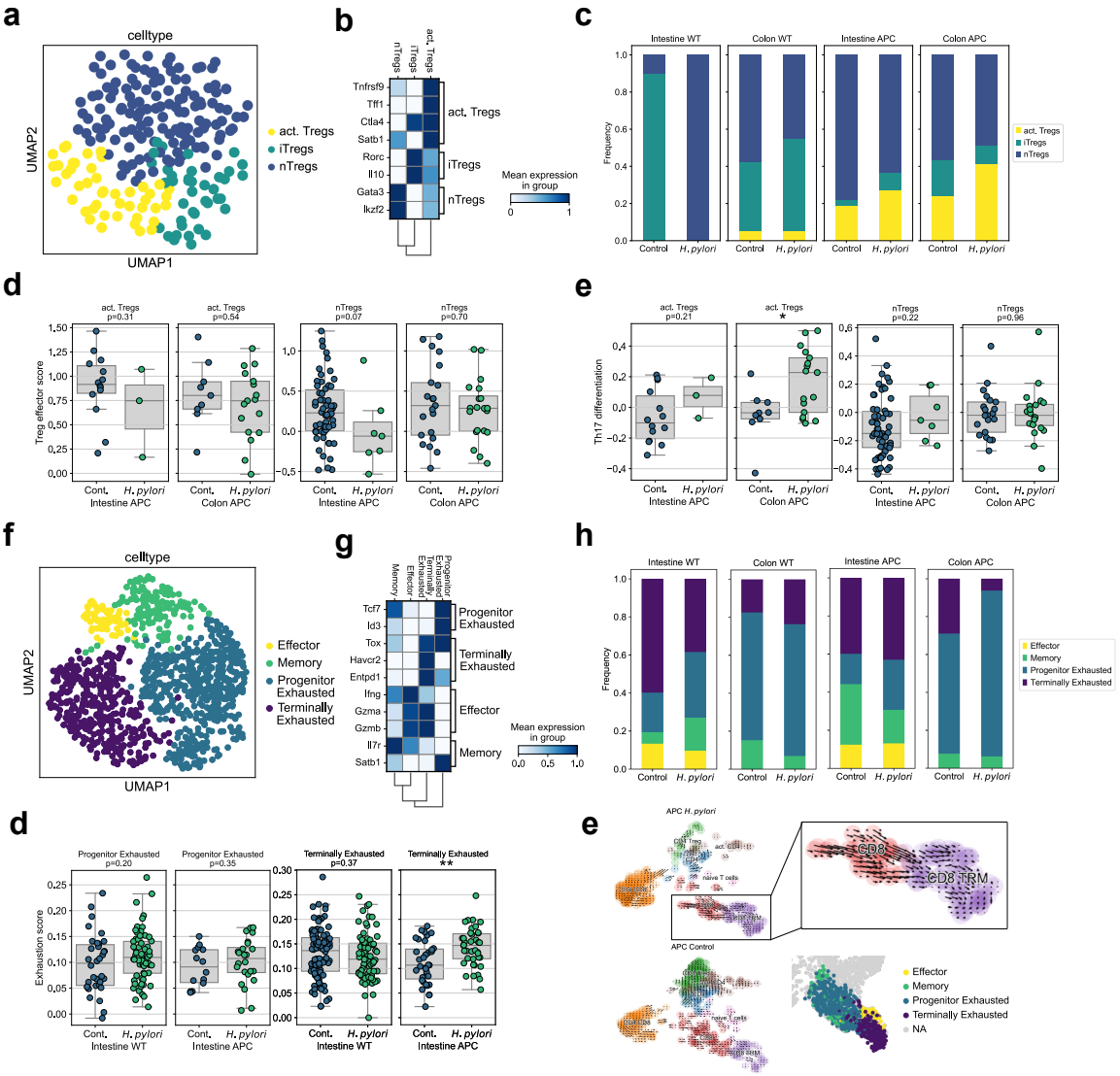

Figure 4.20: *H. pylori* infection dampens regulatory T-cell function and promotes CD8⁺ T-cell exhaustion.
(a) Unsupervised clustering and annotation of Treg cluster as UMAP, n=217 cells. activated Tregs = act. Tregs, iTregs = peripherally induced Tregs, nTregs = thymically derived Tregs. (b) Gene matrix of marker genes used for annotation of Treg subclusters. (c) Relative frequency of Treg cell types in intestine and colon of A*pc*$^{+/+}$ (WT) and A*pc*$^{+/min}$ (APC) mice, grouped by infection. (d) Gene set score of Treg effector genes, comparing Treg cells from intestine and colon of *H. pylori* infected and non-infected A*pc*$^{+/min}$ mice. (e) Gene set score of Th17 differentiation genes comparing Treg cells from intestine and colon of *H. pylori* infected and non-infected A*pc*$^{+/min}$ mice. (f) Unsupervised clustering and annotation of CD8 and CD8 TRM cluster as UMAP, n=986 cells. (g) Gene matrix of marker genes used for annotation of CD8⁺ subclusters. (h) Relative frequency of CD8 cell types in intestine and colon of WT and APC mice, grouped by infection. (i) Gene set score of exhaustion versus effector signatures, comparing progenitor and terminally exhausted CD8 T-cells in intestine from *H. pylori* infected and non-infected WT and APC mice. (i) RNA velocity analysis plotted as UMAP for single CD3⁺ T cells from *H. pylori* infected (APC *H. pylori*) and non-infected A*pc*$^{+/min}$ mice (APC Control). The directional flow of the velocity arrows between cell clusters shows the projection from the observed state to the predicted future state. Zoom into CD8 T-cell RNA velocity analysis of *H. pylori* infected A*pc*$^{+/min}$ mice and visualization of newly identified CD8 subsets in CD45 UMAP. Each symbol represents one single cell. Statistical significance was determined with Kruskal-Wallis test.

Next, transcriptomic profiles of epithelial cells and the impact of *H. pylori* infection on this compartment were assessed. Pseudo-spatial distribution of epithelial cells along the crypt-villus axis (from base to top) were computed to confirm correct annotation of cell types (228, 229) (Figure 4.21a). *H. pylori* infection is known to strongly induce NF-kB signaling in the stomach, which prompted the question whether activation of this pathway is also

seen in intestinal and colonic cell types. Hence, a score of genes involved in NFkB signaling retrieved from the Kyoto Encyclopedia of Genomes and Genes (KEGG) (230, 231) were computed, which showed higher scores in intestinal enterocytes upon *H. pylori* infection (Figure 4.21b). To confirm the extensively described activation of STAT3 signaling in intestine and colon, the same approach was applied and a score of genes involved in the Jak-STAT signaling pathway was retrieved from KEGG (230, 231). This confirmed an increased activation of this pathway, with significantly higher scores in intestinal stem cells and colonocytes of wildtype mice and proximal enterocytes of mutated mice upon *H. pylori* infection (Figure 4.21c). Considering the detrimental effect of *H. pylori* infection on goblet cells, the goblet cell cluster was subclustered and annotated based on differentiation (232), which resulted in three stages of maturation: immature, characterized by high expression of *Tff3*, intermediate, highly expressing Oasis, and terminal goblet cells, high expression of *Muc2* and *Ktlp4* (Figure 4.21d and 4.21e). The correct cell type annotation was confirmed by plotting the expression of *Muc* genes across the different clusters, with terminal goblet cells showing the highest expression (Figure 4.21f). Frequencies across intestinal genotypes were distinctly affected by *H. pylori* infection, with a switch to less differentiated goblet cells (Figure 4.21g). To assess the functionality of the goblet cells, the expression of antimicrobial peptide genes, including *Reg3b* and *Reg3g*, which are known to play a role in response to pathogens and inflammation, was determined. Those peptides were found to be reduced upon *H. pylori* infection (Figure 4.21h). To explain the absolute loss of goblet cells detected by PAS staining, cellular dynamics of goblet cells by means of RNA velocities were studied. In WT mice, less directionality from the stem cell cluster towards the goblet cluster and at the same time more directionality towards colonocyte cluster upon *H. pylori* infection were observed. This phenotype was further pronounced in APC mice, indicating a skewed differentiation of stem cells rather into colonocytes than goblet cells (Figure 4.21i). To get insight into the effect of *H. pylori* infection on tumor cells, differentially expressed genes (DEG) upon infection were identified and gene list annotations of the upregulated genes (-log10p>0.05, log2fc >1) were performed, which revealed that DEG were involved in negative regulation of immune cell proliferation and response, indicating an immune evasion phenotype (Figure 4.21j). Based on previous reports, NOTCH signaling is responsible for tumor microenvironment remodeling towards metastasis and poor prognosis in CRC (233). The NOTCH score from Jackstadt et al. was adapted and showed an increased score in intestinal tumor cells and fibroblasts upon infection (Figure 4.21k).

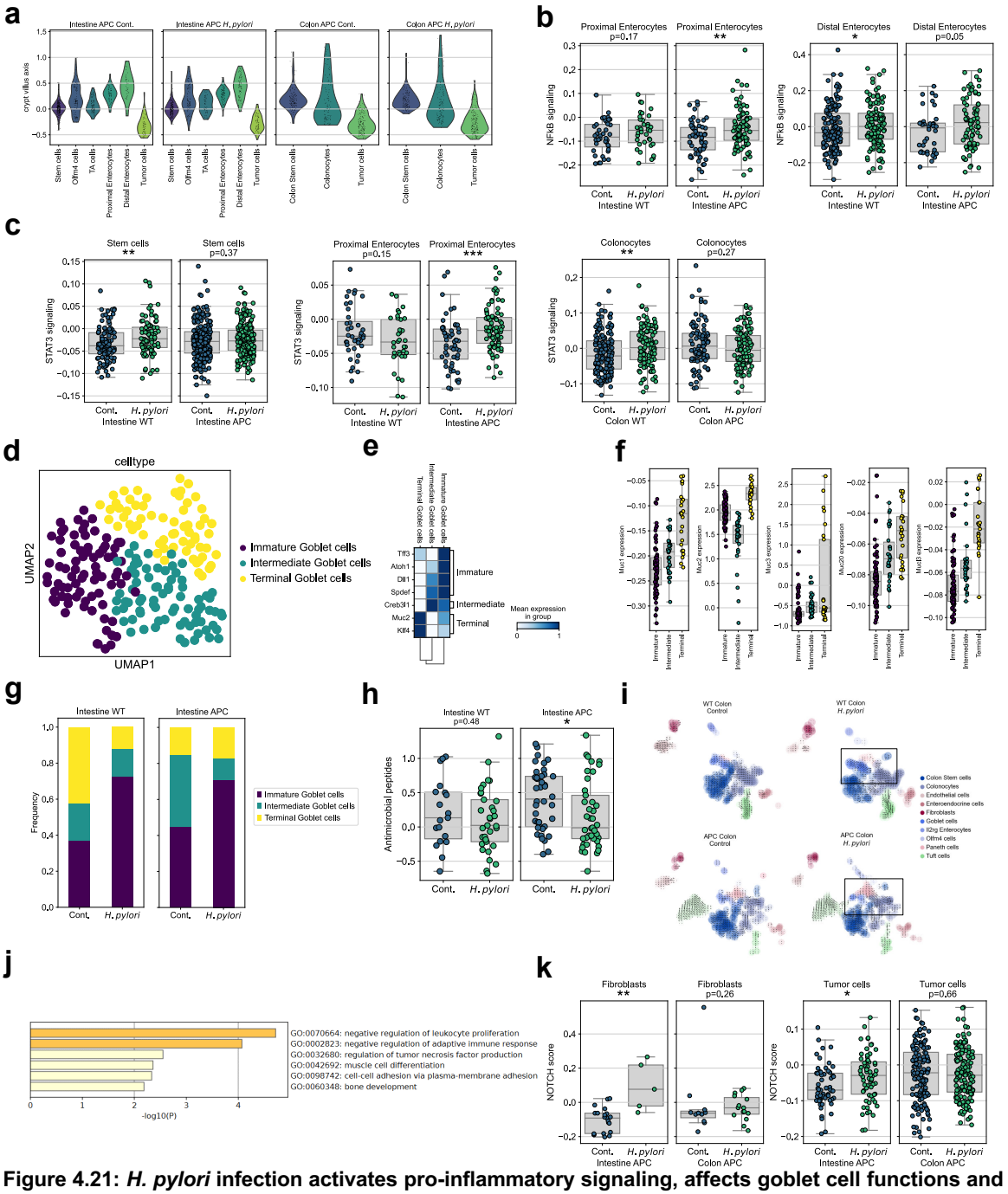

Figure 4.21: *H. pylori* infection activates pro-inflammatory signaling, affects goblet cell functions and induces tumor cell immune evasion.

(a) Pseudo-spatial distribution of stem-cell, enterocyte and tumor cell clusters along the crypt villus axis in intestine and colon of A*pc*$^{+/+}$ (WT) and A*pc*$^{+/min}$ (APC) mice. (b) Gene set score of NFkB signaling genes, comparing epithelial subsets of intestine and colon from *H. pylori* infected and non-infected WT and APC mice. (c) Gene set score of STAT3 signaling genes, comparing epithelial subsets of intestine and colon from *H. pylori* infected and non-infected WT and APC mice. (d) Unsupervised clustering and reannotation of goblet cluster as UMAP, n=218 cells. (e) Gene matrix of marker genes used for annotation of Goblet cell subclusters. (f) Expression of several mucin genes across different Goblet cell subtypes. (g) Relative frequency of goblet subtypes in intestine of WT and APC mice, grouped by infection. (h) Gene set score of antimicrobial peptide genes, comparing goblet cells of intestine from *H. pylori* infected and non-infected WT and APC mice. (i) RNA velocity analysis plotted as UMAP for single EPCAM^{+} cells from intestine of non-infected (left) and *H. pylori* infected WT and APC mice (right). Velocity-inferred cell to cell interactions are shown for stem cell clusters, tumor cells, enterocyte clusters and goblet cells. (j) Gene annotation of differentially expressed genes in tumor cells of *H. pylori* infected APC, log2fc>1, -log10corrected p value <0.05. (k) NOTCH gene set score of tumor cells and fibroblasts from intestine and colon of *H. pylori* infected and non-infected Apc$^{+/min}$ mice (APC) Each symbol represents one single cell. Statistical significance was determined with Kruskal-Wallis test.

In summary, these findings revealed a detrimental effect of *H. pylori* infection on both the immune and epithelial cell compartment. By interfering with regulatory T cell and $CD8^+$ T-cell functions, known to be essential for tumor immune surveillance, as well as reduced goblet cell functionality and hampered differentiation of epithelial cells, transcriptomic profiling revealed that *H. pylori* infection establishes a tumor promoting niche in the intestine and colon, which ultimately may contribute to the increased tumor development and reduced survival in *H. pylori* infected $Apc^{+/min}$ mice.

4.3. Characterization of the influence of *H. pylori* infection on inflammation and signaling pathways in human colon

4.3.1. *H. pylori* induced immune and epithelial signature can be translated into human colon

Finally, the *H. pylori* induced phenotype observed in mice was confirmed in biopsies of human colon. Therefore, 148 colon biopsies derived from endoscopy as well as FFPE biopsies of healthy individuals were analyzed. Histological as well as serological screening allowed to distinguish between currently *H. pylori* infected individuals, *H. pylori* eradicated and *H. pylori* negative individuals (Figure 4.22a). This human cohort displayed evenly distributed patient characteristics regarding age and sex, and approximately one third of the patients was currently positive for *H. pylori* or has been eradicated (Figure 4.22a).

The first aim was to assess the putative effects of *H. pylori* infection on the colonic immune response in human biopsies. *H. pylori* positive and also eradicated individuals exhibited a trend towards higher infiltration of $CD3^+$ T-cells into colonic tissue (Figure 4.22b). This trend was confirmed via flow cytometry and, furthermore, a trend towards higher $CD4^+$ to $CD8^+$ ratio in eradicated and currently infected patients compared to non-infected patients was observed (Figure 4.22c). When assessing Tregs, lower amounts were detected by flow cytometry in currently infected patients and interestingly, eradicated patients seemed to have almost the same numbers of Tregs as negative patients (Figure 4.22d). This reduction of regulatory T-cells was corroborated by multiplexed chip cytometry, which provided additional insight into the loss of intraepithelial T-cells in *H. pylori* positive individuals (Figure 4.22e). Next, the effects of *H. pylori* on STAT3 signaling in human colon were identified and showed more activation of STAT3 in patients suffering from active *H. pylori* infection, however not in eradicated patients (Figure 4.22f), matching to the phenotype in eradicated mice. Likewise, currently infected patients displayed a loss of goblet cells, which however was less pronounced in eradicated patients (Figure 4.22g).

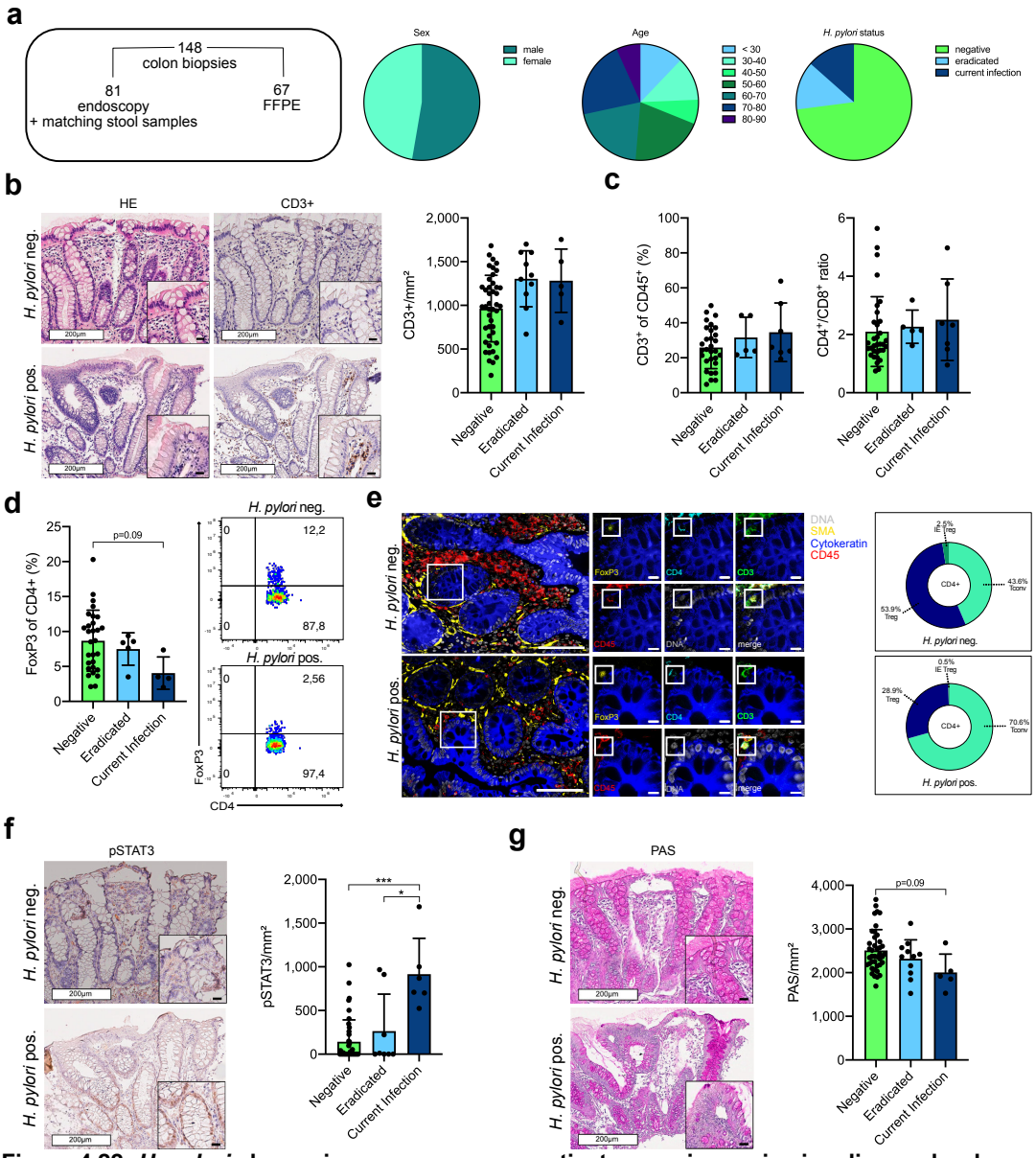

Figure 4.22: *H. pylori* shapes immune response, activates carcinogenic signaling and reduces goblet cells in human colon.

(a) Study design and patient characteristics: 148 colon biopsies were collected, of those 81 from colonoscopies and 67 as FFPE samples. Sex and age distribution as well as *H. pylori* status (negative, eradicated and currently infected) across patients are shown as parts of whole plots. (b) Representative HE and CD3$^+$ pictures of colonic human tissue are shown. White scale bars correspond to 200 µm, black scale bars to 20 µm. Quantification of total CD3$^+$ positive cells per mm^2 are shown. (c) Flow cytometric analysis of *H. pylori* positive and negative colon biopsies were conducted. Frequencies of CD3$^+$ cells of CD45$^+$ cells and CD4$^+$ to CD8$^+$ cell ratio are shown. gated on live, single cells, CD45$^+$ and CD3$^+$. (d) FoxP3$^+$ cells of CD4$^+$ T-cells, gated on live, single cells, CD45$^+$ and CD3$^+$ are shown and representative pseudocolor plots of *H. pylori* positive (current infection) and negative individuals are included. (e) Representative pictures of human colon tissue stained by multiplexed chip cytometry. FoxP3$^+$ cell, defined by intranuclear FoxP3$^+$, CD4$^+$, CD3$^+$ and CD45$^+$ staining is shown for *H. pylori* negative and positive tissue. Large scale bar corresponds to 100µm, small scale bar to 10µm. Automatic image processing of multiplexed chip cytometry on colon tissue determines CD4$^+$ T-cell properties in *H. pylori* positive and negative individuals: frequencies of conventional T-cells (Tconv), regulatory T-cells (Treg) and intraepithelial regulatory T-cells (IE Treg) are shown. (f) Representative pSTAT3 pictures of colonic tissue from *H. pylori* infected (current infection) and non-infected patients are shown. Quantification of intraepithelial pSTAT3 positive cells per mm^2 are shown. (g) Representative PAS pictures of colonic tissue from *H. pylori* infected (current infection) and non-infected patients are shown. Quantification of PAS positive cells per mm^2 are shown. White scale bars correspond to 200 µm, black scale bars to 20 µm. Each symbol represents one patient. Bars denote median. Statistical significance was determined with one-way ANOVA with Tukey's multiple comparisons in case of normal distribution, otherwise with Kruskal Wallis test with Dunn's multiple comparisons, *p<0.05, **p<0.01, ***p>0.001.

4.3.2. *H. pylori* infection affects microbiota in humans

As shown before, *H. pylori* infection has a severe impact on microbiota along the gastrointestinal tract in mice. Therefore, microbiota compositions of matching stool samples from patients with endoscopic colon biopsies were assessed.

No distinct patterns in relative frequencies at phyla level were observed upon taxonomic binning between negative, eradicated and patients with active infection (Fig. 4.23a). When looking into alpha-diversity, a tendency towards less species richness in patients with active *H. pylori* infection was detected (Figure 4.23b). However, a difference in β-diversity between actively *H. pylori* infected and negative patients ($p=0.062$), but not between *H. pylori* eradicated and negative patients ($p=0.552$) could be observed (Figure 4.23c). Furthermore, tendencies towards lower *Firmicutes/Bacteroidetes* ratio in both eradicated and currently infected compared to negative patients was found (Figure 4.23c), which, together with a reduction of alpha-diversity, indicates signs of dysbiosis. Differentially abundant species between *H. pylori* negative and *H. pylori* positive individuals were calculated and revealed that, among others, *Prevotella* and *Peptostreptococcales* were enriched in *H. pylori* positive patients (Figure 4.23d), species found in a previous meta-analysis to be increased in CRC patients (234).

Altogether, this analysis reveals that *H. pylori* affects microbiota compositions in human patients, which are depending on the status of *H. pylori* infection, with evident differences between active infection and patients who underwent eradication.

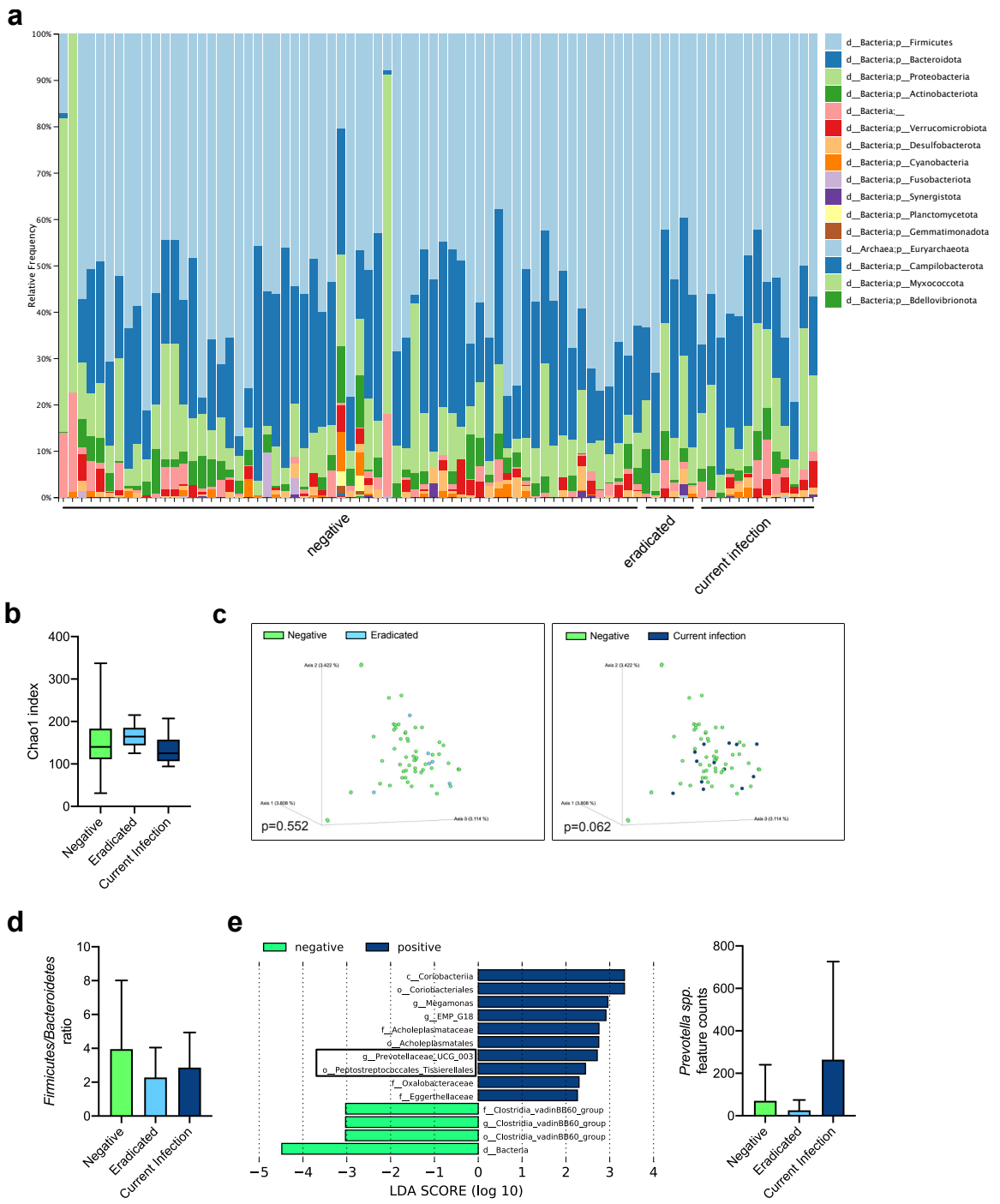

Figure 4.23: *H. pylori* shapes gut microbiota in humans.
(a) Taxonomic binning showing relative frequencies at phyla level in stool of patients. (b) Chao1 index as an indicator of alpha-diversity shown for negative, eradicated and currently infected individuals. (c) Bray-Curtis dissimilarity depicting beta-diversity between *H. pylori* infected and eradicated as well as H. pylori infected and non-infected patients. Statistical significance was determined with PERMANOVA. (d) Ratio of feature counts from *Firmicutes* and *Bacteroidetes* phyla. (e) LEfSe analysis depicting differentially abundant features in patients upon H. pylori infection and feature counts of Prevotella species (spp.). Chao1 index depicted as box and whiskers, from min to max. Feature counts shown as bar plots, indicating mean with standard deviation.

To sum up, those data provide evidence that the phenotype induced upon *H. pylori* infection in mouse models, including a shift towards a pro-inflammatory immune response concomitant with a reduction of regulatory immune cells, the activation of pro-carcinogenic signaling, the reduction of mucus-producing goblet cells and changes of microbiota compositions, can be observed in humans. These findings indicate that *H. pylori* promoted

colorectal carcinogenesis is a multifactorial process, which might be ameliorated and even prevented, if patients at risk are eradicated.

5. Discussion

H. pylori infection is the main risk factor for gastric cancer development and although colonizing the stomach, chronic infection has been shown to be related to a variety of extragastric diseases (235). Among these, growing evidence has stressed an association between *H. pylori* and CRC, with meta-analyses stating a up to 2-fold increased risk upon infection (146, 148-151). However, despite robust epidemiological data, experimental evidence supporting this association and the underlying mechanisms remained elusive.
The effect of *H. pylori* on intestinal and colonic homeostasis was examined by initially characterizing infected C57Bl/6 mice. To investigate the impact on CRC development and progression, two APC mouse models (*Apc*$^{+/1638N}$ and *Apc*$^{+/min}$ mice) were utilized, which developed twice as many tumors upon infection. Mechanisms leading to this exaggerated tumorigenesis revealed to be connected to *H. pylori*'s effects on intestinal and colonic immune, epithelial signaling and microbial signatures. Finally, those signatures were evaluated in a human cohort compromising *H. pylori* positive, eradicated and negative patients.
In the following sections, the observed phenotype and the mechanistic contribution of these effects to colorectal carcinogenesis will be discussed in detail.

5.1. *H. pylori* shapes intestinal immune response and signaling

H. pylori infection is known to trigger a cascade of inflammatory processes, which originate from priming at the Peyer's Patches and the mesenteric lymph nodes (MLN) of the small intestine (59, 60). In the stomach, the elicited response is mainly CD4$^+$ T-cell mediated, consisting of a mixed Th1/Th17 response, which is counteracted by an increase of Tregs, which is required for bacterial persistence. The immune response induced upon *H. pylori* infection is crucial for the development of precancerous lesions in the stomach (236). Therefore, within this study, the immune response elicited in the intestine and colon upon *H. pylori* infection was characterized in depth in order to determine its contribution to colorectal carcinogenesis.

The assessment of gastrointestinal epithelia for T-cell infiltration revealed an overall increase in CD3$^+$ T-cells upon *H. pylori* infection not only in the stomach, but also in the proximal as well as the distal intestine and the colon of mice as well as in the human cohort. Infecting C57Bl/6 mice for 3 different time points, namely 4, 12 and 24 weeks, resembled acute, intermediate, and chronic infection settings and allowed to interpret the infection dynamics over time. These findings led to the following conclusions. First, *H. pylori* was stably colonizing over time and was not cleared by the immune system, which makes the infection of mice in a C57Bl/6 background with the strain PMSS1 (a mouse

adapted strain able to translocate CagA, short for pre-mouse Sidney Strain1 (237)) a suitable model to study long-term effects of *H. pylori* infection and its impact on colorectal carcinogenesis. Second, the sensing of the pathogen, which is known to occur in the lymphoid organs of the intestine (59, 60), was most probably leading to a homing of lymphocytes not only to the infected stomach, but also to the intestine and colon, leading to a chronic inflammatory response throughout the intestinal tract. Chronic inflammation has been reported as an independent risk factor for CRC in patients suffering from ulcerative colitis (UC) and this risk increases with time, from 2% after 10 years, over 8% after 20 years, to 18%, after 30 years of disease (238, 239). This strongly supports the hypothesis, that the chronic inflammatory response elicited upon *H. pylori* infection in intestine and colon is contributing to the increased risk for CRC. To understand the mechanisms triggering this chronic inflammatory response and considering the largely T-cell driven immune response upon *H. pylori* in the stomach, intestinal and colonic T-cells were characterized in further detail.

When looking at T-cell subsets, an increase in $CD8^+$ T-cells was observed, while $CD4^+$ T-cells were reduced upon infection. This has been reported in previous studies, such as mouse models of *H. pylori* infection showing the same trend in the stomach mucosa as well as in ex-vivo stimulated gastric lymphocytes (41, 240). In contrast to mice, *H. pylori* infection leads to an increase of both $CD4^+$ and $CD8^+$ T-cells in human gastric tissue (241), which was also found to be the case in colon biopsies.

As the T-cell response in the stomach has been mostly attributed to T-helper cells, the focus of this study remained on $CD4^+$ T-cells, which revealed a reduction of Tregs and a specific, pro-inflammatory Th17 response. The reduction of Tregs was highly unexpected, as in the stomach, Tregs are upregulated in response to infection and balance the strong pro-inflammatory response. Also, Treg induction plays a major role in the known impact of *H. pylori* on the lung, where this induction results in protection from asthma development (237). In the murine intestine and colon as well as in the human cohort, however, Tregs were consistently reduced. This reduction most certainly further contributes to intestinal inflammation, which is supported by the clinical phenotypes of IBD and patients suffering from immunodysregulation polyendocrinopathy enteropathy X-linked (IPEX) syndrome, where the reduction or lack of functional $FOXP3^+$ Tregs results in severe gastrointestinal inflammation and allergies (242, 243). Furthermore, intestinal Tregs are known to be of utmost importance in their role to maintain a balance between allowance of nutrient uptake and commensal colonization while simultaneously monitoring possible harmful substances and invading pathogens (244). Besides the reduction of Tregs in the lamina propria, a loss of Tregs in the intraepithelial compartment in *H. pylori* infected mice was observed. The close proximity of these cells to the intestinal lumen and the known necessity of

intraepithelial $CD4^+$ T-cells in intestinal barrier homeostasis and immunoregulatory balance underline a perturbation of these functions upon *H. pylori* infection (245, 246).
However, as the sole reduction in Tregs does not consider their functionality, their transcriptional profile was assessed on a single-cell level. The distribution of the different Treg subtypes was clearly affected by *H. pylori* infection: while in the intestine of naïve WT mice, iTregs accounted for the majority of Tregs and the remaining 10% were identified as nTregs, infection skewed this composition to consist exclusively of nTregs while lacking iTregs. It is generally accepted, that induction of $ROR\gamma t^+$ iTregs in the periphery is strongly dependent on the microbiota (247, 248). To identify possible species responsible for iTreg induction, GF mice were colonized with single species, which revealed that members of several phyla and genera, including *Clostridiae* and *Bacteroidia*, were able to restore $ROR\gamma t^+$ iTregs to levels of SPF mice. *Foxp3-cre/Rorc*$^{fl/fl}$ mice, which lack RORγt in their Tregs, displayed an impaired ability to regulate inflammatory responses, and they produced higher levels of IL-17 and IFNγ. Consequently, chemically induced colitis led to more severe colitis scores and histopathology (248). Furthermore, it has been shown that $ROR\gamma t^+$ iTregs express high levels of *Il10*, *Ctla4* and *Icos*, which are known to be crucial for the suppressive capacities of Tregs, thereby controlling colitis and intestinal inflammation (249). This phenotype was further supported by an overall loss of effector properties of $GATA3^+$ nTregs and act. Tregs in *H. pylori* infected mice, which was detected by means of a Treg effector score (225). In addition to this loss of suppressive capacities and shifting in subpopulations of Tregs, a reprogramming towards a Th17 phenotype was observed upon *H. pylori* infection. It has been shown that $Il17^+$ $FoxP3^+$ T-cells display a pro-inflammatory phenotype and express not only IL-17, but also IFNγ and thereby suppress T-cell activation (250). This population has been found to be enriched in patients with Crohn's Disease (CD) and CRC (251, 252). Furthermore, it has been shown, that they might be involved in CRC initiation and progression via the increase of cancer promoting markers like CD44 and EpCAM, as well as phosphorylated Akt and p38 – important for cell proliferation and tumor progression (251). Additionally, $Il17^+$ $FoxP3^+$ T-cells have been linked to $CD8^+$ T-cell suppression, which further potentiates tumor immune evasion and supposedly promotes tumor progression (252).
This loss of regulatory T-cells, shifting of Treg subpopulations and reprogramming towards a Th17 phenotype indicates a severe interference of *H. pylori* with intestinal immune homeostasis and suggests a detrimental impact on the regulation of inflammatory responses, which in combination with pro-inflammatory responses may mechanistically link chronic inflammation to tumor development.
The specific, pro-inflammatory $CD4^+$ T-cell response was characterized by IL-17 production of intestinal lymphocytes upon stimulation with whole *H. pylori* lysate,

suggesting an antigen-specific response. Furthermore, *Il17a* expression levels in intestinal and colonic tissue revealed tendencies towards upregulation, indicating a pro-inflammatory, Th17 mediated response in the intestine and colon upon *H. pylori* infection. It is well known, that in the stomach, *H. pylori* infection of mice leads to a strong upregulation of *Il17a* (41). Interestingly, IL-17 was not only found to be increased in *H. pylori* positive patients with gastritis (253), but also in the serum of gastric cancer patients. Furthermore, mRNA expression of IL-17 was upregulated in gastric cancer tissue of *H. pylori* infected individuals (254-256). Accordingly, it is tempting to speculate, that IL-17 induced upon *H. pylori* infection might be a mechanism contributing to colorectal carcinogenesis. In fact, IL-17 has been suggested to promote carcinogenesis via chronic tissue inflammation, not only in CRC, but also in other cancer entities, like ovarian cancer (257, 258). Furthermore, a study assessing the outcome of colorectal cancer patients revealed, that tumors exhibiting Th17 signatures, including RORC, IL17, IL23 and STAT3, were linked to poorer prognosis (259). This unfavorable role of Th17 responses in cancer immunity is further promoted and influenced by perturbations of gut microbiota. Several microbial species have been shown to induce IL-17 signatures at the epithelial interface with the gut lumen, including segmented filamentous bacteria (SFB) and *enterotoxigenic Bacteroides fragilis* (ETBF) (260, 261). While SFB are neither related to disease progression nor cancer and rather enhance mucosal immunity, ETBF induced IL-17 production has been shown to endorse colon cancer initiation and progression in $Apc^{+/min}$ mice (262). Another study confirmed this phenotype, deciphering that the mechanism behind this was IL-17 induced STAT3 signaling (263). This matches to the epithelial phenotype observed in both WT and tumor mice upon *H. pylori* infection as well as in *H. pylori* “currently infected” individuals, namely an increase in STAT3 signaling activation in both intestine and colon. Tissue levels of STAT3 in CRC patients have been shown to negatively correlate with tumor invasion, progression and survival (264-266). Furthermore, persistent STAT3 activation has been related to cell proliferation and tumor growth in CRC (267). In fact, an increase in proliferation detected by means of Ki67 staining was already observable in intestine and colon of WT mice upon *H. pylori* infection, which suggests, that *H. pylori* can distantly deregulate proliferation, which is known as a prerequisite for carcinogenesis (268). This leaves the question, which mechanism was leading to STAT3 activation upon infection. One possible mechanism could be the activation via microbial signals, which would be supported by the lower intestinal, and in the colon even absent, STAT3 activation in *H. pylori* infected germ-free mice (discussed in section 5.4). Furthermore, it has been shown that IL-6 and IL-11 mediated STAT3 signaling in cancer-associated fibroblasts drives colorectal carcinogenesis (269). Gene expression analysis of intestinal and colonic tissue, which would also include signals from fibroblasts, however,

did not reveal a clear picture of involvement of these cytokines in the activation of this pathway. This supports the concept, that the chronic inflammatory response upon *H. pylori* triggers the activation of epithelial signaling pathways, which eventually promote intestinal and colonic tumor development. Therefore, it is tempting to speculate that in this scenario, IL-17 induced STAT3 signaling is a potent mediator to induce tumor initiation in the colon of a mouse model, that preferentially develops adenomas in the small intestine (195). Furthermore, a study reported a reduced recruitment of Tregs upon STAT3 activation into colonic tissue (270), which would further add significance to the speculation, that STAT3 mediated regulation of immune cells promotes tumor growth upon *H. pylori* infection.

All these effects observed upon *H. pylori* infection in the colon, including a strong pro-inflammatory response, paired with activation of carcinogenic signaling and increased proliferation, let assume that *H. pylori* infection on its own is sufficient enough to create a tumorigenic environment comparable with other colitis and tumor stimulating agents, such as azoxymethane (AOM) and dextran sodium sulphate (DSS). This is of utmost importance, as *Apc* mouse models are known for their limitation as surrogates of human CRC, developing adenomas mostly in the intestine and not in the colon (271, 272).

5.2. *H. pylori* interferes with microbiota compositions and impairs goblet cell function

The microbiota are known to orchestrate major physiological functions of the gut and its disturbance has a detrimental impact on disease development, progression and outcome. The contribution of alterations in microbiota compositions to accelerating inflammation as well as cancer have been described widely (273, 274). The extent of disturbances in microbiota compositions and contribution of certain microbial genera to the cancer promoting effects of *H. pylori* have been examined extensively throughout this study and involved the analysis of tissue-adherent as well as luminal microbiota of the gastrointestinal tract of C57BL/6 mice as well as colon tumor models $Apc^{+/1638N}$ and $Apc^{+/min}$. Furthermore, stool samples of the human cohort were assessed for microbial alterations.

A decrease in α-diversity, an indicator of species richness and microbial diversity within one sample, was observed in the intestine and colon of *H. pylori* infected mice as well as in *H. pylori* infected patients. Furthermore, measures of community diversity revealed separation of the groups according to infection status, emphasizing the effect of *H. pylori* infection on the microbiota of the gastrointestinal tract. A loss of diversity has been described as a common feature of dysbiosis in a variety of diseases of the gastrointestinal tract, including IBD, irritable bowel syndrome (IBS) and colorectal cancer (275-277). It has been shown in both murine and human studies, that *H. pylori* infection induces states of

dysbiosis (76, 278). Importantly, not only the stomach microbiota are susceptible to infection, but also the distant intestine has shown to be affected (76). The composition of the microbiota is highly susceptible to diet, metabolic markers, inflammation, host genetics and therapeutic interventions (274). One could hypothesize that *H. pylori* infection induces a dysbiotic state via distinct mechanisms. First, inflammatory processes elicited upon infection, which have been characterized extensively within this study, may have a detrimental impact on the intestinal microbiota. Mouse models have shown that infection with pathogens like *Citrobacter rodentium* and *Salmonella enterica* serovar *typhimurium* or inflammation induced by dextran sodium sulfate or deficiency in *Il10*, compromise microbial balance and lead to overgrowth of pathobionts (279, 280). Ultimately, this overgrowth induced by inflammation leads to CRC promotion, as it was shown with members of the Enterobacteriaceae family (281). Another mechanism contributing to dysbiosis could be the impact of *H. pylori* on distinct epithelial cell populations, namely mucus producing goblet cells and antimicrobial-peptide secreting Paneth cells, which have been observed to be impaired upon infection. A mouse model deficient in NLRP6 inflammasome, known as a key regulator of colonic homeostasis by regulating mucus-self renewal, proliferation and secretion, revealed that disturbed secretion of mucus and antimicrobial-peptides supports dysbiosis (282, 283).

This notion of *H. pylori* manipulating the balance between mucus replenishment and degradation was further supported by close monitoring of microbial species differentially abundant upon *H. pylori* infection, which revealed a favorable niche for mucus-degrading bacteria. *Akkermansia spp.* and *Ruminococcus spp.* were enriched consistently along the intestinal tract in both wild type and tumor mice. Even though *Akkermansia muciniphila* have been associated with rather beneficial effects, including inverse correlations with disease entities like IBD, diabetes and obesity (284, 285), as well as to have a predictive role in response to PD-1 checkpoint inhibitors (286), several studies have attributed potential disease promoting effects to this species. These include that in case of fiber-deprivation, mucus degrading bacteria, including *Akkermansia muciniphila*, switch their nutritional source to the intestinal mucus layer, which results in an impaired intestinal barrier. This impaired barrier facilitates invasion of enteric pathogens and has been shown to lead to lethal colitis upon infection with *Citrobacter rodentium* (287). In another study, *Akkermansia muciniphila* has been shown to induce colitis in both germ-free and SPF *Il10*$^{-/-}$ mice and that its abundance is determined by NLRP6 in an IL-18 dependent manner, suggesting a potential pathogenic role of the bacteria in a susceptible host (288). Interestingly, a study carried out in germ-free mice, which were subjected to chemically induced CRC via AOM DSS treatment after receiving microbiota transfers from either healthy or CRC patients, revealed, that *Akkermansia spp.* were among the taxa correlating

positively with a high tumor burden (289). Along that line, differential abundance testing in the human cohort of this study did not detect species involved in mucus degradation. However, *Prevotallae spp.* and species of the order *Peptostreptococcales* revealed to be enriched in *H. pylori* positive individuals. Those two species have been shown to be enriched in CRC patients, as shown by a meta-analysis of more than 700 cases identifying a core signature of CRC (234).

The exact mechanism, by which an increased abundance of *Akkermansia spp.* upon *H. pylori* infection might contribute to CRC remains unclear. One could assume, that mucus degradation allows closer interaction of commensals with the intestinal mucosa and therefore drives inflammatory processes. The observed decrease in goblet cells might further pronounce this effect, however, it is not clear, whether and how these two observed phenotypes are related.

Impaired goblet cell function has been described as a pathogenic feature of IBD, more precisely the dysregulation of mucin-synthesis leading to barrier dysfunction, which facilitates bacterial penetration (290). Furthermore, loss of goblet cells has been found in inflamed tissue of both UC and CD patients, indicating a role of inflammation in this process (291). Goblet cell depletion has been observed in several studies of DSS induced colitis, and subsequent bacterial invasion drove the infiltration of immune cells and progression of colitis (292-294). Furthermore, it was shown, that *Muc2* levels did not correlate with loss of goblet cells, which were either unaltered or even increased, and that those levels varied based on the location within the colon (294). This is in concordance with the observed variations in *Muc2* mRNA expression within this study.

The loss of goblet cells could be also attributed to a failure in the differentiation of those specialized cells from the secretory lineage of stem cells. It has been shown, that *ATOH1*, known to drive terminal differentiation of goblet cells, is downregulated in CRC and that this terminal differentiation is inhibited by NOTCH signaling (295, 296). A study showed that inhibition of NOTCH signaling lead to preferential differentiation of stem cells to goblet cells, emphasizing that NOTCH signaling is mediating the lineage differentiation of those specialized epithelial cells (297). Indeed, NOTCH signaling was found to be enhanced upon *H. pylori* infection, indicating that the loss of goblet cells observed in *H. pylori* infected mice might be caused by a failed lineage differentiation.

RNA velocity further supports this speculation, that goblet cells fail to fully differentiate under inflammatory conditions caused by *H. pylori* infection: directionalities from stem towards goblet cell clusters seemed to be reduced in comparison to non-infected mice, possibly explaining the absolute loss of specialized, mucus producing cells.

These studies support the hypothesis, that goblet cell depletion and resulting barrier dysfunction further drives inflammatory processes in the intestine and colon induced upon *H. pylori* infection and might therefore be involved in colorectal carcinogenesis.

5.3. *H. pylori* modulates the tumor environment

To explore the molecular mechanisms involved in the acceleration of tumor development and to get insight into the processes leading to the severe, at times lethal phenotype in *Apc*$^{+/min}$ mice upon *H. pylori* infection, possible factors influencing the tumor microenvironment as well as transcriptomic profiles of tumor cells were investigated by means of single-cell RNA sequencing of immune and epithelial cells. Phenotype and density of tumor-infiltrating immune cells are known to be decisive in the progression, outcome and therapy response of various cancer entities, above all in regard to cytotoxic T-cells (298). Next to the reduction of regulatory T-cells and their phenotypic switch towards Th17 cells, CD8$^+$ T-cell exhaustion was observed in *Apc*$^{+/min}$ mice upon *H. pylori* infection. Exhausted CD8$^+$ T-cells have been proposed to be subdivided into two groups, namely progenitor exhausted and terminally exhausted T-cells (299, 300). Besides their observed differential expression of PD-1 and other inhibitory molecules and exhaustion markers, such as Tim-3, Tox and CXCR5, importantly, these two subpopulations are distinguished functionally by their ability to proliferate after immune-checkpoint blockade (299, 301). Those progenitor exhausted T-cells have been shown to possess the ability to differentiate into highly cytotoxic, tumor-infiltrating lymphocytes and thereby control tumor growth and therapy response (226). Both progenitor and terminally exhausted CD8$^+$ T-cells displayed higher exhaustion scores upon *H. pylori* infection and the overall CD8$^+$ T-cell population showed pronounced dynamics towards the terminally exhausted cluster compared to non-infected tumor mice. These data lead to the impression, that *H. pylori* promotes tumor immune evasion, which was further supported by pathway enrichment analysis of differentially expressed genes in tumor cells upon infection, revealing immune evasion signatures.

Indeed, in human CRC tissue, high infiltrates of memory and effector CD8$^+$ T-cells correlated with less metastasis, less tumor progression and better survival (302). In line with this, *H. pylori* seemed to increase NOTCH signaling in tumor cells and fibroblasts of *Apc*$^{+/min}$ mice, which was shown to reshape the tumor microenvironment towards metastasis and found to correlate with poor prognosis in CRC (233).

These data suggest that *H. pylori* favors terminal T-cell exhaustion and immune evasion in tumor cells, and thereby creates an immune suppressive, possibly pre-metastatic tumor environment.

5.4. *H. pylori* induced phenotype is normalized upon eradication and is partly depending on the presence of microbiota

Eradication of *H. pylori* infection is the gold-standard treatment in risk stratified patients and has been shown to be highly preventive in terms of morbidity to infection (303). In the course of this study, the effect of eradication on the phenotype observed in intestine and colon upon *H. pylori* infection was evaluated. This revealed that the *H. pylori* induced effects on immune and epithelial signatures, but most importantly also on tumor development in *Apc*$^{+/1638N}$ mice, normalized to levels of non-infected controls. Similarly, eradication of *H. pylori* in gastric cancer prone INS-GAS mice resulted in cancer prevention (304). Another study performed in Mongolian gerbils confirmed the reduced gastric cancer incidence in *H. pylori* eradicated compared to *H. pylori* infected animals (305). Interestingly, in both studies the time point of eradication was decisive for the outcome, with early intervention being superior in terms of incidence and severity of cancer lesions compared to later intervention. In this study, early intervention after 4 weeks of infection proved to be efficient in tumor prevention in *Apc*$^{+/1638N}$ mice, however it still needs to be determined whether eradication after later time points of infection would still positively impact tumor development and disease progression in this mouse model.

As a side observation besides the normalization of *H. pylori* induced effects, the eradication treatment and the various time spans of “recovery”, indicating the time between antibiotic administration and sacrifice of the mice, highlighted the detrimental impact of antibiotic intake on certain immune and epithelial cell populations. Especially Tregs and goblet cells seemed to be affected. The unfavorable impact of antibiotic exposure on Treg frequency in the gut has been related to microbial depletion (306, 307). Also, goblet cell functions have been described to highly depend on microbial signals (308). However, several studies in humans and mice show, that microbial dysbiosis after antibiotic intake was mostly restored after 1 to 1.5 months in adults and children (309, 310) and in even less than 1 month in mice (311). Nevertheless, the study conducted in mice also showed, that normal microbial evolution occurring with aging could not be restored after a follow-up period of 6 months (311). Those findings are mostly consistent with phenotypes in germ-free mice, supporting the fact that many immune and epithelial functions in the gut are heavily reliant on microbial signals.

Within this study, additional to eradication experiments, which allowed to attribute the described effects specifically to *H. pylori* infection, the role of the microbiota in *H. pylori* driven carcinogenesis was determined by infection and transferring stool of *H. pylori* infected mice into germ-free *Apc*$^{+/1638N}$ mice. The fact, that the effects on the intestinal and colonic immune response were still observable in germ-free mice and that eradication experiments reversed the observed immune phenotype, reinforce the concept, that those

effects can be attributed specifically to *H. pylori* infection and are not a consequence of other factors, such as the microbiota. In contrast, the activation of STAT3 signaling seemed to be highly depending on the presence of microbiota, as e.g. in the colon, almost no signal was detectable in germ-free mice. Indeed, mice with antibiotically depleted microbiota exhibited a loss of STAT3 signaling, which was reconstituted upon fecal microbiota transplantation (FMT) (312). Furthermore, it has been shown in $Apc^{+/min}$ mice, that tumor growth was accelerated via microbial induced c-Jun/JNK and STAT3 signaling (313), which matches to the observation, that germ-free $Apc^{+/1638N}$ mice, exhibiting almost no STAT3 signaling, developed less tumors upon *H. pylori* infection than mice housed under SPF conditions. Additionally, our findings from transferring stool of *H. pylori*-infected SPF mice into germ-free Apc+/1638N mice, where we observed an accelerated tumor development in comparison to stool transferred from non-infected mice, support the hypothesis, that microbial induction of STAT3 signaling might be crucial in the tumor promoting effects of *H. pylori*.

Taken together, these findings allow the following conclusions. First, the disturbances in microbiota are a critical component in the tumor promoting effect of *H. pylori*. Additionally, the immune response was still affected by *H. pylori* infection in germ-free mice but apparently not sufficient to induce the full cancer promoting effect as observed in conventionally raised mice. Finally, the fact that stool transfer was sufficient to accelerate tumor development implies that a multifactorial process, including not only a pro-inflammatory environment, but also certain microbiota signatures, activated STAT3 signaling and impaired goblet cell functions, underlies the cancer promoting effects of *H. pylori*.

5.5. *H. pylori* affects immune, epithelial and microbial signatures in human colon

Finally, it was attempted to corroborate those described signatures in a cohort of human patients. The analysis of colon biopsies revealed increased T-cell infiltration, reduction of regulatory T-cells, activation of STAT3 signaling, loss of goblet cells and perturbations in microbiota compositions in *H. pylori* infected individuals. Stratifying *H. pylori* status of this human cohort into “currently infected“ and “eradicated”, which however has the limitation that the time of eradication was not known and could thereby be biased, revealed similar results as detected upon eradication of mice: the observed phenotype in eradicated patients was obviously mitigated or, in case of STAT3 activation, even significantly lower than in currently infected patients. This not only indicates that the effects described to occur in response to *H. pylori* infection in the colon can be attributed to *H. pylori* infection, as they seem to be reversible upon eradication, also, it is of utmost clinical importance, as it justifies the assumption, that eradication of *H. pylori* infection would be a preventive

option not only for gastric cancer, but also for CRC. Current guidelines recommend eradication of *H. pylori* infection in the following cases: peptic ulcer, MALT lymphoma, functional dyspepsia after endoscopy, ITP, refractory iron deficiency anemia, upper gastrointestinal bleeding while on acetylsalicylic acid (ASA) or non-steroidal anti-inflammatory drugs (NSAID), ASA or NSAID long-term intake with medical history of peptic ulcer disease and gastric cancer risk patients (314). This study provides experimental basis to include CRC risk patients in those guidelines. In line with that, it supports the inclusion of *H. pylori* infection into risk assessment of patients with increased risk for CRC development.

In concordance with the changes observed in mouse models, those findings allow the assumption that *H. pylori* infection might favor a pre-cancerous microbial niche in the human colon, which in combination with inflammation, carcinogenic signaling and other environmental and risk factors could foster the development of CRC.

5.6. *H. pylori* induced colorectal carcinogenesis: a proposed model of underlying mechanisms

Compelling evidence supports an increased risk for CRC development in *H. pylori* infected individuals. However, a causality or underlying mechanism has not been verified yet. *H. pylori's* relationship with increased CRC development could be attributed to two distinct modes of action. On one side, *H. pylori* could exert its cancer promoting effects in a direct manner, providing that the bacterium is present in the stool or colon tissue of patients. However, this presence was only seldomly detected (315-317) and would stand against an exclusive ecological niche of *H. pylori* within the stomach and the very well described, intricate host-pathogen relation here. Another mechanism would be an indirect effect, which seems to be more probable when considering the effects of the bacterium on other extragastric organs, such as the lung.

This study supports the notion that *H. pylori* infection exerts its colon cancer promoting effects via (i) creating a pro-inflammatory environment, including T-cell exhaustion and reduced as well as pathogenically rewired Tregs, (ii) activating pro-inflammatory and pro-carcinogenic STAT3 signaling, (iii) reducing mucus producing goblet cells and (iv) modulating the microbiota towards a dysbiotic state and mucus degradation (Figure 5.1).

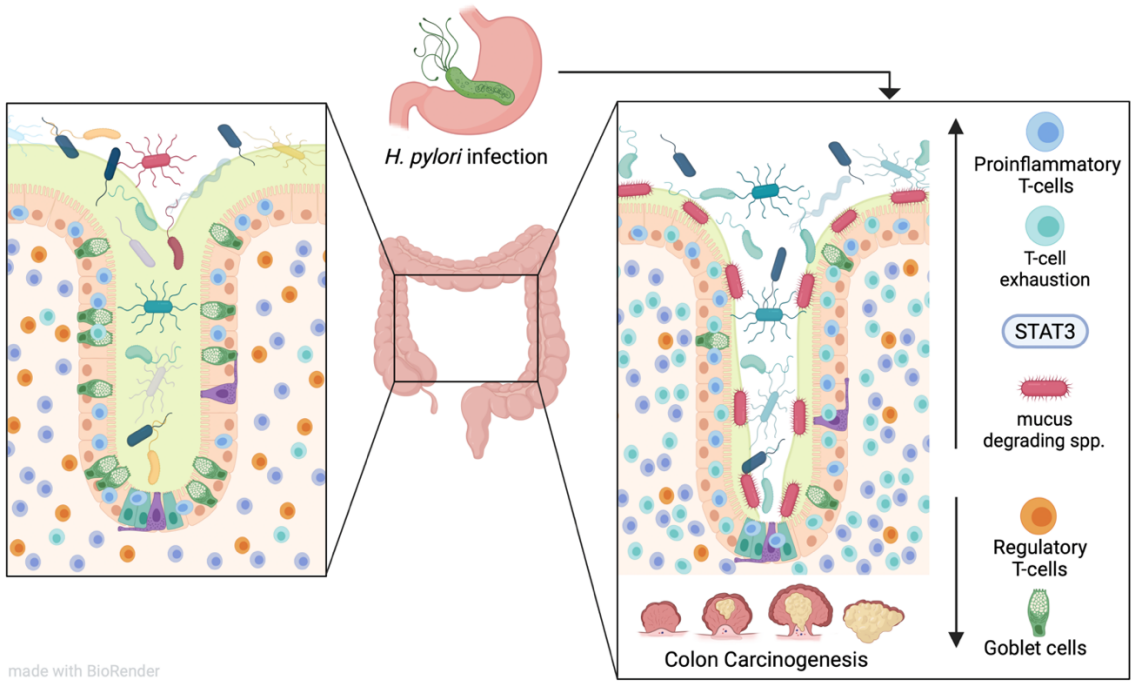

Figure 5.1: *H. pylori* induced indirect effects promote colon carcinogenesis

Left panel: Healthy colon epithelia are in a symbiotic, balanced state, characterized by diverse microbiota and balanced immune and epithelial cell populations. Right panel: upon *H. pylori* infection, colonic homeostasis is disturbed, manifested by an increase of proinflammatory T-cells, T-cell exhaustion, STAT3 activation and mucus-degrading bacteria and concomitant reduction of regulatory T-cells and goblet cells – eventually contributing to colon carcinogenesis. Created with Biorender.com.

5.7. Conclusion and outlook

This study provides first experimental evidence of *H. pylori* inducing colorectal carcinogenesis and describes mechanisms involved in this association. Eradication experiments performed in both wild type and tumor mouse models show a reversibility of the underlying effects as well as a normalization of the accelerated tumor development. Moreover, the clinical relevance of these findings was corroborated in a cohort of human colon biopsies, which reflected the phenotype observed in mouse models and indicated a decline of the effects in eradicated patients.

Those findings strongly encourage and support the association of *H. pylori* with an increased risk for CRC development and provide convincing evidence to include *H. pylori* status into an adapted risk score for CRC. Furthermore, it indicates that eradication might be an effective measure to reduce this risk. Considering a PAR of *H. pylori* positive individuals to develop CRC of nearly 30%, eradication therapy would prevent more than 150.000 CRC cases per year in Europe (152). Long term studies including *H. pylori* positive patients undergoing eradication therapy are required to ultimately confirm this suggestion. Furthermore, phenotyping of cancer tissue derived from polyps, adenomas, and carcinomas of *H. pylori* positive patients would be worth investigating, to determine the influence of *H. pylori* infection on colon cancer progression. Finally, considering the worldwide emerging antibiotic resistance, the findings of this study in terms of *H. pylori* as a major health threat, support the importance of investigation for alternative treatment options for *H. pylori* infection, including *H. pylori* specific phages or vaccination strategies.

Abbreviations

act. Tregs	activated Tregs
APC	*Apc*$^{+/min}$ mice
APCs	antigen-presenting cells
ASA	acetylsalicylic acid
ASVs	amplicon sequence variants
BabA	blood group antigen binding adhesin
BHI	brain-heart-infusion
CAC	colitis-associated cancer
CagA	cytotoxin-associated gene A
cagPAI	cag pathogenicity island
CEACAM	carcinoembryonic antigen-related cell adhesion molecules
CFU	colony forming units
CIMP	CpG island methylator phenotype
CMS	consensus molecular subtypes
CRC	colorectal cancer
C57Bl/6 mice	WT mice
DAB	diaminobenzidine
DCs	dendritic cells
FAP	familial adenomatous polyposis coli
FCS	fetal calve serum
FMT	fecal microbiota transplantation
FoxP3	forkhead box P3
FSC	forward scatter
GERD	gastro-esophageal reflux disease
gGT	γ-glutamyltranspeptidase
GIN	gastrointestinal intraepithelial neoplasia
HRP	horseradish peroxidase
IBD	inflammatory bowel disease
IBS	irritable bowel syndrome
IFNγ	interferon-γ
IL	interleukin
INS-GAS	insulin-gastrin
IPEX	immunodysregulation polyendocrinopathy enteropathy X-linked
IRF-3	interferon regulatory factor 3
iTregs	peripherally induced Tregs
LEfSe	linear discriminant analysis effect size

LPS	lipopolysaccharide
MAMPs	microbe-associated molecular patterns
MALT	mucosa-associated lymphoid tissue
MHCII	major-histocompatibility complex molecule class II
MSI	microsatellite instability
NF-κB	nuclear factor 'kappa-light-chain-enhancer' of activated B-cells
NFW	nuclease-free water
NOD1	nucleotide-binding ologomerization domain 1
nTregs	thymically derived Tregs
NSAID	non-steroidal anti-inflammatory drugs
OMP	outer membrane protein
PAMPs	pathogen associated molecular patterns
PAR	population attributable risk
PAS	periodic acid Schiff
PBS	phosphate-buffered saline
pSTAT3	phosphorylated STAT3
SabA	sialic acid-binding adhesin
SCNA	somatic copy number alterations
SPF	specific pathogen free
SSC	side scatter
STAT3	signal transducer and activator of transcription 3
TGF-β	transforming-growth-factor ß
TLRs	toll-like receptors
TNFα	tumor necrosis factor-α
Tregs	regulatory T-cells
TRM	tissue resident memory
T4SS	type IV secretion system
UMAP	Uniform Manifold Approximation and Projection
VacA	vacuolating cytotoxin gene A
WC	Wilkins-Chalgren

Figures

Figure 1.1: Percentages of *H. pylori* infected individuals worldwide.
Figure 1.2: TLR-mediated signaling as paradigm of simultaneous manipulation and evasion of immune mechanisms by *H. pylori*.
Figure 1.3: Summary of risk and protective factors of CRC
Figure 3.1: *H. pylori* infection setup.
Figure 3.2: Eradication of *H. pylori* infection.
Figure 3.3: Gating strategy
Figure 4.1: WT mice were successfully infected with *H. pylori* strain PMSS1 for 4, 12 and 24 weeks.
Figure 4.2: *H. pylori* infection induces pro-inflammatory T-cell responses in intestine and colon.
Figure 4.3: Immune response elicited upon *H. pylori* infection in intestinal and colonic tissue.
Figure 4.4: *H. pylori* infection leads to loss of intraepithelial regulatory T cells in colon tissue.
Figure 4.5: *H. pylori* infection activates STAT3 signaling in intestine and colon.
Figure 4.6: *H. pylori* infection drives proliferation in intestinal and colonic tissue.
Figure 4.7: *H. pylori* reduces mucus producing cells in intestine and colon.
Figure 4.8: *H. pylori* infection affects gastrointestinal microbiota.
Figure 4.9: *H. pylori* infected WT mice were successfully eradicated.
Figure 4.10: Eradication therapy reverses *H. pylori* induced phenotype in C57Bl/6 mice.
Figure 4.11: *H. pylori* promotes tumor development in $Apc^{+/1638N}$ and $Apc^{+/min}$ mice.
Figure 4.12: *H. pylori* induces proinflammatory T-cell response in $Apc^{+/1638N}$ and $Apc^{+/min}$ mice.
Figure 4.13: *H. pylori* enhances activation of STAT3 signaling in $Apc^{+/1638N}$ and $Apc^{+/min}$ mice.
Figure 4.14: *H. pylori* reduces mucus producing cells in $Apc^{+/1638N}$ and $Apc^{+/min}$ mice.
Figure 4.15: *H. pylori* infection shapes gastrointestinal microbiota of $Apc^{+/1638N}$ mice.
Figure 4.16: *H. pylori* infection shapes gastrointestinal microbiota of $Apc^{+/min}$ mice.
Figure 4.17: *H. pylori*'s cancer promoting effects are depending on the presence of gut microbiota.
Figure 4.18: *H. pylori*'s cancer promoting effects are reversible upon eradication.
Figure 4.19: Single cell RNA sequencing of immune and epithelial cells from *H. pylori* infected $Apc^{+/min}$ and $Apc^{+/+}$ mice
Figure 4.20: *H. pylori* infection dampens regulatory T-cell function and promotes $CD8^+$ T-cell exhaustion

Figure 4.21: *H. pylori* infection activates pro-inflammatory signaling, affects goblet cell functions and induces tumor cell immune evasion.
Figure 4.22: *H. pylori* shapes immune response, activates carcinogenic signaling and reduces goblet cells in human colon.
Figure 4.23: *H. pylori* shapes gut microbiota in humans.
Figure 5.1: *H. pylori* induced indirect effects promote colon carcinogenesis

Tables

Table 1.1: *H. pylori*'s role in extragastric diseases
Table 1.2: Selected mouse models of colorectal cancer
Table 3.1: Instruments used within this study
Table 3.2: Consumables used within this study
Table 3.3: Chemicals used within this study
Table 3.4: Buffers and solutions used within this study
Table 3.5: Assays and kits used within this study
Table 3.6: Softwares and Packages used within this study
Table 3.7: HE staining
Table 3.8: Antibodies used for immunohistochemical evaluation
Table 3.9: PAS staining
Table 3.10: cDNA master mix
Table 3.11: cDNA cycling conditions
Table 3.12: qPCR master mix
Table 3.13: qPCR cycling conditions
Table 3.14: Primer sequences used for qPCR
Table 3.15: Antibodies used for ChipCytometry
Table 3.16: Antibodies used for flow cytometry
Table 3.17: 16S rRNA primer sequence
Table 3.18: PCR conditions for amplification of 16S rRNA gene

Acknowledgements

The completion of my Ph.D. was the most challenging and demanding, and simultaneously most rewarding and educational time of my life. This unique experience would not have been possible without a variety of people, that I would like to thank in the following section.

I would firstly like to express my deep gratitude to my advisor Prof. Dr. Markus Gerhard for the opportunity to join his group and to immerse myself into the unbelievably fascinating world of science. I am beyond thankful for the trust and support that I have received throughout the years. Along that line, my deepest appreciation goes to PD Dr. Raquel Mejías-Luque, for being an endlessly supportive and encouraging mentor. It has been a privilege to learn and thrive under your guidance.

Furthermore, I would like to thank my Ph.D. mentors Prof. Dr. Klaus-Peter Janssen and Prof. Dr. Dirk Haller for their valued guidance, the fruitful discussions and their contribution to my personal and scientific development. Along that line, I want to thank everyone in our SFB, which enriched my Ph.D. journey on so many levels: the highly fascinating and encouraging scientific environment, the collaborations and possibilities that came with it and most importantly the people I met and became friends with. I cannot highlight enough what huge role this research environment played throughout this time.

I would also like to thank my group members for creating such an enjoyable working environment. The support, understanding and encouragement for each other and fun we had as a group was something that easily overcame many struggles that come along with a Ph.D. Veronika Engelsberger deserves a special acknowledgement, you made it very easy to supervise a Master student and I am very proud, that you will continue with this project – I could not imagine anyone better.

Also, I am very thankful for the people I met during this time, with whom I share unforgettable moments and true friendships: Sebastian Jarosch and Anna Sichler, Karin Taxauer and Becky Sienel, Anna Brutau Abia and Youssef Hamway, Ruolan Gong and Xue Li, Anna Meier and Nyssa Cullin. Finally, I want to thank my family and friends who always believed in me, encouraged me to follow my dreams and continue to do so whatever the future might bring.

And as always, Alisa Dietl, you played the most important role during the last 4 years. I cannot thank you enough, you are a true inspiration and your endless, unconditional support make me believe that I can do anything that I have ever dreamed of.

6. References

1. Hooi JKY, Lai WY, Ng WK, Suen MMY, Underwood FE, Tanyingoh D, et al. Global Prevalence of Helicobacter pylori Infection: Systematic Review and Meta-Analysis. Gastroenterology. 2017;153(2):420-9.
2. Marshall BJ, Warren JR. Unidentified curved bacilli in the stomach of patients with gastritis and peptic ulceration. Lancet. 1984;1(8390):1311-5.
3. Yokota S, Konno M, Fujiwara S, Toita N, Takahashi M, Yamamoto S, et al. Intrafamilial, Preferentially Mother-to-Child and Intraspousal, Helicobacter pylori Infection in Japan Determined by Mutilocus Sequence Typing and Random Amplified Polymorphic DNA Fingerprinting. Helicobacter. 2015;20(5):334-42.
4. Kayali S, Manfredi M, Gaiani F, Bianchi L, Bizzarri B, Leandro G, et al. Helicobacter pylori, transmission routes and recurrence of infection: state of the art. Acta Biomed. 2018;89(8-S):72-6.
5. Nagy P, Johansson S, Molloy-Bland M. Systematic review of time trends in the prevalence of Helicobacter pylori infection in China and the USA. Gut Pathog. 2016;8:8.
6. Weeks DL, Eskandari S, Scott DR, Sachs G. A H+-gated urea channel: the link between Helicobacter pylori urease and gastric colonization. Science. 2000;287(5452):482-5.
7. Sycuro LK, Pincus Z, Gutierrez KD, Biboy J, Stern CA, Vollmer W, et al. Peptidoglycan crosslinking relaxation promotes Helicobacter pylori's helical shape and stomach colonization. Cell. 2010;141(5):822-33.
8. Schreiber S, Konradt M, Groll C, Scheid P, Hanauer G, Werling HO, et al. The spatial orientation of Helicobacter pylori in the gastric mucus. Proc Natl Acad Sci U S A. 2004;101(14):5024-9.
9. Danon SJ, O'Rourke JL, Moss ND, Lee A. The importance of local acid production in the distribution of Helicobacter felis in the mouse stomach. Gastroenterology. 1995;108(5):1386-95.
10. Lee A, Dixon MF, Danon SJ, Kuipers E, Megraud F, Larsson H, et al. Local acid production and Helicobacter pylori: a unifying hypothesis of gastroduodenal disease. Eur J Gastroenterol Hepatol. 1995;7(5):461-5.
11. Testerman TL, McGee DJ, Mobley HLT. Adherence and Colonization. In: Mobley HLT, Mendz GL, Hazell SL, editors. Helicobacter pylori: Physiology and Genetics. Washington (DC)2001.
12. Aspholm-Hurtig M, Dailide G, Lahmann M, Kalia A, Ilver D, Roche N, et al. Functional adaptation of BabA, the H. pylori ABO blood group antigen binding adhesin. Science. 2004;305(5683):519-22.
13. Boren T, Falk P, Roth KA, Larson G, Normark S. Attachment of Helicobacter pylori to human gastric epithelium mediated by blood group antigens. Science. 1993;262(5141):1892-5.
14. Mahdavi J, Sonden B, Hurtig M, Olfat FO, Forsberg L, Roche N, et al. Helicobacter pylori SabA adhesin in persistent infection and chronic inflammation. Science. 2002;297(5581):573-8.
15. Prinz C, Schoniger M, Rad R, Becker I, Keiditsch E, Wagenpfeil S, et al. Key importance of the Helicobacter pylori adherence factor blood group antigen binding adhesin during chronic gastric inflammation. Cancer Res. 2001;61(5):1903-9.
16. Isiadinso OO, Sullivan JF. The problems of vascular access for hemodialysis in juvenile diabetics with end-stage renal disease. Angiology. 1975;26(7):569-71.
17. Sakamoto S, Watanabe T, Tokumaru T, Takagi H, Nakazato H, Lloyd KO. Expression of Lewisa, Lewisb, Lewisx, Lewisy, siayl-Lewisa, and sialyl-Lewisx blood group antigens in human gastric carcinoma and in normal gastric tissue. Cancer Res. 1989;49(3):745-52.
18. Sheu BS, Odenbreit S, Hung KH, Liu CP, Sheu SM, Yang HB, et al. Interaction between host gastric Sialyl-Lewis X and H. pylori SabA enhances H. pylori density in patients lacking gastric Lewis B antigen. Am J Gastroenterol. 2006;101(1):36-44.
19. Senkovich OA, Yin J, Ekshyyan V, Conant C, Traylor J, Adegboyega P, et al. Helicobacter pylori AlpA and AlpB bind host laminin and influence gastric inflammation in gerbils. Infect Immun. 2011;79(8):3106-16.

20. Lu H, Wu JY, Beswick EJ, Ohno T, Odenbreit S, Haas R, et al. Functional and intracellular signaling differences associated with the Helicobacter pylori AlpAB adhesin from Western and East Asian strains. J Biol Chem. 2007;282(9):6242-54.
21. Odenbreit S, Faller G, Haas R. Role of the alpAB proteins and lipopolysaccharide in adhesion of Helicobacter pylori to human gastric tissue. Int J Med Microbiol. 2002;292(3-4):247-56.
22. Javaheri A, Kruse T, Moonens K, Mejias-Luque R, Debraekeleer A, Asche CI, et al. Helicobacter pylori adhesin HopQ engages in a virulence-enhancing interaction with human CEACAMs. Nat Microbiol. 2016;2:16189.
23. Koniger V, Holsten L, Harrison U, Busch B, Loell E, Zhao Q, et al. Helicobacter pylori exploits human CEACAMs via HopQ for adherence and translocation of CagA. Nat Microbiol. 2016;2:16188.
24. Kwok T, Zabler D, Urman S, Rohde M, Hartig R, Wessler S, et al. Helicobacter exploits integrin for type IV secretion and kinase activation. Nature. 2007;449(7164):862-6.
25. Mueller D, Tegtmeyer N, Brandt S, Yamaoka Y, De Poire E, Sgouras D, et al. c-Src and c-Abl kinases control hierarchic phosphorylation and function of the CagA effector protein in Western and East Asian Helicobacter pylori strains. J Clin Invest. 2012;122(4):1553-66.
26. Papadakos KS, Sougleri IS, Mentis AF, Hatziloukas E, Sgouras DN. Presence of terminal EPIYA phosphorylation motifs in Helicobacter pylori CagA contributes to IL-8 secretion, irrespective of the number of repeats. PLoS One. 2013;8(2):e56291.
27. Nagase L, Hayashi T, Senda T, Hatakeyama M. Dramatic increase in SHP2 binding activity of Helicobacter pylori Western CagA by EPIYA-C duplication: its implications in gastric carcinogenesis. Sci Rep. 2015;5:15749.
28. Lind J, Backert S, Hoffmann R, Eichler J, Yamaoka Y, Perez-Perez GI, et al. Systematic analysis of phosphotyrosine antibodies recognizing single phosphorylated EPIYA-motifs in CagA of East Asian-type Helicobacter pylori strains. BMC Microbiol. 2016;16(1):201.
29. Lind J, Backert S, Pfleiderer K, Berg DE, Yamaoka Y, Sticht H, et al. Systematic analysis of phosphotyrosine antibodies recognizing single phosphorylated EPIYA-motifs in CagA of Western-type Helicobacter pylori strains. PLoS One. 2014;9(5):e96488.
30. Parsonnet J, Friedman GD, Orentreich N, Vogelman H. Risk for gastric cancer in people with CagA positive or CagA negative Helicobacter pylori infection. Gut. 1997;40(3):297-301.
31. Kaparakis M, Turnbull L, Carneiro L, Firth S, Coleman HA, Parkington HC, et al. Bacterial membrane vesicles deliver peptidoglycan to NOD1 in epithelial cells. Cell Microbiol. 2010;12(3):372-85.
32. Viala E, Pouyssegur J. Regulation of tumor cell motility by ERK mitogen-activated protein kinases. Ann N Y Acad Sci. 2004;1030:208-18.
33. Allison CC, Kufer TA, Kremmer E, Kaparakis M, Ferrero RL. Helicobacter pylori induces MAPK phosphorylation and AP-1 activation via a NOD1-dependent mechanism. J Immunol. 2009;183(12):8099-109.
34. Suarez G, Romero-Gallo J, Piazuelo MB, Wang G, Maier RJ, Forsberg LS, et al. Modification of Helicobacter pylori Peptidoglycan Enhances NOD1 Activation and Promotes Cancer of the Stomach. Cancer Res. 2015;75(8):1749-59.
35. Kuck D, Kolmerer B, Iking-Konert C, Krammer PH, Stremmel W, Rudi J. Vacuolating cytotoxin of Helicobacter pylori induces apoptosis in the human gastric epithelial cell line AGS. Infect Immun. 2001;69(8):5080-7.
36. Terebiznik MR, Raju D, Vazquez CL, Torbricki K, Kulkarni R, Blanke SR, et al. Effect of Helicobacter pylori's vacuolating cytotoxin on the autophagy pathway in gastric epithelial cells. Autophagy. 2009;5(3):370-9.
37. Muller A, Oertli M, Arnold IC. H. pylori exploits and manipulates innate and adaptive immune cell signaling pathways to establish persistent infection. Cell Commun Signal. 2011;9(1):25.
38. Atherton JC, Cao P, Peek RM, Jr., Tummuru MK, Blaser MJ, Cover TL. Mosaicism in vacuolating cytotoxin alleles of Helicobacter pylori. Association of specific vacA types with cytotoxin production and peptic ulceration. J Biol Chem. 1995;270(30):17771-7.
39. Rhead JL, Letley DP, Mohammadi M, Hussein N, Mohagheghi MA, Eshagh Hosseini M, et al. A new Helicobacter pylori vacuolating cytotoxin determinant, the intermediate region, is associated with gastric cancer. Gastroenterology. 2007;133(3):926-36.

40. Shibayama K, Wachino J, Arakawa Y, Saidijam M, Rutherford NG, Henderson PJ. Metabolism of glutamine and glutathione via gamma-glutamyltranspeptidase and glutamate transport in Helicobacter pylori: possible significance in the pathophysiology of the organism. Mol Microbiol. 2007;64(2):396-406.
41. Wustner S, Anderl F, Wanisch A, Sachs C, Steiger K, Nerlich A, et al. Helicobacter pylori gamma-glutamyl transferase contributes to colonization and differential recruitment of T cells during persistence. Sci Rep. 2017;7(1):13636.
42. Oertli M, Noben M, Engler DB, Semper RP, Reuter S, Maxeiner J, et al. Helicobacter pylori gamma-glutamyl transpeptidase and vacuolating cytotoxin promote gastric persistence and immune tolerance. Proc Natl Acad Sci U S A. 2013;110(8):3047-52.
43. Gong M, Ling SS, Lui SY, Yeoh KG, Ho B. Helicobacter pylori gamma-glutamyl transpeptidase is a pathogenic factor in the development of peptic ulcer disease. Gastroenterology. 2010;139(2):564-73.
44. Cullen TW, Giles DK, Wolf LN, Ecobichon C, Boneca IG, Trent MS. Helicobacter pylori versus the host: remodeling of the bacterial outer membrane is required for survival in the gastric mucosa. PLoS Pathog. 2011;7(12):e1002454.
45. Rubin EJ, Trent MS. Colonize, evade, flourish: how glyco-conjugates promote virulence of Helicobacter pylori. Gut Microbes. 2013;4(6):439-53.
46. Andersen-Nissen E, Smith KD, Strobe KL, Barrett SL, Cookson BT, Logan SM, et al. Evasion of Toll-like receptor 5 by flagellated bacteria. Proc Natl Acad Sci U S A. 2005;102(26):9247-52.
47. Pachathundikandi SK, Tegtmeyer N, Arnold IC, Lind J, Neddermann M, Falkeis-Veits C, et al. T4SS-dependent TLR5 activation by Helicobacter pylori infection. Nat Commun. 2019;10(1):5717.
48. Rad R, Ballhorn W, Voland P, Eisenacher K, Mages J, Rad L, et al. Extracellular and intracellular pattern recognition receptors cooperate in the recognition of Helicobacter pylori. Gastroenterology. 2009;136(7):2247-57.
49. Sun X, Zhang M, El-Zataari M, Owyang SY, Eaton KA, Liu M, et al. TLR2 mediates Helicobacter pylori-induced tolerogenic immune response in mice. PLoS One. 2013;8(9):e74595.
50. Otani K, Tanigawa T, Watanabe T, Nadatani Y, Sogawa M, Yamagami H, et al. Toll-like receptor 9 signaling has anti-inflammatory effects on the early phase of Helicobacter pylori-induced gastritis. Biochem Biophys Res Commun. 2012;426(3):342-9.
51. Necchi V, Manca R, Ricci V, Solcia E. Evidence for transepithelial dendritic cells in human H. pylori active gastritis. Helicobacter. 2009;14(3):208-22.
52. Tanaka H, Yoshida M, Nishiumi S, Ohnishi N, Kobayashi K, Yamamoto K, et al. The CagA protein of Helicobacter pylori suppresses the functions of dendritic cell in mice. Arch Biochem Biophys. 2010;498(1):35-42.
53. Kaebisch R, Mejias-Luque R, Prinz C, Gerhard M. Helicobacter pylori cytotoxin-associated gene A impairs human dendritic cell maturation and function through IL-10-mediated activation of STAT3. J Immunol. 2014;192(1):316-23.
54. Kabisch R, Semper RP, Wustner S, Gerhard M, Mejias-Luque R. Helicobacter pylori gamma-Glutamyltranspeptidase Induces Tolerogenic Human Dendritic Cells by Activation of Glutamate Receptors. J Immunol. 2016;196(10):4246-52.
55. Suzuki T, Kato K, Ohara S, Noguchi K, Sekine H, Nagura H, et al. Localization of antigen-presenting cells in Helicobacter pylori-infected gastric mucosa. Pathol Int. 2002;52(4):265-71.
56. Pagliari M, Munari F, Toffoletto M, Lonardi S, Chemello F, Codolo G, et al. Helicobacter pylori Affects the Antigen Presentation Activity of Macrophages Modulating the Expression of the Immune Receptor CD300E through miR-4270. Front Immunol. 2017;8:1288.
57. Ye G, Barrera C, Fan X, Gourley WK, Crowe SE, Ernst PB, et al. Expression of B7-1 and B7-2 costimulatory molecules by human gastric epithelial cells: potential role in CD4+ T cell activation during Helicobacter pylori infection. J Clin Invest. 1997;99(7):1628-36.
58. Fan X, Crowe SE, Behar S, Gunasena H, Ye G, Haeberle H, et al. The effect of class II major histocompatibility complex expression on adherence of Helicobacter pylori and induction of apoptosis in gastric epithelial cells: a mechanism for T helper cell type 1-mediated damage. J Exp Med. 1998;187(10):1659-69.

59. Shi Y, Liu XF, Zhuang Y, Zhang JY, Liu T, Yin Z, et al. Helicobacter pylori-induced Th17 responses modulate Th1 cell responses, benefit bacterial growth, and contribute to pathology in mice. J Immunol. 2010;184(9):5121-9.
60. Nagai S, Mimuro H, Yamada T, Baba Y, Moro K, Nochi T, et al. Role of Peyer's patches in the induction of Helicobacter pylori-induced gastritis. Proc Natl Acad Sci U S A. 2007;104(21):8971-6.
61. Bamford KB, Fan X, Crowe SE, Leary JF, Gourley WK, Luthra GK, et al. Lymphocytes in the human gastric mucosa during Helicobacter pylori have a T helper cell 1 phenotype. Gastroenterology. 1998;114(3):482-92.
62. Quiding-Jarbrink M, Lundin BS, Lonroth H, Svennerholm AM. CD4+ and CD8+ T cell responses in Helicobacter pylori-infected individuals. Clin Exp Immunol. 2001;123(1):81-7.
63. Hitzler I, Kohler E, Engler DB, Yazgan AS, Muller A. The role of Th cell subsets in the control of Helicobacter infections and in T cell-driven gastric immunopathology. Front Immunol. 2012;3:142.
64. Crabtree JE, Shallcross TM, Heatley RV, Wyatt JI. Mucosal tumour necrosis factor alpha and interleukin-6 in patients with Helicobacter pylori associated gastritis. Gut. 1991;32(12):1473-7.
65. Karttunen R, Karttunen T, Ekre HP, MacDonald TT. Interferon gamma and interleukin 4 secreting cells in the gastric antrum in Helicobacter pylori positive and negative gastritis. Gut. 1995;36(3):341-5.
66. Yamamoto T, Kita M, Ohno T, Iwakura Y, Sekikawa K, Imanishi J. Role of tumor necrosis factor-alpha and interferon-gamma in Helicobacter pylori infection. Microbiol Immunol. 2004;48(9):647-54.
67. Smythies LE, Waites KB, Lindsey JR, Harris PR, Ghiara P, Smith PD. Helicobacter pylori-induced mucosal inflammation is Th1 mediated and exacerbated in IL-4, but not IFN-gamma, gene-deficient mice. J Immunol. 2000;165(2):1022-9.
68. Gray BM, Fontaine CA, Poe SA, Eaton KA. Complex T cell interactions contribute to Helicobacter pylori gastritis in mice. Infect Immun. 2013;81(3):740-52.
69. Garhart CA, Heinzel FP, Czinn SJ, Nedrud JG. Vaccine-induced reduction of Helicobacter pylori colonization in mice is interleukin-12 dependent but gamma interferon and inducible nitric oxide synthase independent. Infect Immun. 2003;71(2):910-21.
70. Shiomi S, Toriie A, Imamura S, Konishi H, Mitsufuji S, Iwakura Y, et al. IL-17 is involved in Helicobacter pylori-induced gastric inflammatory responses in a mouse model. Helicobacter. 2008;13(6):518-24.
71. Mizuno T, Ando T, Nobata K, Tsuzuki T, Maeda O, Watanabe O, et al. Interleukin-17 levels in Helicobacter pylori-infected gastric mucosa and pathologic sequelae of colonization. World J Gastroenterol. 2005;11(40):6305-11.
72. Velin D, Favre L, Bernasconi E, Bachmann D, Pythoud C, Saiji E, et al. Interleukin-17 is a critical mediator of vaccine-induced reduction of Helicobacter infection in the mouse model. Gastroenterology. 2009;136(7):2237-46 e1.
73. Harris PR, Wright SW, Serrano C, Riera F, Duarte I, Torres J, et al. Helicobacter pylori gastritis in children is associated with a regulatory T-cell response. Gastroenterology. 2008;134(2):491-9.
74. Kandulski A, Wex T, Kuester D, Peitz U, Gebert I, Roessner A, et al. Naturally occurring regulatory T cells (CD4+, CD25high, FOXP3+) in the antrum and cardia are associated with higher H. pylori colonization and increased gene expression of TGF-beta1. Helicobacter. 2008;13(4):295-303.
75. Matsumoto Y, Blanchard TG, Drakes ML, Basu M, Redline RW, Levine AD, et al. Eradication of Helicobacter pylori and resolution of gastritis in the gastric mucosa of IL-10-deficient mice. Helicobacter. 2005;10(5):407-15.
76. Kienesberger S, Cox LM, Livanos A, Zhang XS, Chung J, Perez-Perez GI, et al. Gastric Helicobacter pylori Infection Affects Local and Distant Microbial Populations and Host Responses. Cell Rep. 2016;14(6):1395-407.
77. Ge Z, Sheh A, Feng Y, Muthupalani S, Ge L, Wang C, et al. Helicobacter pylori-infected C57BL/6 mice with different gastrointestinal microbiota have contrasting gastric pathology, microbial and host immune responses. Sci Rep. 2018;8(1):8014.
78. Rolig AS, Cech C, Ahler E, Carter JE, Ottemann KM. The degree of Helicobacter pylori-triggered inflammation is manipulated by preinfection host microbiota. Infect Immun. 2013;81(5):1382-9.

79. Lofgren JL, Whary MT, Ge Z, Muthupalani S, Taylor NS, Mobley M, et al. Lack of commensal flora in Helicobacter pylori-infected INS-GAS mice reduces gastritis and delays intraepithelial neoplasia. Gastroenterology. 2011;140(1):210-20.
80. Bik EM, Eckburg PB, Gill SR, Nelson KE, Purdom EA, Francois F, et al. Molecular analysis of the bacterial microbiota in the human stomach. Proc Natl Acad Sci U S A. 2006;103(3):732-7.
81. Maldonado-Contreras A, Goldfarb KC, Godoy-Vitorino F, Karaoz U, Contreras M, Blaser MJ, et al. Structure of the human gastric bacterial community in relation to Helicobacter pylori status. ISME J. 2011;5(4):574-9.
82. Li XX, Wong GL, To KF, Wong VW, Lai LH, Chow DK, et al. Bacterial microbiota profiling in gastritis without Helicobacter pylori infection or non-steroidal anti-inflammatory drug use. PLoS One. 2009;4(11):e7985.
83. Yang I, Woltemate S, Piazuelo MB, Bravo LE, Yepez MC, Romero-Gallo J, et al. Different gastric microbiota compositions in two human populations with high and low gastric cancer risk in Colombia. Sci Rep. 2016;6:18594.
84. Zheng W, Miao J, Luo L, Long G, Chen B, Shu X, et al. The Effects of Helicobacter pylori Infection on Microbiota Associated With Gastric Mucosa and Immune Factors in Children. Front Immunol. 2021;12:625586.
85. Brawner KM, Kumar R, Serrano CA, Ptacek T, Lefkowitz E, Morrow CD, et al. Helicobacter pylori infection is associated with an altered gastric microbiota in children. Mucosal Immunol. 2017;10(5):1169-77.
86. Cover TL, Blaser MJ. Helicobacter pylori in health and disease. Gastroenterology. 2009;136(6):1863-73.
87. Herrera V, Parsonnet J. Helicobacter pylori and gastric adenocarcinoma. Clin Microbiol Infect. 2009;15(11):971-6.
88. Basso D, Zambon CF, Letley DP, Stranges A, Marchet A, Rhead JL, et al. Clinical relevance of Helicobacter pylori cagA and vacA gene polymorphisms. Gastroenterology. 2008;135(1):91-9.
89. Gerhard M, Lehn N, Neumayer N, Boren T, Rad R, Schepp W, et al. Clinical relevance of the Helicobacter pylori gene for blood-group antigen-binding adhesin. Proc Natl Acad Sci U S A. 1999;96(22):12778-83.
90. Yamaoka Y, Kikuchi S, el-Zimaity HM, Gutierrez O, Osato MS, Graham DY. Importance of Helicobacter pylori oipA in clinical presentation, gastric inflammation, and mucosal interleukin 8 production. Gastroenterology. 2002;123(2):414-24.
91. El-Omar EM, Carrington M, Chow WH, McColl KE, Bream JH, Young HA, et al. Interleukin-1 polymorphisms associated with increased risk of gastric cancer. Nature. 2000;404(6776):398-402.
92. Joossens JV, Hill MJ, Elliott P, Stamler R, Lesaffre E, Dyer A, et al. Dietary salt, nitrate and stomach cancer mortality in 24 countries. European Cancer Prevention (ECP) and the INTERSALT Cooperative Research Group. Int J Epidemiol. 1996;25(3):494-504.
93. Fox JG, Beck P, Dangler CA, Whary MT, Wang TC, Shi HN, et al. Concurrent enteric helminth infection modulates inflammation and gastric immune responses and reduces helicobacter-induced gastric atrophy. Nat Med. 2000;6(5):536-42.
94. Uemura N, Okamoto S, Yamamoto S, Matsumura N, Yamaguchi S, Yamakido M, et al. Helicobacter pylori infection and the development of gastric cancer. N Engl J Med. 2001;345(11):784-9.
95. Wong BC, Lam SK, Wong WM, Chen JS, Zheng TT, Feng RE, et al. Helicobacter pylori eradication to prevent gastric cancer in a high-risk region of China: a randomized controlled trial. JAMA. 2004;291(2):187-94.
96. Chiang TH, Chang WJ, Chen SL, Yen AM, Fann JC, Chiu SY, et al. Mass eradication of Helicobacter pylori to reduce gastric cancer incidence and mortality: a long-term cohort study on Matsu Islands. Gut. 2021;70(2):243-50.
97. Gravina AG, Zagari RM, De Musis C, Romano L, Loguercio C, Romano M. Helicobacter pylori and extragastric diseases: A review. World J Gastroenterol. 2018;24(29):3204-21.
98. Mendall MA, Goggin PM, Molineaux N, Levy J, Toosy T, Strachan D, et al. Relation of Helicobacter pylori infection and coronary heart disease. Br Heart J. 1994;71(5):437-9.

99. Lai CY, Yang TY, Lin CL, Kao CH. Helicobacter pylori infection and the risk of acute coronary syndrome: a nationwide retrospective cohort study. Eur J Clin Microbiol Infect Dis. 2015;34(1):69-74.
100. Matsuura E, Kobayashi K, Matsunami Y, Shen L, Quan N, Makarova M, et al. Autoimmunity, infectious immunity, and atherosclerosis. J Clin Immunol. 2009;29(6):714-21.
101. Chen Y, Segers S, Blaser MJ. Association between Helicobacter pylori and mortality in the NHANES III study. Gut. 2013;62(9):1262-9.
102. Alvarez-Arellano L, Maldonado-Bernal C. Helicobacter pylori and neurological diseases: Married by the laws of inflammation. World J Gastrointest Pathophysiol. 2014;5(4):400-4.
103. Wang ZW, Li Y, Huang LY, Guan QK, Xu DW, Zhou WK, et al. Helicobacter pylori infection contributes to high risk of ischemic stroke: evidence from a meta-analysis. J Neurol. 2012;259(12):2527-37.
104. Huang WS, Yang TY, Shen WC, Lin CL, Lin MC, Kao CH. Association between Helicobacter pylori infection and dementia. J Clin Neurosci. 2014;21(8):1355-8.
105. Doulberis M, Kotronis G, Thomann R, Polyzos SA, Boziki M, Gialamprinou D, et al. Review: Impact of Helicobacter pylori on Alzheimer's disease: What do we know so far? Helicobacter. 2018;23(1).
106. Cook KW, Crooks J, Hussain K, O'Brien K, Braitch M, Kareem H, et al. Helicobacter pylori infection reduces disease severity in an experimental model of multiple sclerosis. Front Microbiol. 2015;6:52.
107. Fasano A, Bove F, Gabrielli M, Petracca M, Zocco MA, Ragazzoni E, et al. The role of small intestinal bacterial overgrowth in Parkinson's disease. Mov Disord. 2013;28(9):1241-9.
108. Huang HK, Wang JH, Lei WY, Chen CL, Chang CY, Liou LS. Helicobacter pylori infection is associated with an increased risk of Parkinson's disease: A population-based retrospective cohort study. Parkinsonism Relat Disord. 2018;47:26-31.
109. Shen X, Yang H, Wu Y, Zhang D, Jiang H. Meta-analysis: Association of Helicobacter pylori infection with Parkinson's diseases. Helicobacter. 2017;22(5).
110. Dardiotis E, Sokratous M, Tsouris Z, Siokas V, Mentis AA, Aloizou AM, et al. Association between Helicobacter pylori infection and Guillain-Barre Syndrome: A meta-analysis. Eur J Clin Invest. 2020;50(5):e13218.
111. Chiba S, Sugiyama T, Yonekura K, Tanaka S, Matsumoto H, Fujii N, et al. An antibody to VacA of Helicobacter pylori in cerebrospinal fluid from patients with Guillain-Barre syndrome. J Neurol Neurosurg Psychiatry. 2002;73(1):76-8.
112. Kountouras J, Deretzi G, Zavos C, Karatzoglou P, Touloumis L, Nicolaides T, et al. Association between Helicobacter pylori infection and acute inflammatory demyelinating polyradiculoneuropathy. Eur J Neurol. 2005;12(2):139-43.
113. Argenziano G, Donnarumma G, Iovene MR, Arnese P, Baldassarre MA, Baroni A. Incidence of anti-Helicobacter pylori and anti-CagA antibodies in rosacea patients. Int J Dermatol. 2003;42(8):601-4.
114. Gravina A, Federico A, Ruocco E, Lo Schiavo A, Masarone M, Tuccillo C, et al. Helicobacter pylori infection but not small intestinal bacterial overgrowth may play a pathogenic role in rosacea. United European Gastroenterol J. 2015;3(1):17-24.
115. Campanati A, Ganzetti G, Martina E, Giannoni M, Gesuita R, Bendia E, et al. Helicobacter pylori infection in psoriasis: results of a clinical study and review of the literature. Int J Dermatol. 2015;54(5):e109-14.
116. Ozkasap S, Yarali N, Isik P, Bay A, Kara A, Tunc B. The role of prohepcidin in anemia due to Helicobacter pylori infection. Pediatr Hematol Oncol. 2013;30(5):425-31.
117. Muhsen K, Cohen D. Helicobacter pylori infection and iron stores: a systematic review and meta-analysis. Helicobacter. 2008;13(5):323-40.
118. Blecker U, Renders F, Lanciers S, Vandenplas Y. Syncopes leading to the diagnosis of a Helicobacter pylori positive chronic active haemorrhagic gastritis. Eur J Pediatr. 1991;150(8):560-1.
119. Lahner E, Persechino S, Annibale B. Micronutrients (Other than iron) and Helicobacter pylori infection: a systematic review. Helicobacter. 2012;17(1):1-15.
120. Campuzano-Maya G. Hematologic manifestations of Helicobacter pylori infection. World J Gastroenterol. 2014;20(36):12818-38.

121. Gasbarrini A, Franceschi F, Tartaglione R, Landolfi R, Pola P, Gasbarrini G. Regression of autoimmune thrombocytopenia after eradication of Helicobacter pylori. Lancet. 1998;352(9131):878.
122. Yang GH, Wu JS, Yang YC, Huang YH, Lu FH, Chang CJ. Gastric Helicobacter pylori infection associated with risk of diabetes mellitus, but not prediabetes. J Gastroenterol Hepatol. 2014;29(10):1794-9.
123. Hsieh MC, Wang SS, Hsieh YT, Kuo FC, Soon MS, Wu DC. Helicobacter pylori infection associated with high HbA1c and type 2 diabetes. Eur J Clin Invest. 2013;43(9):949-56.
124. Zhou X, Liu W, Gu M, Zhou H, Zhang G. Helicobacter pylori infection causes hepatic insulin resistance by the c-Jun/miR-203/SOCS3 signaling pathway. J Gastroenterol. 2015;50(10):1027-40.
125. Oertli M, Sundquist M, Hitzler I, Engler DB, Arnold IC, Reuter S, et al. DC-derived IL-18 drives Treg differentiation, murine Helicobacter pylori-specific immune tolerance, and asthma protection. J Clin Invest. 2012;122(3):1082-96.
126. Chen Y, Blaser MJ. Inverse associations of Helicobacter pylori with asthma and allergy. Arch Intern Med. 2007;167(8):821-7.
127. Sumida Y, Kanemasa K, Imai S, Mori K, Tanaka S, Shimokobe H, et al. Helicobacter pylori infection might have a potential role in hepatocyte ballooning in nonalcoholic fatty liver disease. J Gastroenterol. 2015;50(9):996-1004.
128. Chen CX, Mao YS, Foster P, Zhu ZW, Du J, Guo CY. Possible association between Helicobacter pylori infection and nonalcoholic fatty liver disease. Appl Physiol Nutr Metab. 2017;42(3):295-301.
129. Fukuda Y, Bamba H, Okui M, Tamura K, Tanida N, Satomi M, et al. Helicobacter pylori infection increases mucosal permeability of the stomach and intestine. Digestion. 2001;63 Suppl 1:93-6.
130. Ki MR, Goo MJ, Park JK, Hong IH, Ji AR, Han SY, et al. Helicobacter pylori accelerates hepatic fibrosis by sensitizing transforming growth factor-beta1-induced inflammatory signaling. Lab Invest. 2010;90(10):1507-16.
131. Krasinskas AM, Yao Y, Randhawa P, Dore MP, Sepulveda AR. Helicobacter pylori may play a contributory role in the pathogenesis of primary sclerosing cholangitis. Dig Dis Sci. 2007;52(9):2265-70.
132. Nilsson HO, Taneera J, Castedal M, Glatz E, Olsson R, Wadstrom T. Identification of Helicobacter pylori and other Helicobacter species by PCR, hybridization, and partial DNA sequencing in human liver samples from patients with primary sclerosing cholangitis or primary biliary cirrhosis. J Clin Microbiol. 2000;38(3):1072-6.
133. Leone N, Pellicano R, Brunello F, Cutufia MA, Berrutti M, Fagoonee S, et al. Helicobacter pylori seroprevalence in patients with cirrhosis of the liver and hepatocellular carcinoma. Cancer Detect Prev. 2003;27(6):494-7.
134. Tu QV, Okoli AS, Kovach Z, Mendz GL. Hepatocellular carcinoma: prevalence and molecular pathogenesis of Helicobacter spp. Future Microbiol. 2009;4(10):1283-301.
135. Wang F, Xia P, Wu F, Wang D, Wang W, Ward T, et al. Helicobacter pylori VacA disrupts apical membrane-cytoskeletal interactions in gastric parietal cells. J Biol Chem. 2008;283(39):26714-25.
136. Nordenstedt H, Nilsson M, Johnsen R, Lagergren J, Hveem K. Helicobacter pylori infection and gastroesophageal reflux in a population-based study (The HUNT Study). Helicobacter. 2007;12(1):16-22.
137. Kandulski A, Malfertheiner P. Helicobacter pylori and gastroesophageal reflux disease. Curr Opin Gastroenterol. 2014;30(4):402-7.
138. Raghunath A, Hungin AP, Wooff D, Childs S. Prevalence of Helicobacter pylori in patients with gastro-oesophageal reflux disease: systematic review. BMJ. 2003;326(7392):737.
139. Ghoshal UC, Chourasia D. Gastroesophageal Reflux Disease and Helicobacter pylori: What May Be the Relationship? J Neurogastroenterol Motil. 2010;16(3):243-50.
140. Fischbach LA, Graham DY, Kramer JR, Rugge M, Verstovsek G, Parente P, et al. Association between Helicobacter pylori and Barrett's esophagus: a case-control study. Am J Gastroenterol. 2014;109(3):357-68.

141. Rokkas T, Pistiolas D, Sechopoulos P, Robotis I, Margantinis G. Relationship between Helicobacter pylori infection and esophageal neoplasia: a meta-analysis. Clin Gastroenterol Hepatol. 2007;5(12):1413-7, 7 e1-2.
142. Engler DB, Leonardi I, Hartung ML, Kyburz A, Spath S, Becher B, et al. Helicobacter pylori-specific protection against inflammatory bowel disease requires the NLRP3 inflammasome and IL-18. Inflamm Bowel Dis. 2015;21(4):854-61.
143. Koch KN, Muller A. Helicobacter pylori activates the TLR2/NLRP3/caspase-1/IL-18 axis to induce regulatory T-cells, establish persistent infection and promote tolerance to allergens. Gut Microbes. 2015;6(6):382-7.
144. Higgins PD, Johnson LA, Luther J, Zhang M, Sauder KL, Blanco LP, et al. Prior Helicobacter pylori infection ameliorates Salmonella typhimurium-induced colitis: mucosal crosstalk between stomach and distal intestine. Inflamm Bowel Dis. 2011;17(6):1398-408.
145. Castano-Rodriguez N, Kaakoush NO, Lee WS, Mitchell HM. Dual role of Helicobacter and Campylobacter species in IBD: a systematic review and meta-analysis. Gut. 2017;66(2):235-49.
146. Butt J, Epplein M. Helicobacter pylori and colorectal cancer-A bacterium going abroad? PLoS Pathog. 2019;15(8):e1007861.
147. Butt J, Jenab M, Pawlita M, Tjonneland A, Kyro C, Boutron-Ruault MC, et al. Antibody Responses to Helicobacter pylori and Risk of Developing Colorectal Cancer in a European Cohort. Cancer Epidemiol Biomarkers Prev. 2020;29(7):1475-81.
148. Wu Q, Yang ZP, Xu P, Gao LC, Fan DM. Association between Helicobacter pylori infection and the risk of colorectal neoplasia: a systematic review and meta-analysis. Colorectal Dis. 2013;15(7):e352-64.
149. Choi DS, Seo SI, Shin WG, Park CH. Risk for Colorectal Neoplasia in Patients With Helicobacter pylori Infection: A Systematic Review and Meta-analysis. Clin Transl Gastroenterol. 2020;11(2):e00127.
150. Zuo Y, Jing Z, Bie M, Xu C, Hao X, Wang B. Association between Helicobacter pylori infection and the risk of colorectal cancer: A systematic review and meta-analysis. Medicine (Baltimore). 2020;99(37):e21832.
151. Lu D, Wang M, Ke X, Wang Q, Wang J, Li D, et al. Association Between H. pylori Infection and Colorectal Polyps: A Meta-Analysis of Observational Studies. Front Med (Lausanne). 2021;8:706036.
152. Sung H, Ferlay J, Siegel RL, Laversanne M, Soerjomataram I, Jemal A, et al. Global Cancer Statistics 2020: GLOBOCAN Estimates of Incidence and Mortality Worldwide for 36 Cancers in 185 Countries. CA Cancer J Clin. 2021;71(3):209-49.
153. Keum N, Giovannucci E. Global burden of colorectal cancer: emerging trends, risk factors and prevention strategies. Nat Rev Gastroenterol Hepatol. 2019;16(12):713-32.
154. Armaghany T, Wilson JD, Chu Q, Mills G. Genetic alterations in colorectal cancer. Gastrointest Cancer Res. 2012;5(1):19-27.
155. Cancer Genome Atlas N. Comprehensive molecular characterization of human colon and rectal cancer. Nature. 2012;487(7407):330-7.
156. Brannon AR, Vakiani E, Sylvester BE, Scott SN, McDermott G, Shah RH, et al. Comparative sequencing analysis reveals high genomic concordance between matched primary and metastatic colorectal cancer lesions. Genome Biol. 2014;15(8):454.
157. Dow LE, O'Rourke KP, Simon J, Tschaharganeh DF, van Es JH, Clevers H, et al. Apc Restoration Promotes Cellular Differentiation and Reestablishes Crypt Homeostasis in Colorectal Cancer. Cell. 2015;161(7):1539-52.
158. Kedrin D, Gala MK. Genetics of the serrated pathway to colorectal cancer. Clin Transl Gastroenterol. 2015;6:e84.
159. Leggett B, Whitehall V. Role of the serrated pathway in colorectal cancer pathogenesis. Gastroenterology. 2010;138(6):2088-100.
160. Bond CE, McKeone DM, Kalimutho M, Bettington ML, Pearson SA, Dumenil TD, et al. RNF43 and ZNRF3 are commonly altered in serrated pathway colorectal tumorigenesis. Oncotarget. 2016;7(43):70589-600.
161. Yan HHN, Lai JCW, Ho SL, Leung WK, Law WL, Lee JFY, et al. RNF43 germline and somatic mutation in serrated neoplasia pathway and its association with BRAF mutation. Gut. 2017;66(9):1645-56.

162. Itzkowitz SH, Yio X. Inflammation and cancer IV. Colorectal cancer in inflammatory bowel disease: the role of inflammation. Am J Physiol Gastrointest Liver Physiol. 2004;287(1):G7-17.
163. Jess T, Rungoe C, Peyrin-Biroulet L. Risk of colorectal cancer in patients with ulcerative colitis: a meta-analysis of population-based cohort studies. Clin Gastroenterol Hepatol. 2012;10(6):639-45.
164. Robles AI, Traverso G, Zhang M, Roberts NJ, Khan MA, Joseph C, et al. Whole-Exome Sequencing Analyses of Inflammatory Bowel Disease-Associated Colorectal Cancers. Gastroenterology. 2016;150(4):931-43.
165. Grady WM, Carethers JM. Genomic and epigenetic instability in colorectal cancer pathogenesis. Gastroenterology. 2008;135(4):1079-99.
166. Carethers JM, Jung BH. Genetics and Genetic Biomarkers in Sporadic Colorectal Cancer. Gastroenterology. 2015;149(5):1177-90 e3.
167. Guinney J, Dienstmann R, Wang X, de Reynies A, Schlicker A, Soneson C, et al. The consensus molecular subtypes of colorectal cancer. Nat Med. 2015;21(11):1350-6.
168. Flossmann E, Rothwell PM, British Doctors Aspirin T, the UKTIAAT. Effect of aspirin on long-term risk of colorectal cancer: consistent evidence from randomised and observational studies. Lancet. 2007;369(9573):1603-13.
169. Thun MJ, Namboodiri MM, Heath CW, Jr. Aspirin use and reduced risk of fatal colon cancer. N Engl J Med. 1991;325(23):1593-6.
170. Lakatos PL, Lakatos L. Risk for colorectal cancer in ulcerative colitis: changes, causes and management strategies. World J Gastroenterol. 2008;14(25):3937-47.
171. Yu H, Pardoll D, Jove R. STATs in cancer inflammation and immunity: a leading role for STAT3. Nat Rev Cancer. 2009;9(11):798-809.
172. Sakamoto K, Maeda S, Hikiba Y, Nakagawa H, Hayakawa Y, Shibata W, et al. Constitutive NF-kappaB activation in colorectal carcinoma plays a key role in angiogenesis, promoting tumor growth. Clin Cancer Res. 2009;15(7):2248-58.
173. Fridman WH, Pages F, Sautes-Fridman C, Galon J. The immune contexture in human tumours: impact on clinical outcome. Nat Rev Cancer. 2012;12(4):298-306.
174. Wang K, Kim MK, Di Caro G, Wong J, Shalapour S, Wan J, et al. Interleukin-17 receptor a signaling in transformed enterocytes promotes early colorectal tumorigenesis. Immunity. 2014;41(6):1052-63.
175. Grivennikov SI, Wang K, Mucida D, Stewart CA, Schnabl B, Jauch D, et al. Adenoma-linked barrier defects and microbial products drive IL-23/IL-17-mediated tumour growth. Nature. 2012;491(7423):254-8.
176. Cheng Y, Ling Z, Li L. The Intestinal Microbiota and Colorectal Cancer. Front Immunol. 2020;11:615056.
177. Cullin N, Azevedo Antunes C, Straussman R, Stein-Thoeringer CK, Elinav E. Microbiome and cancer. Cancer Cell. 2021;39(10):1317-41.
178. Castellarin M, Warren RL, Freeman JD, Dreolini L, Krzywinski M, Strauss J, et al. Fusobacterium nucleatum infection is prevalent in human colorectal carcinoma. Genome Res. 2012;22(2):299-306.
179. Han YW, Shi W, Huang GT, Kinder Haake S, Park NH, Kuramitsu H, et al. Interactions between periodontal bacteria and human oral epithelial cells: Fusobacterium nucleatum adheres to and invades epithelial cells. Infect Immun. 2000;68(6):3140-6.
180. Zhang S, Li C, Liu J, Geng F, Shi X, Li Q, et al. Fusobacterium nucleatum promotes epithelial-mesenchymal transiton through regulation of the lncRNA MIR4435-2HG/miR-296-5p/Akt2/SNAI1 signaling pathway. FEBS J. 2020;287(18):4032-47.
181. Dalmasso G, Cougnoux A, Delmas J, Darfeuille-Michaud A, Bonnet R. The bacterial genotoxin colibactin promotes colon tumor growth by modifying the tumor microenvironment. Gut Microbes. 2014;5(5):675-80.
182. Nougayrede JP, Homburg S, Taieb F, Boury M, Brzuszkiewicz E, Gottschalk G, et al. Escherichia coli induces DNA double-strand breaks in eukaryotic cells. Science. 2006;313(5788):848-51.
183. Wu S, Rhee KJ, Zhang M, Franco A, Sears CL. Bacteroides fragilis toxin stimulates intestinal epithelial cell shedding and gamma-secretase-dependent E-cadherin cleavage. J Cell Sci. 2007;120(Pt 11):1944-52.

184. Chung L, Thiele Orberg E, Geis AL, Chan JL, Fu K, DeStefano Shields CE, et al. Bacteroides fragilis Toxin Coordinates a Pro-carcinogenic Inflammatory Cascade via Targeting of Colonic Epithelial Cells. Cell Host Microbe. 2018;23(2):203-14 e5.
185. Boleij A, Hechenbleikner EM, Goodwin AC, Badani R, Stein EM, Lazarev MG, et al. The Bacteroides fragilis toxin gene is prevalent in the colon mucosa of colorectal cancer patients. Clin Infect Dis. 2015;60(2):208-15.
186. Haghi F, Goli E, Mirzaei B, Zeighami H. The association between fecal enterotoxigenic B. fragilis with colorectal cancer. BMC Cancer. 2019;19(1):879.
187. Chen HM, Yu YN, Wang JL, Lin YW, Kong X, Yang CQ, et al. Decreased dietary fiber intake and structural alteration of gut microbiota in patients with advanced colorectal adenoma. Am J Clin Nutr. 2013;97(5):1044-52.
188. Ou J, DeLany JP, Zhang M, Sharma S, O'Keefe SJ. Association between low colonic short-chain fatty acids and high bile acids in high colon cancer risk populations. Nutr Cancer. 2012;64(1):34-40.
189. Dermadi D, Valo S, Ollila S, Soliymani R, Sipari N, Pussila M, et al. Western Diet Deregulates Bile Acid Homeostasis, Cell Proliferation, and Tumorigenesis in Colon. Cancer Res. 2017;77(12):3352-63.
190. Genua F, Raghunathan V, Jenab M, Gallagher WM, Hughes DJ. The Role of Gut Barrier Dysfunction and Microbiome Dysbiosis in Colorectal Cancer Development. Front Oncol. 2021;11:626349.
191. Coleman OI, Haller D. Microbe-Mucus Interface in the Pathogenesis of Colorectal Cancer. Cancers (Basel). 2021;13(4).
192. Velcich A, Yang W, Heyer J, Fragale A, Nicholas C, Viani S, et al. Colorectal cancer in mice genetically deficient in the mucin Muc2. Science. 2002;295(5560):1726-9.
193. Van der Sluis M, De Koning BA, De Bruijn AC, Velcich A, Meijerink JP, Van Goudoever JB, et al. Muc2-deficient mice spontaneously develop colitis, indicating that MUC2 is critical for colonic protection. Gastroenterology. 2006;131(1):117-29.
194. Schmitt M, Greten FR. The inflammatory pathogenesis of colorectal cancer. Nat Rev Immunol. 2021;21(10):653-67.
195. Burtin F, Mullins CS, Linnebacher M. Mouse models of colorectal cancer: Past, present and future perspectives. World J Gastroenterol. 2020;26(13):1394-426.
196. Papanikolaou A, Wang QS, Papanikolaou D, Whiteley HE, Rosenberg DW. Sequential and morphological analyses of aberrant crypt foci formation in mice of differing susceptibility to azoxymethane-induced colon carcinogenesis. Carcinogenesis. 2000;21(8):1567-72.
197. Neufert C, Becker C, Neurath MF. An inducible mouse model of colon carcinogenesis for the analysis of sporadic and inflammation-driven tumor progression. Nat Protoc. 2007;2(8):1998-2004.
198. Moser AR, Pitot HC, Dove WF. A dominant mutation that predisposes to multiple intestinal neoplasia in the mouse. Science. 1990;247(4940):322-4.
199. Fodde R, Edelmann W, Yang K, van Leeuwen C, Carlson C, Renault B, et al. A targeted chain-termination mutation in the mouse Apc gene results in multiple intestinal tumors. Proc Natl Acad Sci U S A. 1994;91(19):8969-73.
200. Janssen KP, Alberici P, Fsihi H, Gaspar C, Breukel C, Franken P, et al. APC and oncogenic KRAS are synergistic in enhancing Wnt signaling in intestinal tumor formation and progression. Gastroenterology. 2006;131(4):1096-109.
201. Boutin AT, Liao WT, Wang M, Hwang SS, Karpinets TV, Cheung H, et al. Oncogenic Kras drives invasion and maintains metastases in colorectal cancer. Genes Dev. 2017;31(4):370-82.
202. Drost J, van Jaarsveld RH, Ponsioen B, Zimberlin C, van Boxtel R, Buijs A, et al. Sequential cancer mutations in cultured human intestinal stem cells. Nature. 2015;521(7550):43-7.
203. Roper J, Tammela T, Cetinbas NM, Akkad A, Roghanian A, Rickelt S, et al. In vivo genome editing and organoid transplantation models of colorectal cancer and metastasis. Nat Biotechnol. 2017;35(6):569-76.
204. Winawer SJ, Fletcher RH, Miller L, Godlee F, Stolar MH, Mulrow CD, et al. Colorectal cancer screening: clinical guidelines and rationale. Gastroenterology. 1997;112(2):594-642.
205. Dekker E, Tanis PJ, Vleugels JLA, Kasi PM, Wallace MB. Colorectal cancer. Lancet. 2019;394(10207):1467-80.

206. Wolf FA, Angerer P, Theis FJ. SCANPY: large-scale single-cell gene expression data analysis. Genome Biol. 2018;19(1):15.
207. La Manno G, Soldatov R, Zeisel A, Braun E, Hochgerner H, Petukhov V, et al. RNA velocity of single cells. Nature. 2018;560(7719):494-8.
208. Bergen V, Lange M, Peidli S, Wolf FA, Theis FJ. Generalizing RNA velocity to transient cell states through dynamical modeling. Nat Biotechnol. 2020;38(12):1408-14.
209. van Zanten SJ, Kolesnikow T, Leung V, O'Rourke JL, Lee A. Gastric transitional zones, areas where Helicobacter treatment fails: results of a treatment trial using the Sydney strain mouse model. Antimicrob Agents Chemother. 2003;47(7):2249-55.
210. Ralser A, Dietl A, Jarosch S, Engelsberger V, Wanisch A, Janssen KP, et al. Helicobacter pylori promotes colorectal carcinogenesis by deregulating intestinal immunity and inducing a mucus-degrading microbiota signature. medRxiv. 2022:2022.06.16.22276474.
211. Jarosch S, Köhlen J, Sarker RSJ, Steiger K, Janssen KP, Christians A, et al. Multiplexed imaging and automated signal quantification in formalin-fixed paraffin-embedded tissues by ChipCytometry. Cell Reports Methods. 2021;1(7).
212. Reitmeier S, Kiessling S, Neuhaus K, Haller D. Comparing Circadian Rhythmicity in the Human Gut Microbiome. STAR Protoc. 2020;1(3):100148.
213. Reitmeier S, Kiessling S, Clavel T, List M, Almeida EL, Ghosh TS, et al. Arrhythmic Gut Microbiome Signatures Predict Risk of Type 2 Diabetes. Cell Host Microbe. 2020;28(2):258-72 e6.
214. Zoetendal EG, Heilig HG, Klaassens ES, Booijink CC, Kleerebezem M, Smidt H, et al. Isolation of DNA from bacterial samples of the human gastrointestinal tract. Nat Protoc. 2006;1(2):870-3.
215. Turnbaugh PJ, Hamady M, Yatsunenko T, Cantarel BL, Duncan A, Ley RE, et al. A core gut microbiome in obese and lean twins. Nature. 2009;457(7228):480-4.
216. Kozich JJ, Westcott SL, Baxter NT, Highlander SK, Schloss PD. Development of a dual-index sequencing strategy and curation pipeline for analyzing amplicon sequence data on the MiSeq Illumina sequencing platform. Appl Environ Microbiol. 2013;79(17):5112-20.
217. Bolyen E, Rideout JR, Dillon MR, Bokulich NA, Abnet CC, Al-Ghalith GA, et al. Reproducible, interactive, scalable and extensible microbiome data science using QIIME 2. Nat Biotechnol. 2019;37(8):852-7.
218. Segata N, Izard J, Waldron L, Gevers D, Miropolsky L, Garrett WS, et al. Metagenomic biomarker discovery and explanation. Genome Biol. 2011;12(6):R60.
219. Luecken MD, Theis FJ. Current best practices in single-cell RNA-seq analysis: a tutorial. Mol Syst Biol. 2019;15(6):e8746.
220. Zhu C, Song K, Shen Z, Quan Y, Tan B, Luo W, et al. Roseburia intestinalis inhibits interleukin17 excretion and promotes regulatory T cells differentiation in colitis. Mol Med Rep. 2018;17(6):7567-74.
221. Akeus P, Langenes V, von Mentzer A, Yrlid U, Sjoling A, Saksena P, et al. Altered chemokine production and accumulation of regulatory T cells in intestinal adenomas of APC(Min/+) mice. Cancer Immunol Immunother. 2014;63(8):807-19.
222. Becht E, McInnes L, Healy J, Dutertre CA, Kwok IWH, Ng LG, et al. Dimensionality reduction for visualizing single-cell data using UMAP. Nat Biotechnol. 2018.
223. Osman A, Yan B, Li Y, Pavelko KD, Quandt J, Saadalla A, et al. TCF-1 controls Treg cell functions that regulate inflammation, CD8(+) T cell cytotoxicity and severity of colon cancer. Nat Immunol. 2021;22(9):1152-62.
224. Miragaia RJ, Gomes T, Chomka A, Jardine L, Riedel A, Hegazy AN, et al. Single-Cell Transcriptomics of Regulatory T Cells Reveals Trajectories of Tissue Adaptation. Immunity. 2019;50(2):493-504 e7.
225. Vasanthakumar A, Liao Y, Teh P, Pascutti MF, Oja AE, Garnham AL, et al. The TNF Receptor Superfamily-NF-kappaB Axis Is Critical to Maintain Effector Regulatory T Cells in Lymphoid and Non-lymphoid Tissues. Cell Rep. 2017;20(12):2906-20.
226. Miller BC, Sen DR, Al Abosy R, Bi K, Virkud YV, LaFleur MW, et al. Subsets of exhausted CD8(+) T cells differentially mediate tumor control and respond to checkpoint blockade. Nat Immunol. 2019;20(3):326-36.
227. Wherry EJ, Ha SJ, Kaech SM, Haining WN, Sarkar S, Kalia V, et al. Molecular signature of CD8+ T cell exhaustion during chronic viral infection. Immunity. 2007;27(4):670-84.

228. Parikh K, Antanaviciute A, Fawkner-Corbett D, Jagielowicz M, Aulicino A, Lagerholm C, et al. Colonic epithelial cell diversity in health and inflammatory bowel disease. Nature. 2019;567(7746):49-55.
229. Moor AE, Harnik Y, Ben-Moshe S, Massasa EE, Rozenberg M, Eilam R, et al. Spatial Reconstruction of Single Enterocytes Uncovers Broad Zonation along the Intestinal Villus Axis. Cell. 2018;175(4):1156-67 e15.
230. Kanehisa M, Goto S. KEGG: kyoto encyclopedia of genes and genomes. Nucleic Acids Res. 2000;28(1):27-30.
231. Subramanian A, Tamayo P, Mootha VK, Mukherjee S, Ebert BL, Gillette MA, et al. Gene set enrichment analysis: a knowledge-based approach for interpreting genome-wide expression profiles. Proc Natl Acad Sci U S A. 2005;102(43):15545-50.
232. Asada R, Saito A, Kawasaki N, Kanemoto S, Iwamoto H, Oki M, et al. The endoplasmic reticulum stress transducer OASIS is involved in the terminal differentiation of goblet cells in the large intestine. J Biol Chem. 2012;287(11):8144-53.
233. Jackstadt R, van Hooff SR, Leach JD, Cortes-Lavaud X, Lohuis JO, Ridgway RA, et al. Epithelial NOTCH Signaling Rewires the Tumor Microenvironment of Colorectal Cancer to Drive Poor-Prognosis Subtypes and Metastasis. Cancer Cell. 2019;36(3):319-36 e7.
234. Wirbel J, Pyl PT, Kartal E, Zych K, Kashani A, Milanese A, et al. Meta-analysis of fecal metagenomes reveals global microbial signatures that are specific for colorectal cancer. Nat Med. 2019;25(4):679-89.
235. Franceschi F, Covino M, Roubaud Baudron C. Review: Helicobacter pylori and extragastric diseases. Helicobacter. 2019;24 Suppl 1:e12636.
236. Valenzuela MA, Canales J, Corvalan AH, Quest AF. Helicobacter pylori-induced inflammation and epigenetic changes during gastric carcinogenesis. World J Gastroenterol. 2015;21(45):12742-56.
237. Arnold IC, Dehzad N, Reuter S, Martin H, Becher B, Taube C, et al. Helicobacter pylori infection prevents allergic asthma in mouse models through the induction of regulatory T cells. J Clin Invest. 2011;121(8):3088-93.
238. Eaden JA, Abrams KR, Mayberry JF. The risk of colorectal cancer in ulcerative colitis: a meta-analysis. Gut. 2001;48(4):526-35.
239. Rubin DT, Huo D, Kinnucan JA, Sedrak MS, McCullom NE, Bunnag AP, et al. Inflammation is an independent risk factor for colonic neoplasia in patients with ulcerative colitis: a case-control study. Clin Gastroenterol Hepatol. 2013;11(12):1601-8 e1-4.
240. Ruiz VE, Sachdev M, Zhang S, Wen S, Moss SF. Isolating, immunophenotyping and ex vivo stimulation of CD4+ and CD8+ gastric lymphocytes during murine Helicobacter pylori infection. J Immunol Methods. 2012;384(1-2):157-63.
241. Nurgalieva ZZ, Conner ME, Opekun AR, Zheng CQ, Elliott SN, Ernst PB, et al. B-cell and T-cell immune responses to experimental Helicobacter pylori infection in humans. Infect Immun. 2005;73(5):2999-3006.
242. Torgerson TR, Linane A, Moes N, Anover S, Mateo V, Rieux-Laucat F, et al. Severe food allergy as a variant of IPEX syndrome caused by a deletion in a noncoding region of the FOXP3 gene. Gastroenterology. 2007;132(5):1705-17.
243. Singh B, Read S, Asseman C, Malmstrom V, Mottet C, Stephens LA, et al. Control of intestinal inflammation by regulatory T cells. Immunol Rev. 2001;182:190-200.
244. Sharma A, Rudra D. Emerging Functions of Regulatory T Cells in Tissue Homeostasis. Front Immunol. 2018;9:883.
245. Hoytema van Konijnenburg DP, Mucida D. Intraepithelial lymphocytes. Curr Biol. 2017;27(15):R737-R9.
246. Sujino T, London M, Hoytema van Konijnenburg DP, Rendon T, Buch T, Silva HM, et al. Tissue adaptation of regulatory and intraepithelial CD4(+) T cells controls gut inflammation. Science. 2016;352(6293):1581-6.
247. Ohnmacht C, Park JH, Cording S, Wing JB, Atarashi K, Obata Y, et al. MUCOSAL IMMUNOLOGY. The microbiota regulates type 2 immunity through RORgammat(+) T cells. Science. 2015;349(6251):989-93.
248. Sefik E, Geva-Zatorsky N, Oh S, Konnikova L, Zemmour D, McGuire AM, et al. MUCOSAL IMMUNOLOGY. Individual intestinal symbionts induce a distinct population of RORgamma(+) regulatory T cells. Science. 2015;349(6251):993-7.
249. Yang BH, Hagemann S, Mamareli P, Lauer U, Hoffmann U, Beckstette M, et al. Foxp3(+) T cells expressing RORgammat represent a stable regulatory T-cell effector lineage

with enhanced suppressive capacity during intestinal inflammation. Mucosal Immunol. 2016;9(2):444-57.
250. Kryczek I, Wu K, Zhao E, Wei S, Vatan L, Szeliga W, et al. IL-17+ regulatory T cells in the microenvironments of chronic inflammation and cancer. J Immunol. 2011;186(7):4388-95.
251. Yang S, Wang B, Guan C, Wu B, Cai C, Wang M, et al. Foxp3+IL-17+ T cells promote development of cancer-initiating cells in colorectal cancer. J Leukoc Biol. 2011;89(1):85-91.
252. Ma C, Dong X. Colorectal cancer-derived Foxp3(+) IL-17(+) T cells suppress tumour-specific CD8+ T cells. Scand J Immunol. 2011;74(1):47-51.
253. Caruso R, Fina D, Paoluzi OA, Del Vecchio Blanco G, Stolfi C, Rizzo A, et al. IL-23-mediated regulation of IL-17 production in Helicobacter pylori-infected gastric mucosa. Eur J Immunol. 2008;38(2):470-8.
254. Pinchuk IV, Morris KT, Nofchissey RA, Earley RB, Wu JY, Ma TY, et al. Stromal cells induce Th17 during Helicobacter pylori infection and in the gastric tumor microenvironment. PLoS One. 2013;8(1):e53798.
255. Li Q, Li Q, Chen J, Liu Y, Zhao X, Tan B, et al. Prevalence of Th17 and Treg cells in gastric cancer patients and its correlation with clinical parameters. Oncol Rep. 2013;30(3):1215-22.
256. Zhang B, Rong G, Wei H, Zhang M, Bi J, Ma L, et al. The prevalence of Th17 cells in patients with gastric cancer. Biochem Biophys Res Commun. 2008;374(3):533-7.
257. Miyahara Y, Odunsi K, Chen W, Peng G, Matsuzaki J, Wang RF. Generation and regulation of human CD4+ IL-17-producing T cells in ovarian cancer. Proc Natl Acad Sci U S A. 2008;105(40):15505-10.
258. Le Gouvello S, Bastuji-Garin S, Aloulou N, Mansour H, Chaumette MT, Berrehar F, et al. High prevalence of Foxp3 and IL17 in MMR-proficient colorectal carcinomas. Gut. 2008;57(6):772-9.
259. Tosolini M, Kirilovsky A, Mlecnik B, Fredriksen T, Mauger S, Bindea G, et al. Clinical impact of different classes of infiltrating T cytotoxic and helper cells (Th1, th2, treg, th17) in patients with colorectal cancer. Cancer Res. 2011;71(4):1263-71.
260. Atarashi K, Tanoue T, Ando M, Kamada N, Nagano Y, Narushima S, et al. Th17 Cell Induction by Adhesion of Microbes to Intestinal Epithelial Cells. Cell. 2015;163(2):367-80.
261. Ivanov, II, Atarashi K, Manel N, Brodie EL, Shima T, Karaoz U, et al. Induction of intestinal Th17 cells by segmented filamentous bacteria. Cell. 2009;139(3):485-98.
262. Housseau F, Wu S, Wick EC, Fan H, Wu X, Llosa NJ, et al. Redundant Innate and Adaptive Sources of IL17 Production Drive Colon Tumorigenesis. Cancer Res. 2016;76(8):2115-24.
263. Wick EC, Rabizadeh S, Albesiano E, Wu X, Wu S, Chan J, et al. Stat3 activation in murine colitis induced by enterotoxigenic Bacteroides fragilis. Inflamm Bowel Dis. 2014;20(5):821-34.
264. Ji K, Zhang M, Chu Q, Gan Y, Ren H, Zhang L, et al. The Role of p-STAT3 as a Prognostic and Clinicopathological Marker in Colorectal Cancer: A Systematic Review and Meta-Analysis. PLoS One. 2016;11(8):e0160125.
265. Kusaba T, Nakayama T, Yamazumi K, Yakata Y, Yoshizaki A, Inoue K, et al. Activation of STAT3 is a marker of poor prognosis in human colorectal cancer. Oncol Rep. 2006;15(6):1445-51.
266. Morikawa T, Baba Y, Yamauchi M, Kuchiba A, Nosho K, Shima K, et al. STAT3 expression, molecular features, inflammation patterns, and prognosis in a database of 724 colorectal cancers. Clin Cancer Res. 2011;17(6):1452-62.
267. Corvinus FM, Orth C, Moriggl R, Tsareva SA, Wagner S, Pfitzner EB, et al. Persistent STAT3 activation in colon cancer is associated with enhanced cell proliferation and tumor growth. Neoplasia. 2005;7(6):545-55.
268. Hanahan D, Weinberg RA. The hallmarks of cancer. Cell. 2000;100(1):57-70.
269. Heichler C, Scheibe K, Schmied A, Geppert CI, Schmid B, Wirtz S, et al. STAT3 activation through IL-6/IL-11 in cancer-associated fibroblasts promotes colorectal tumour development and correlates with poor prognosis. Gut. 2020;69(7):1269-82.
270. Nguyen AV, Wu YY, Liu Q, Wang D, Nguyen S, Loh R, et al. STAT3 in epithelial cells regulates inflammation and tumor progression to malignant state in colon. Neoplasia. 2013;15(9):998-1008.

271. Cooper HS, Everley L, Chang WC, Pfeiffer G, Lee B, Murthy S, et al. The role of mutant Apc in the development of dysplasia and cancer in the mouse model of dextran sulfate sodium-induced colitis. Gastroenterology. 2001;121(6):1407-16.
272. Tanaka T, Kohno H, Suzuki R, Hata K, Sugie S, Niho N, et al. Dextran sodium sulfate strongly promotes colorectal carcinogenesis in Apc(Min/+) mice: inflammatory stimuli by dextran sodium sulfate results in development of multiple colonic neoplasms. Int J Cancer. 2006;118(1):25-34.
273. Ni J, Wu GD, Albenberg L, Tomov VT. Gut microbiota and IBD: causation or correlation? Nat Rev Gastroenterol Hepatol. 2017;14(10):573-84.
274. Levy M, Kolodziejczyk AA, Thaiss CA, Elinav E. Dysbiosis and the immune system. Nat Rev Immunol. 2017;17(4):219-32.
275. Durban A, Abellan JJ, Jimenez-Hernandez N, Salgado P, Ponce M, Ponce J, et al. Structural alterations of faecal and mucosa-associated bacterial communities in irritable bowel syndrome. Environ Microbiol Rep. 2012;4(2):242-7.
276. Ahn J, Sinha R, Pei Z, Dominianni C, Wu J, Shi J, et al. Human gut microbiome and risk for colorectal cancer. J Natl Cancer Inst. 2013;105(24):1907-11.
277. Norman JM, Handley SA, Baldridge MT, Droit L, Liu CY, Keller BC, et al. Disease-specific alterations in the enteric virome in inflammatory bowel disease. Cell. 2015;160(3):447-60.
278. Guo Y, Zhang Y, Gerhard M, Gao JJ, Mejias-Luque R, Zhang L, et al. Effect of Helicobacter pylori on gastrointestinal microbiota: a population-based study in Linqu, a high-risk area of gastric cancer. Gut. 2020;69(9):1598-607.
279. Stecher B, Robbiani R, Walker AW, Westendorf AM, Barthel M, Kremer M, et al. Salmonella enterica serovar typhimurium exploits inflammation to compete with the intestinal microbiota. PLoS Biol. 2007;5(10):2177-89.
280. Lupp C, Robertson ML, Wickham ME, Sekirov I, Champion OL, Gaynor EC, et al. Host-mediated inflammation disrupts the intestinal microbiota and promotes the overgrowth of Enterobacteriaceae. Cell Host Microbe. 2007;2(3):204.
281. Arthur JC, Perez-Chanona E, Muhlbauer M, Tomkovich S, Uronis JM, Fan TJ, et al. Intestinal inflammation targets cancer-inducing activity of the microbiota. Science. 2012;338(6103):120-3.
282. Elinav E, Strowig T, Kau AL, Henao-Mejia J, Thaiss CA, Booth CJ, et al. NLRP6 inflammasome regulates colonic microbial ecology and risk for colitis. Cell. 2011;145(5):745-57.
283. Levy M, Thaiss CA, Zeevi D, Dohnalova L, Zilberman-Schapira G, Mahdi JA, et al. Microbiota-Modulated Metabolites Shape the Intestinal Microenvironment by Regulating NLRP6 Inflammasome Signaling. Cell. 2015;163(6):1428-43.
284. Schneeberger M, Everard A, Gomez-Valades AG, Matamoros S, Ramirez S, Delzenne NM, et al. Akkermansia muciniphila inversely correlates with the onset of inflammation, altered adipose tissue metabolism and metabolic disorders during obesity in mice. Sci Rep. 2015;5:16643.
285. Plovier H, Everard A, Druart C, Depommier C, Van Hul M, Geurts L, et al. A purified membrane protein from Akkermansia muciniphila or the pasteurized bacterium improves metabolism in obese and diabetic mice. Nat Med. 2017;23(1):107-13.
286. Derosa L, Routy B, Thomas AM, Iebba V, Zalcman G, Friard S, et al. Intestinal Akkermansia muciniphila predicts clinical response to PD-1 blockade in patients with advanced non-small-cell lung cancer. Nat Med. 2022;28(2):315-24.
287. Desai MS, Seekatz AM, Koropatkin NM, Kamada N, Hickey CA, Wolter M, et al. A Dietary Fiber-Deprived Gut Microbiota Degrades the Colonic Mucus Barrier and Enhances Pathogen Susceptibility. Cell. 2016;167(5):1339-53 e21.
288. Seregin SS, Golovchenko N, Schaf B, Chen J, Pudlo NA, Mitchell J, et al. NLRP6 Protects Il10(-/-) Mice from Colitis by Limiting Colonization of Akkermansia muciniphila. Cell Rep. 2017;19(4):733-45.
289. Baxter NT, Zackular JP, Chen GY, Schloss PD. Structure of the gut microbiome following colonization with human feces determines colonic tumor burden. Microbiome. 2014;2:20.
290. Sheng YH, Hasnain SZ, Florin TH, McGuckin MA. Mucins in inflammatory bowel diseases and colorectal cancer. J Gastroenterol Hepatol. 2012;27(1):28-38.

291. Gersemann M, Becker S, Kubler I, Koslowski M, Wang G, Herrlinger KR, et al. Differences in goblet cell differentiation between Crohn's disease and ulcerative colitis. Differentiation. 2009;77(1):84-94.
292. Johansson ME, Gustafsson JK, Sjoberg KE, Petersson J, Holm L, Sjovall H, et al. Bacteria penetrate the inner mucus layer before inflammation in the dextran sulfate colitis model. PLoS One. 2010;5(8):e12238.
293. Dharmani P, Leung P, Chadee K. Tumor necrosis factor-alpha and Muc2 mucin play major roles in disease onset and progression in dextran sodium sulphate-induced colitis. PLoS One. 2011;6(9):e25058.
294. Renes IB, Boshuizen JA, Van Nispen DJ, Bulsing NP, Buller HA, Dekker J, et al. Alterations in Muc2 biosynthesis and secretion during dextran sulfate sodium-induced colitis. Am J Physiol Gastrointest Liver Physiol. 2002;282(2):G382-9.
295. Leow CC, Romero MS, Ross S, Polakis P, Gao WQ. Hath1, down-regulated in colon adenocarcinomas, inhibits proliferation and tumorigenesis of colon cancer cells. Cancer Res. 2004;64(17):6050-7.
296. Katoh M, Katoh M. Notch signaling in gastrointestinal tract (review). Int J Oncol. 2007;30(1):247-51.
297. van Es JH, van Gijn ME, Riccio O, van den Born M, Vooijs M, Begthel H, et al. Notch/gamma-secretase inhibition turns proliferative cells in intestinal crypts and adenomas into goblet cells. Nature. 2005;435(7044):959-63.
298. van der Leun AM, Thommen DS, Schumacher TN. CD8(+) T cell states in human cancer: insights from single-cell analysis. Nat Rev Cancer. 2020;20(4):218-32.
299. Im SJ, Hashimoto M, Gerner MY, Lee J, Kissick HT, Burger MC, et al. Defining CD8+ T cells that provide the proliferative burst after PD-1 therapy. Nature. 2016;537(7620):417-21.
300. Paley MA, Kroy DC, Odorizzi PM, Johnnidis JB, Dolfi DV, Barnett BE, et al. Progenitor and terminal subsets of CD8+ T cells cooperate to contain chronic viral infection. Science. 2012;338(6111):1220-5.
301. He R, Hou S, Liu C, Zhang A, Bai Q, Han M, et al. Follicular CXCR5- expressing CD8(+) T cells curtail chronic viral infection. Nature. 2016;537(7620):412-28.
302. Pages F, Berger A, Camus M, Sanchez-Cabo F, Costes A, Molidor R, et al. Effector memory T cells, early metastasis, and survival in colorectal cancer. N Engl J Med. 2005;353(25):2654-66.
303. Kamboj AK, Cotter TG, Oxentenko AS. Helicobacter pylori: The Past, Present, and Future in Management. Mayo Clin Proc. 2017;92(4):599-604.
304. Lee CW, Rickman B, Rogers AB, Ge Z, Wang TC, Fox JG. Helicobacter pylori eradication prevents progression of gastric cancer in hypergastrinemic INS-GAS mice. Cancer Res. 2008;68(9):3540-8.
305. Romero-Gallo J, Harris EJ, Krishna U, Washington MK, Perez-Perez GI, Peek RM, Jr. Effect of Helicobacter pylori eradication on gastric carcinogenesis. Lab Invest. 2008;88(3):328-36.
306. Nutsch K, Chai JN, Ai TL, Russler-Germain E, Feehley T, Nagler CR, et al. Rapid and Efficient Generation of Regulatory T Cells to Commensal Antigens in the Periphery. Cell Rep. 2016;17(1):206-20.
307. Smith PM, Howitt MR, Panikov N, Michaud M, Gallini CA, Bohlooly YM, et al. The microbial metabolites, short-chain fatty acids, regulate colonic Treg cell homeostasis. Science. 2013;341(6145):569-73.
308. Knoop KA, McDonald KG, McCrate S, McDole JR, Newberry RD. Microbial sensing by goblet cells controls immune surveillance of luminal antigens in the colon. Mucosal Immunol. 2015;8(1):198-210.
309. Yassour M, Vatanen T, Siljander H, Hamalainen AM, Harkonen T, Ryhanen SJ, et al. Natural history of the infant gut microbiome and impact of antibiotic treatment on bacterial strain diversity and stability. Sci Transl Med. 2016;8(343):343ra81.
310. Palleja A, Mikkelsen KH, Forslund SK, Kashani A, Allin KH, Nielsen T, et al. Recovery of gut microbiota of healthy adults following antibiotic exposure. Nat Microbiol. 2018;3(11):1255-65.
311. Laubitz D, Typpo K, Midura-Kiela M, Brown C, Barberan A, Ghishan FK, et al. Dynamics of Gut Microbiota Recovery after Antibiotic Exposure in Young and Old Mice (A Pilot Study). Microorganisms. 2021;9(3).

312. Wang J, Wang P, Tian H, Tian F, Zhang Y, Zhang L, et al. Aryl hydrocarbon receptor/IL-22/Stat3 signaling pathway is involved in the modulation of intestinal mucosa antimicrobial molecules by commensal microbiota in mice. Innate Immun. 2018;24(5):297-306.
313. Li Y, Kundu P, Seow SW, de Matos CT, Aronsson L, Chin KC, et al. Gut microbiota accelerate tumor growth via c-jun and STAT3 phosphorylation in APCMin/+ mice. Carcinogenesis. 2012;33(6):1231-8.
314. Fischbach W, Malfertheiner P, Lynen Jansen P, Bolten W, Bornschein J, Buderus S, et al. S2k-Guideline Helicobacter pylori and gastroduodenal ulcer disease. Z Gastroenterol. 2017;55(2):167-206.
315. Soylu A, Ozkara S, Alis H, Dolay K, Kalayci M, Yasar N, et al. Immunohistochemical testing for Helicobacter Pylori existence in neoplasms of the colon. BMC Gastroenterol. 2008;8:35.
316. Jones M, Helliwell P, Pritchard C, Tharakan J, Mathew J. Helicobacter pylori in colorectal neoplasms: is there an aetiological relationship? World J Surg Oncol. 2007;5:51.
317. Grahn N, Hmani-Aifa M, Fransen K, Soderkvist P, Monstein HJ. Molecular identification of Helicobacter DNA present in human colorectal adenocarcinomas by 16S rDNA PCR amplification and pyrosequencing analysis. J Med Microbiol. 2005;54(Pt 11):1031-5.